Spring 2013

Improving bottom-up and top-down estimates of carbon fluxes in the Midwestern USA

Aditsuda Jamroensan
University of Iowa

IMPROVING BOTTOM-UP AND TOP-DOWN ESTIMATES OF

CARBON FLUXES IN THE MIDWESTERN USA

by

Aditsuda Jamroensan

<u>An Abstract</u>

Of a thesis submitted in partial fulfillment
of the requirements for the Doctor of
Philosophy degree in Civil and Environmental Engineering
in the Graduate College of
The University of Iowa

May 2013

Thesis Supervisors: Professor Gregory R. Carmichael
Associate Professor Charles Stanier

ABSTRACT

Carbon dioxide (CO_2) is the leading contributor to global warming and climate change. The increases in fossil fuel emissions, deforestation, and changes of land use have resulted in increased CO_2 levels in the atmosphere from 280 ppm in 1765 to 390 ppm in 2010. Carbon mitigation policies for managing the biosphere to increase net CO_2 uptake are dependent upon accurate knowledge of the biosphere fluxes. However, Northern Hemisphere bottom-up and top-down biosphere flux estimates show significant discrepancies, especially in North America. In this study, we design an analysis framework that integrates observations with models with the goal of reducing some of the key uncertainties in estimating CO_2 fluxes and concentrations in the Midwest, USA.

In this research, the biosphere model, WRF-VPRM model (Ahmadov et al., 2007) is used to simulate CO_2 biosphere fluxes and atmospheric CO_2 concentrations in the Midwest, USA at high spatial resolution. Reducing uncertainties in the predictions is accomplished by improving the model transport configurations (i.e. the WRF planetary boundary layer (PBL) scheme, the number of vertical layers and the horizontal resolution), utilizing a more detailed land cover map, optimizing VPRM photosynthesis and respiratory parameters for major crops (i.e. corn and soybean) against flux towers, and integrating CO_2 tall tower observations and model through a top-down data assimilation method to improve the VPRM model parameters and in turn improving the flux and concentration estimates.

The WRF-VPRM model configuration with the YonSei University PBL scheme produced the most accurate CO_2 concentration predictions at the WBI tower at all three tower levels with the maximum error reduction of 17.1%. Increasing the number of vertical layers improved the CO_2 estimates during nighttime and early morning, especially at 30 m, where the error was reduced by a maximum of ~ 20%. The differences in the monthly average net fluxes over the State of Iowa between the high

resolution WRF-VPRM model and coarse resolution Carbon Tracker were significant, 71%, 18%, and 62% in June, July, and August, respectively.

The fluxes calculated by the VPRM model are primarily dependent on 4 model parameters, half saturation value of photosynthesis (PAR_0), light use efficiency (λ), and respiration parameters (α and β). These parameters are specific to vegetation types, regions, and time period. The default settings do not distinguish between corn and soybean, which are major crops in the Midwest and have significant different photosynthesis rates. When corn and soybean are explicitly included in the model, the flux estimate changed by 31.3% at 12 pm and 24.5% at 12 am.

Two different methods were used to optimize for the VPRM model parameters which are optimization against Ameriflux NEE and using a top-down variational method. The simulation using optimized parameters from the variational method reduced the error during the daytime from 11.6 ppm to 7.8 ppm. The average fluxes optimized using the variational method changed by 17% and 38.6% at 12 pm and 12 am, respectively. The more accurate VPRM parameters lead to the more accurate biosphere fluxes, which will ease the evaluation of benefits of different carbon mitigation policies.

Abstract Approved: _____
                                                Thesis Supervisor

                                             _____
                                                Title and Department

                                             _____
                                                Date

                                             _____
                                                Thesis Supervisor

                                             _____
                                                Title and Department

                                             _____
                                                Date

IMPROVING BOTTOM-UP AND TOP-DOWN ESTIMATES OF

CARBON FLUXES IN THE MIDWESTERN USA

by

Aditsuda Jamroensan

A thesis submitted in partial fulfillment
of the requirements for the Doctor of
Philosophy degree in Civil and Environmental Engineering
in the Graduate College of
The University of Iowa

May 2013

Thesis Supervisor: Professor Gregory R. Carmichael
                    Associate Professor Charles Stanier

Graduate College
The University of Iowa
Iowa City, Iowa

CERTIFICATE OF APPROVAL

_____

PH.D. THESIS

_____

This is to certify that the Ph.D. thesis of

Aditsuda Jamroensan

has been approved by the Examining Committee
for the thesis requirement for the Doctor of Philosophy
degree in Civil and Environmental Engineering at the May 2013 graduation.

Thesis Committee: _____
                                  Gregory Carmichael, Thesis Supervisor

                              _____
                                  Charles Stanier, Thesis Supervisor

                              _____
                                  Jerold Schnoor

                              _____
                                  William Eichinger

                              _____
                                  Thanos Papanicolaou

                              _____
                                  Scott Spak

To my family and friends who have encouraged me during my Ph.D.

ACKNOWLEDGMENTS

I would like to thank my advisors, Professor Gregory Carmichael and Associate Professor Charles Stanier, for the encouragement they have given me since the beginning of my Ph.D. study until the end. They have not only taught me scientific knowledge but also taught me to share and to encourage others. Their patience and sincerity have and will empower me to success. I promise I will do the same to others. Thank you for never giving up on me.

I would also like to thank my colleagues Pallavi Marrapu, Pablo Saide, Jaemeen Baek, Man Yu, and Yafang Chen. Thank you for all the support and suggestions. I appreciate the friendship you all have given me. We became best friends after all and will be forever.

Last but not least, I would like to thank my friends, my husband, Andrew Kiekhaefer, and my family for their constant support and sacrifices. Thank you Mom and Dad for always believing in me and cheering me up. I love you all very much.

ABSTRACT

Carbon dioxide (CO_2) is the leading contributor to global warming and climate change. The increases in fossil fuel emissions, deforestation, and changes of land use have resulted in increased CO_2 levels in the atmosphere from 280 ppm in 1765 to 390 ppm in 2010. Carbon mitigation policies for managing the biosphere to increase net CO_2 uptake are dependent upon accurate knowledge of the biosphere fluxes. However, Northern Hemisphere bottom-up and top-down biosphere flux estimates show significant discrepancies, especially in North America. In this study, we design an analysis framework that integrates observations with models with the goal of reducing some of the key uncertainties in estimating CO_2 fluxes and concentrations in the Midwest, USA.

In this research, the biosphere model, WRF-VPRM model (Ahmadov et al., 2007) is used to simulate CO_2 biosphere fluxes and atmospheric CO_2 concentrations in the Midwest, USA at high spatial resolution. Reducing uncertainties in the predictions is accomplished by improving the model transport configurations (i.e. the WRF planetary boundary layer (PBL) scheme, the number of vertical layers and the horizontal resolution), utilizing a more detailed land cover map, optimizing VPRM photosynthesis and respiratory parameters for major crops (i.e. corn and soybean) against flux towers, and integrating CO_2 tall tower observations and model through a top-down data assimilation method to improve the VPRM model parameters and in turn improving the flux and concentration estimates.

The WRF-VPRM model configuration with the YonSei University PBL scheme produced the most accurate CO_2 concentration predictions at the WBI tower at all three tower levels with the maximum error reduction of 17.1%. Increasing the number of vertical layers improved the CO_2 estimates during nighttime and early morning, especially at 30 m, where the error was reduced by a maximum of ~ 20%. The differences in the monthly average net fluxes over the State of Iowa between the high

resolution WRF-VPRM model and coarse resolution Carbon Tracker were significant, 71%, 18%, and 62% in June, July, and August, respectively.

The fluxes calculated by the VPRM model are primarily dependent on 4 model parameters, half saturation value of photosynthesis (PAR_0), light use efficiency (λ), and respiration parameters (α and β). These parameters are specific to vegetation types, regions, and time period. The default settings do not distinguish between corn and soybean, which are major crops in the Midwest and have significant different photosynthesis rates. When corn and soybean are explicitly included in the model, the flux estimate changed by 31.3% at 12 pm and 24.5% at 12 am.

Two different methods were used to optimize for the VPRM model parameters which are optimization against Ameriflux NEE and using a top-down variational method. The simulation using optimized parameters from the variational method reduced the error during the daytime from 11.6 ppm to 7.8 ppm. The average fluxes optimized using the variational method changed by 17% and 38.6% at 12 pm and 12 am, respectively. The more accurate VPRM parameters lead to the more accurate biosphere fluxes, which will ease the evaluation of benefits of different carbon mitigation policies.

TABLE OF CONTENTS

LIST OF FIGURES

xii

CHAPTER 1 INTRODUCTION

1.1 Background and Significant

Carbon dioxide is the single most important greenhouse gas and warms the Earth's surface due to its ability to absorb infrared radiation (thermal radiation) emitted by land and ocean (IPCC, 2007). An increase in CO_2 emissions to the atmosphere will increase the warming, and as a result, the evaporation of water will increase, which further intensifies the warming and increases water vapor. Carbon dioxide is mainly generated from burning of fossil fuels, cement production, and release of carbon due to land use changes, e.g., deforestation and biomass burning. About 9 gigatons of carbon each year are released due to human activities (NASA, 2011). Plants and the biosphere can uptake about half of that carbon dioxide as a carbon source through photosynthesis. Since the fossil fuel carbon generated cannot be completely absorbed by the ocean and terrestrial biosphere on a fast enough time scale, the global carbon budget is currently imbalanced. This leads to an accumulation of carbon dioxide in the atmosphere. The observed global mean concentration reported by National Oceanic and Atmospheric Administration (NOAA) in 2010 was approximately 390 ppm, and rising by about 1.9 ppm/yr. It has increased 30 ppm in the last 17 years. The increase is significant since it has not risen by 30 ppm in the prior 1000 years. Fossil fuel emissions and land use change (primarily deforestation) are responsible for 75% and 25% of human-caused CO_2 emission, respectively (IPCC, 2007).

According to the Intergovernmental Panel on Climate Change 2007 (IPCC, 2007), the impacts associated with the increase in greenhouse gases and land use changes include: an increase in average temperature; change in extremes of temperature; higher intensity and frequency of severe weather (e.g., hurricanes in North Pacific Indian and Southwest Pacific Oceans); and an increase in precipitation over land north of $30^{o}N$ (1900 to 2005) but a decrease in precipitation over the topics since 1970s. These shifts in

precipitation lead to more frequent droughts in some regions. Changes in the cryosphere include the melting of mountain glaciers and ice caps from the Greenland and Antarctic Ice Sheets, which contribute to a rise of mean sea level (1.8 ± 0.5 mm yr^{-1} from 1961 to 2003). Changes in sea levels and ocean temperatures affect the rate of uptake of carbon dioxide by the oceans. It is likely that the ratio of emitted carbon dioxide uptake by the ocean dropped from $42\pm7\%$ during 1750 to 1994 to $37\pm7\%$ during 1980 to 2005 (IPCC, 2007). Additionally, ocean biogeochemistry is changing i.e. the increase in total inorganic carbon content, 118 ± 19 GtC between 1750 and 1994 (and continues to increase) caused decreases in surface ocean pH and oxygen concentrations. The nature and extent of these impacts suggest that policies to stabilize and reduce greenhouse gas emissions are needed.

Carbon mitigation policies focus on reducing anthropogenic CO_2 emissions and managing the biosphere to increase net CO_2 uptake. An example of a land management policy focused on enhancing carbon sequestration is the limiting of deforestation, since forests store large amounts of carbon. Deforestation releases carbon back to the atmosphere, particularly in tropical forests. For example deforestation in Brazil, Indonesia and parts of Africa account for about 20% of greenhouse gas emissions (IPCC, 2007). Forest ecosystems store more carbon than grasslands, which store more carbon than croplands. Changing grasslands and croplands to forest or changing unused land to grassland are also ways of increasing the sequestering of carbon. Crop planting methods, such as reducing tillage and no-tillage planting, are ways of reducing net CO_2 emissions. Land use changes associated with US corn ethanol production is another important issue. The 15 billion gallon Renewable Fuel Standard implied by the Energy Independence and Security Act of 2007 is established to result in carbon emissions in the range between 1167 and 1676 g/gallon (Tyner et al. 2010) or approximately 17.5 to 25.1 million tons of carbon. Corn ethanol fuel seems to have lower environmental impacts compared to fossil fuels such as coal since corn uptakes carbon from the atmosphere during photosynthesis.

Coal fuels, in contrast, release carbon which was stored underground to the atmosphere. However, diverting land from existing forest and grassland, which previously stored large amounts of carbon, will cause the release of it to the atmosphere. The higher price of the crop as more US croplands support ethanol also encourages farmers all over the world to divert more land for corn production, which in turn results in the clearing of more forest and more carbon emissions. Due to the lower crop yield, farmers in other countries often need more land to grow the crops and sometime to try to increase the yield by environmental unfriendly practices such as using more fertilizer and reducing crop rotations (Searchinger et al., 2008). Increased knowledge about carbon dioxide fluxes from the biosphere is required to facilitate cost-effective carbon management policies both at global and regional scales.

Devising effective policies are dependent upon knowledge of carbon source/sink estimates which include the contributions from the biosphere and anthropogenic emissions. Anthropogenic emission inventories are believed to be more certain than estimates of the biosphere fluxes since the anthropogenic emission sources (e.g. industries, automobile, etc.) are known. The estimation of the land-to-atmosphere flux is more uncertain due to the vast diversity and complexity of the terrestrial biosphere. Two approaches are commonly used for the estimates of carbon released from the biosphere: 1) the bottom-up approach which estimates carbon based on plants' photosynthesis and respiration activities and 2) the top-down approach which utilizes atmospheric carbon dioxide concentrations and transport models to retrieve biosphere fluxes. So far, significant discrepancies of the biosphere flux estimates based on the bottom-up and the top-down approaches have been reported. The inversion estimates of Northern Hemisphere land sink are -1.7 (-0.4 to -2.3) GtC yr^{-1}, while the sink obtained from the bottom up approach are -0.98 (-0.38 to -1.6) GtC yr^{-1} (Kurz et al., 1995; Fang et al., 2001; Pacala et al., 2001; Janssens et al., 2003; Shvidenko et al., 2003). The inversion sink value is on average higher than the bottom-up value.

Improving carbon flux estimates can be achieved through several methods. Using high quality and more detailed land cover maps, optimizing biosphere model parameters, and better estimates of shortwave radiation and temperature, are examples of ways to improve the biosphere flux estimates based on the bottom-up approach. Reducing the uncertainty in top-down approaches requires improvements in the forward models and in the observing system. Using higher resolution biosphere and transport models can also improve the estimates.

Tall tower carbon dioxide observations are crucial for both investigating the bottom-up model performances and providing observed CO_2 concentrations for top-down inversion of posterior fluxes. The NOAA Global Monitoring Division (GMD) began making measurement of carbon dioxide and related gases in the continental boundary layer from tall towers since 1990s in order to extent long-term carbon-cycle gas monitoring to continental areas. Currently, there are eight NOAA tall towers in the continental United States. Two of those are located in the study area of this research, the Midwest, USA. The WBI tower which samples the gases at 31 m, 99 m, and 379 m above ground is located in West Branch, Iowa. The LEF tower which takes the samples at 11 m, 30 m, 76 m, 122 m, 244 m, and 396 m above ground is located in Park Falls, Wisconsin. The tall towers provide high temporal continuous measurement of carbon dioxide and carbon monoxide (CO) concentrations and daily flask sampling of other atmospheric trace gases such as CH_4, N_2O, and carbonyl sulfide (COS). Beside the NOAA tall towers, five Ring 2 towers (lower sampling level at 30 m and upper levels at 110-140 m height) were established as part of the Mid-continental Intensive (MCI) campaign aimed to measure the terrestrial carbon balance of the upper Midwest. The towers measured CO_2 mixing ratio continuously for the period April 2007 to October 2009. These observed CO_2 concentrations from tower networks are used for evaluating the model performance and in estimating the biosphere fluxes and mixing ratios as well as utilizing as input in the inversion studies.

1.2 Overview and Objectives

North America is currently a net source of carbon dioxide to the atmosphere. According to the First State of the Carbon Cycle Report (SOCCR report) (CCSP, 2007), fossil fuel emissions from North America accounted for 27% of global fossil-fuel emissions in 2003, with the United States contributing 85% of this total fossil fuel emission. Only 30% (505 Mt C per year ± 50%) of the North America fossil fuel carbon is absorbed by natural sinks. Biosphere flux estimations in North America are highly uncertain (CCSP, 2007; Baker et al., 2006). Baker et al. (2006) reported the North America carbon sink of 0.97 ± 0.36 Gt C per year from 1991-2000 based on inversions of 13 atmospheric transport models. According to the SOCCR report, the North American sink for the year 2003 was approximately 500 Mt of carbon plus or minus 50% (between 250 and 750 Mt C per year). Scientists have focused on understanding and quantifying the carbon budgets over the past decade. The North America Carbon Program (NACP) aims to measure and understand the sources and sinks of carbon dioxide in North America and in adjacent ocean regions. Various regional carbon flux networks (e.g. AmeriFlux and FLUXNET) were constructed to provide continuous observations of ecosystem level exchanges of the gas, water, energy in North America and other continents.

The North America carbon flux uncertainty is an important factor which drives the global uncertainty, and reducing this uncertainty is critical to better understanding of the carbon budgets (IPCC, 2007; Peters et al., 2005). The current best attempt for estimation of biosphere sources/sinks is called Carbon Tracker established by NOAA (Peters et al., 2007). It has shown that the sinks are mainly located in the agricultural regions of the Midwest (36% of the North America total sink). However, the estimation is uncertain due to the coarse resolution of the model (1 degree) and the use of a simplified process model for terrestrial photosynthesis and respiration. High resolution and precise estimates of carbon dioxide biosphere flux estimates and concentrations are invaluable

for carbon management and policy decision makers. This motivates the main objective of this research, which is to develop a methodology to reduce uncertainty in estimates of carbon dioxide biosphere fluxes and concentrations.

The major model used in this research is called WRF-VPRM (Ahmadov et al., 2007). It is an online-coupled air quality and transport model (Weather Research and Forecasting Model: WRF) and a diagnostic biosphere model (Vegetation Photosynthesis and Respiration Model: VPRM). The WRF model version 3, developed at National Center for Atmospheric Research (NCAR) (Skamarock et al., 2008) conserves mass, momentum, dry entropy, and scalars. VPRM is a diagnostic biosphere model developed by Mahadevan et al. (2008), modified from the Vegetation Photosynthesis Model developed by Xiao et al. (2004). WRF-VPRM utilizes simulated downward shortwave radiation and surface temperature at 2 meter from WRF, along with satellite-derived vegetation indices (Enhanced Vegetation Index (EVI) and Land Surface Water Index (LSWI)) and derived parameters from Ameriflux eddy flux towers, to estimate carbon dioxide biosphere fluxes based on empirical equations. The VPRM parameters, light use efficiency (λ), half saturation value of photosynthesis (PAR_0), and parameters for respiration (α and β), specific for each land cover class, are utilized for biosphere flux estimates.

To evaluate flux predictions, the carbon dioxide mixing ratios predicted by a forward model need to be compared against observations (e.g., tall towers and aircraft observations). One of the factors which strongly influences the mixing ratio estimates is atmospheric transport. Two previous regional studies (Ahmadov et al., 2007 and 2009) for carbon dioxide simulation were done in France during the CarboEurope Regional Experiment Strategy (CERES) campaign conducted 16 May - 15 June, 2005. Ahmadov et al. (2009) simulations used a 2-way nesting option with 10 and 2 km outer and inner domains, respectively. The results showed that the model could capture the observed diurnal variability of CO_2 quite well. However, it failed to resolve the high concentrations

of CO_2 during early morning (underestimated by about 10 ppm), when respired CO_2 is retained by the nocturnal boundary layer. Ahmadov et al. (2007) indicated that WRF-VPRM model and observation discrepancies were mainly contributed to inaccuracies in the WRF transport model. Therefore, the first research aim is to find the WRF model settings that most accurately predict the meteorological parameters that effect carbon dioxide estimates is crucial for improving model predictions of biosphere flux and mixing ratios.

The second research objective focuses on improving the bottom-up flux and carbon dioxide concentration estimates by using more detailed land cover maps that distinguish corn (C4 crop) from soybean (C3 crop) and optimizing VPRM model parameters for corn and soybean for a specific region and time period. Although VPRM parameters are specific to vegetation type, location, and time, they are only available for a limited set of crops, regions and time periods. Mahadevan et al. (2008) utilized Ameriflux data during 2000 to 2004 from the sites in the United States and Canada for VPRM parameter optimization, which include corn and soybean. Although corn and soybean were optimized separately in Mahadevan's study, using long periods of observed fluxes can push the parameter values toward lower values than using growing season only data, as plants usually have higher rates of photosynthesis in the growing season as compared to other times of the year. For some vegetation, especially grasslands which have heterogeneous spatial distributions, optimization at the regional scale is needed in order to obtain representative values. Optimizing parameters against Ameriflux tower data in the model domain and during the period of model simulation is expected to yield more representative results and better flux estimates. Currently, WRF-VPRM does not distinguish between C3 and C4 crops. Corn is a C4 plant and can photosynthesize faster under high heat and light conditions than C3 plants like soybean. These C4 plants have higher carbon dioxide uptake through photosynthesis. Therefore, separating the two

major crop types in the study area (corn and soybean) from the other crops is anticipated to improve biosphere flux predictions.

CO$_2$ inversion (i.e., "top-down" approach) is a method used for the biosphere flux estimation from atmospheric CO$_2$ measurements (Gurney et al., 2002; Maksyutov et al., 2003; Peylin et al., 2002; Law et al., 2003; Rodenbeck et al., 2003; Peylin et al., 2005). Top-down approaches utilize carbon dioxide atmospheric observations (e.g., from tall towers, aircraft, ships, and fixed site measurements) along with data assimilation tools to tune the results from a forward model toward observations. In this study, we have applied a CO$_2$ top-down inversion approach using a generalized Bayesian inversion for improving the VPRM parameters derived from the bottom up approach which in turn improves the biosphere flux estimates. The CO$_2$ inversion studies were carried out in August 2008 over the State of Iowa and the Midwest domains at 4 km resolution.

1.3 Specific Objectives

The ability to estimate accurate biosphere fluxes with high resolution is crucial for quantifying net CO$_2$ emission to the atmosphere. The main objective of this research is to develop a methodology to reduce uncertainty in estimates of CO$_2$ fluxes and concentrations by improving current bottom up biosphere and transport model performance and utilizing top-down inversion data assimilation method.

The specific objectives are:

1. Identify the planetary boundary scheme (PBL) which yields the better CO$_2$ estimation using WRF-VPRM biosphere and transport model.

2. Optimize the VPRM biosphere model photosynthesis and respiratory parameters for major crop types in the Midwest i.e., corn and soybean.

3. Utilize a generalized Bayesian inversion method for improving the VPRM model parameters derived from the bottom up approach.

CHAPTER 2 MODEL DESCRIPTIONS AND METHODOLOGY

2.1 Overview of Methodology

The major tool used in this research is the WRF-VPRM transport and biosphere

model version 3.0.1.1 (Ahmadov et al., 2007). The VPRM biosphere model estimates

carbon dioxide biosphere fluxes based on vegetation indices derived from MODIS

satellite data, model parameters, and temperature and radiation from the WRF model.

This method is also referred to as "bottom-up" estimate of carbon dioxide fluxes. High

resolution fossil fuel carbon dioxide (VULCAN) is also incorporated into the model as

another source of the emissions (Gurney et al., 2009). Transport of carbon dioxide is

performed using WRF model resulting in atmospheric carbon dioxide concentrations.

Tall towers are used for comparison to evaluate model accuracy and representing the

truth in 3Dvar data assimilation step to invert for VPRM parameters from the known CO_2

concentrations (also referred to as "top-down" approach).

Bottom-up approaches utilize photosynthesis and respiration information to

estimate the surface fluxes. The VPRM model is used as a tool for calculating the

biosphere fluxes based on the photosynthesis and respiration information along with

meteorological data from the WRF model. Therefore, improving the bottom-up CO_2 flux

and mixing ratio estimates can be achieved by improving the bottom-up model

photosynthesis and respiration parameters and improving the model transport errors. Top-

down approaches or inversion, on the other hand, utilize the atmospheric CO_2

information and invert back to the surface fluxes through the use of transport model and

mathematical equations.

Here, we tried to improve the bottom-up and top-down estimates of the biosphere

fluxes and atmospheric CO2 concentrations by: (1) investigating effects of boundary

layer schemes on atmospheric carbon dioxide mixing ratios; (2) model parameter

estimation by choosing parameters to minimize the differences between VPRM fluxes

and observed fluxes at Ameriflux towers; (3) model parameter estimation by a generalized Bayesian inversion method and minimization of differences between atmospheric CO_2 concentrations and WRF-VPRM concentrations; and (4) evaluation of model CO_2 concentrations versus measurements.

In (3), we optimized VPRM parameters by utilizing atmosphere carbon dioxide observations from tall towers and the inversion method. The inversion of carbon dioxide biosphere fluxes in the Midwest domain was performed during summer 2008 time period using limited-BFGS technique (Liu et al., 1989). Two NOAA tall towers (WBI and LEF) and five Ring2 towers (established for the Mid Continent Intensive program) were used as observations. An overview of the methodology is illustrated in Figure 2.1.
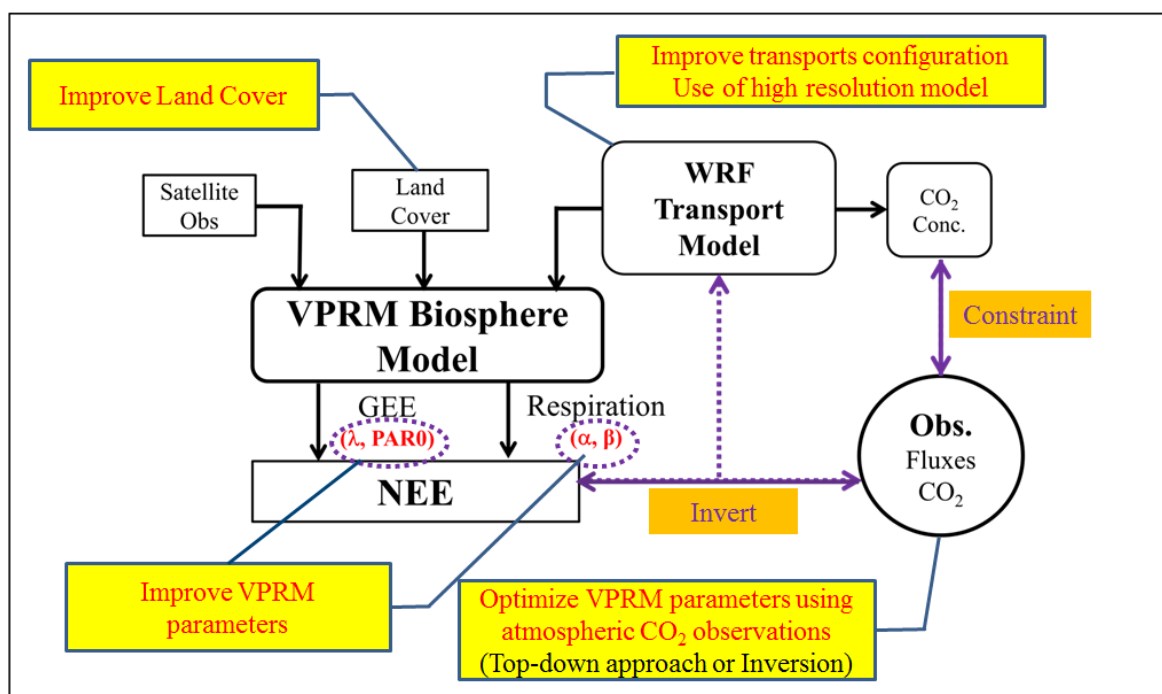
Figure 2.1 Overview of the research methodology

2.2 WRF-VPRM Model Descriptions

The WRF-VPRM model (Ahmadov et al., 2007) is an online coupled model of an atmospheric transport model called Weather Research and Forecasting (WRF) model (Skamarock et al., 2005) and a diagnostic biosphere model called Vegetation Photosynthesis and Respiration Model (VPRM) (Mahadevan et al., 2008). The WRF model is used to estimate meteorological parameters and the carbon dioxide concentrations. It utilizes carbon dioxide emissions (i.e. CO_2 biosphere and anthropogenic fluxes) and returns atmospheric carbon dioxide concentrations. The VPRM model estimates Gross Ecosystem Exchange (GEE), Ecosystem Respiration (R), and Net Ecosystem Exchange (NEE) fluxes based on empirical equations. It utilizes simulated downward shortwave radiation and surface temperature at 2 meter from the WRF model, along with MODIS satellite-derived vegetation indices (Enhanced Vegetation Index (EVI) and Land Surface Water Index (LSWI)) and VPRM photosynthesis and respiration parameters derived from Ameriflux eddy flux towers as inputs. Details of WRF and VPRM models are explained below.

2.3 Weather Research and Forecasting Model (WRF)

Chemistry

The WRF chemistry model version 3.0.1.1 is an air quality model developed at National Center for Atmospheric Research (NCAR) (Skamarock et al., 2005; Grell et al., 2005). The model conserves mass, momentum, dry entropy, and scalars. Examples of configuration options of the WRF chemistry model are as follows:

- o Dry deposition coupled with soil/vegetation scheme;
- o Multiple options for biogenic emissions, anthropogenic emissions, gas-phase chemical mechanisms including RADM2, RACM, CB-4, CBM-Z and Kinetic Pre-Processor (KPP) photolysis schemes, and aerosol schemes;

- o Aerosol indirect effects through interaction with atmospheric radiation, photolysis, and microphysics routines;

- o A tracer transport option; and

- o A subroutine to calculate plume rises to incorporate wildfire emissions.

Transport of CO_2 is treated as a tracer option (only transport without chemical reactions). As a result, the scalar conservation equation is the same as the mass conservation equation. In the scalar conservation equation, 5th order evaluation of horizontal flux divergence (advection) and a 3rd order evaluation of vertical flux coupled with the 3rd order Runge-Kutta time integration scheme are used. A dynamic solver called Advanced Research WRF (ARW) originally referred to as Eulerian mass solver (Skamarock et al., 2008) is used to calculate the transport of the gas. The solver integrates the compressible, non-hydrostatic Euler equations using a terrain-following mass vertical coordinate.

2.4 Vegetation Photosynthesis and Respiration Model
(VPRM) Structure

VPRM is a diagnostic biosphere model developed by Mahadevan et al. (2008). The model was modified from the Vegetation Photosynthesis Model developed by Xiao et al. (2004). It estimates CO_2 biosphere fluxes by incorporating simulated downward shortwave radiation and surface temperature at 2 meter from WRF along with satellite-derived vegetation indices (EVI and LSWI), and derived photosynthesis and respiration parameters from eddy flux towers (Ameriflux networks). The photosynthesis parameters (light use efficiency (λ) and half saturation value of photosynthesis (PAR_0)) and respiration parameters (α and β) are specific for each vegetation type. The model estimates Net Ecosystem Exchange (NEE), Gross Ecosystem Exchange (GEE), and Ecosystem Respiration (R) based on empirical equations as described below.

2.4.1 Net Ecosystem Exchange (NEE)

Net Ecosystem Exchange (NEE) includes the light dependent part (or Gross Ecosystem Exchange, GEE) and the light independent part (or Ecosystem Respiration, R) as shown in equation 2.1.

NEE = - GEE + R   (2.1)

The minus sign in equation 2.1 indicates removal (uptake by the terrestrial biosphere) of carbon dioxide from the atmosphere while the positive sign indicates the release (through respiration) of carbon dioxide to the atmosphere.

2.4.2 Gross Ecosystem Exchange (GEE)

Equations 2.2 to 2.5 (Mahadevan et al., 2008) are used for estimating GEE in the VPRM model.

$$GEE = \lambda \times T_{scale} \; x \; P_{scale} \times W_{scale} \times EVI \times \frac{1}{(1+PAR/PAR_0)} \times PAR \qquad (2.2)$$

$$T_{scale} = \frac{(T-T_{min})(T-T_{max})}{[(T-T_{min})(T-T_{max})-(T-T_{opt})^2]} \qquad (2.3)$$

$$P_{scale} = \frac{1+LSWI}{2} \qquad (2.4)$$

$$W_{scale} = \frac{1+LSWI}{1+LSWI_{max}} \qquad (2.5)$$

Where, PAR_0 is the half-saturation value of plant photosynthesis.

T_{scale} represents the effects of temperature on photosynthesis obtained by equation 2.3 (Raich et al., 1991). T_{min}, T_{max}, and T_{opt} are minimum, maximum and optimal

temperatures for photosynthesis of each vegetation type (Raich et al., 1991; Aber et al., 1992). T_{scale} is assigned to zero when surface temperature is less than the minimum temperature for photosynthesis (Xiao et al., 2004a; Xiao et al., 2004b), which means that photosynthesis activities do not occur when temperature is lower than T_{min} or higher than T_{max}.

Effects of leaf age on photosynthesis of deciduous trees from bud burst to full canopy phase are represented by P_{scale} in equation 2.4 (Xiao et al., 2004a; Xiao et al., 2004b; Boles et al., 2004), where $LSWI_{max}$ is the maximum LSWI at each pixel. EVI helps to indicate phases of plant growth (bud burst, full canopy, or senescence phases) and represents photosynthesis activities. Plant photosynthesis highly correlates with EVI. EVI values range from 0 to 1. The higher the EVI, the more photosynthesis activities occur in a pixel. W_{scale} accounts for the effect of water stress on plant photosynthesis which can be calculated from LSWI as shown in equation 2.5 (Xiao et al., 2004a).

2.4.3 Ecosystem Respiration (R)

Ecosystem Respiration (R) is the light independent part of NEE which can be estimated using equation 2.6. R is temperature dependent. As the temperature increase, the rate of respiration usually increases (Grace et al., 2000; Piovesan et al., 2000). Alpha (α) and Beta (β) are constants specific for a vegetation type and can be derived from CO_2 flux towers. In the VPRM model, respiration from soil microbe and plants both above ground (stem/leaf) and below ground (root) are combined as ecosystem respiration.

$$R = \alpha \times T + \beta \qquad (2.6)$$

2.5 VPRM Input Data

2.5.1 Vegetation Indices

Changes in plant phenology can be observed by tracking the temporal changes of a Vegetation Index, e.g. Normalized Difference Vegetation Index (NDVI) and Enhanced Vegetation Index (EVI). Recent studies show that the MODIS satellite derived EVI correlates better with photosynthesis (Huete et al., 2002; Huete et al., 1997). The LSWI correlates with effects of water stress on plant photosynthesis (Xiao et al., 2004a; Xiao et al., 2004b), therefore, it is used to calculate W_{scale}. Here, the surface reflectance data from the MODIS sensor, onboard the NASA Terra satellite (500 meter spatial resolution 8 days composites MOD09A1, http://modis.gsfc.nasa.gov) are used to calculate the vegetation indices using the VPRM preprocessor program developed by Roberto Kretschmer (http://www.bgc-jena.mpg.de/~rkretsch/vrmpreproc). The MODIS visible red (620–670 nm), near infrared (841–876 nm), visible blue (459–479 nm), and shortwave infrared (1628 – 1652 nm) bands were used in the calculation of the vegetation indices. Healthy green vegetation strongly reflects in the near infrared wavelengths and absorbs visible red and blue for photosynthesis. From equation 2.7, therefore, high values of the EVI correspond to more photosynthesis activity in the pixel. The program first calculates vegetation indices based on land cover grids at 1km resolution using equation 2.7 and 2.8. Then the MODIS MOD09A1 data are re-projected from the original map projection of sinusoidal grid to lat/long coordinates using MODIS Map Projection Tool (https://lpdaac.usgs.gov/lpdaac/tools/modis_reprojection_tool). Aggregation of the re-projected indices to the WRF grid resolution and calculation of minimum and maximum indices at each pixel are processed using the VPRM preprocessor tool.

$$EVI = G \times \frac{(\rho_{nir} - \rho_{red})}{\rho_{nir} + (C_1 \times \rho_{red} - C_2 \times \rho_{blue}) + L} \tag{2.7}$$

$$G = 2.5, C_1 = 6, C_2 = 7.5, L = 1$$

Where, ρ_{nir}, ρ_{red}, ρ_{blue}, and ρ_{swir} are surface reflectance of near infrared, visible red, visible blue and shortwave infrared, respectively.

$$LSWI = \frac{\rho_{nir} - \rho_{swir}}{\rho_{nir} + \rho_{swir}} \tag{2.8}$$

2.5.2 SYNMAP Land Cover Products

The model uses land cover information in estimating the biosphere fluxes. Each land cover type releases/uptakes different amounts of CO_2 depending on VPRM model parameters, plant phenology, water stress, temperature, and radiation. SYNMAP land cover was employed in the studies of effects of transport (Chapter 3). The land cover product was reclassified from 48 land cover classes to 8 VPRM classes in this study. The eight VPRM classes are (1) Trees evergreen, (2) Trees deciduous, (3) Trees mixed, (4)Trees and shrubs, (5) Trees and grasses, (6) Trees and crops, (7) grasses, and (8) Barren, urban and built-up, permanent snow and ice.

SYNMAP was developed based on existing land cover products from NOAA AVHRR, MODIS, and SPOT-VEGETATION satellite sensors (Jung et al., 2006). The land cover products used were: (1) Global Land Cover Characterization Data Base (GLCC) version 2.0 from NOAA AVHRR sensor, 10-day composites with 1-km resolution during the period April 1992 – March 1993 (Loveland et al., 2000); (2) the Global Land Cover 2000 (GLC2000) version 1.0 from SPOT4-VEGETATION sensor, daily product with 1-km resolution during November 1999 and December 2000 (http://wwwvm.jrc.it/glc2000/publications.htm); and (3) TERRA MODIS sensor Level 2 and Level 3, monthly composites with acquisition period January 2001 and December 2001 (Friedl et al., 2002). The three land cover maps were overlaid with geographic (latitude/longitude, Plate Carree) projection with a spatial resolution 30" x 30" (0.008333°). All the maps were clipped to 43,200 column and 17,500 rows which

exclusion of Antarctica (not covered by GLC2000). The disadvantage of using SYNMAP land cover for biosphere flux estimate is that all crops are classified as a single crop type.

2.5.3 Crop Data Layer (CDL) Land Cover Product

The CDL land cover (http://www.nass.usda.gov/research/Cropland/SARS1a.htm) for the year 2008, processed by L. Olsen at Oak Ridge National Laboratory (ORNL), was utilized as a more detailed land cover product to estimate the biosphere fluxes. It has the same projection as SYNMAP with a spatial resolution of 30" x 30" (0.008333^o). Land cover types including crops are classified based on the National Agricultural Statistics Service (NASS) Crop Data Layer. Corn and soybean which are the major crops in the Midwest were also separated. The CDL land cover product was used in VPRM parameter optimization, in assessing the effects of separating corn and soybean, and in data assimilation studies (Chapter 4 to chapter 7). The 55 CDL vegetation types were reclassified to 12 VPRM classes, which include (1) Trees evergreen, (2) Trees deciduous, (3) Trees mixed, (4) Trees and shrubs, (5) Tree and grasses, (6) C3 crops, (7) Soybean, (8) C4 Crop, (9) Corn, (10) Mixed C3/C4 crops, (11) Grasses, and (12) Barren, urban and built-up, permanent snow and ice.

2.5.4 VPRM Parameter

VPRM photosynthesis parameters, λ (μmol CO_2/μmol PPFD) and PAR_0 (μmol PPFD m^{-2} s^{-1}), and respiration parameters, α (μmol CO_2 m^{-2} s^{-1}/^oC) and β (μmol CO_2 m^{-2} s^{-1}), indicate the rates of photosynthesis and respiration of each vegetation type. Lambda is maximum light use efficiency which is affected by water (W_{scale}), temperature (T_{scale}), and plant phenology (P_{scale}). The numbers vary depending on vegetation types, densities, regions, etc. PAR_0 is a half-saturation for photosynthesis which represents the relationship between solar irradiance and photosynthesis. Alpha and Beta are constants of VPRM zero-order respiration equation. The four VPRM parameters for each vegetation type can be derived from tower flux data.

2.6 VULCAN CO_2 Anthropogenic Emission

In this research, the VULCAN CO_2 fossil fuel emission provides anthropogenic CO_2 for the model. VULCAN is a high spatial resolution (10km x 10km and 0.1 x 0.1 degree) and high temporal resolution (hourly) US fossil fuel CO_2 emission inventory of the year 2002 developed by Gurney et al. (2009). It is derived from the local/regional air pollution monitoring combined with census, traffic, and digital road data sets. It consists of CO_2 emission from industrial, commercial, residential, on-road, non-road, utility, and aircraft sectors. The point, non-point, and airport data files come from the Environmental Protection Agency's (EPA) National Emissions Inventory (NEI) for the year 2002. Global Aero2K aircraft CO_2 emissions inventory $1° \times 1°$ degree grid was used for aircraft emission beyond take-off/landing. The on-road mobile emissions are based on a combination of county-level data, from the National Mobile Inventory Model (NMIM) County Database (NCD), and standard internal combustion engine stoichiometry. The non-road emissions are also from NMIM NCD.

2.7 Setup and Run WRF-VPRM

The model domain in the effects of transport studies (Chapter 3) was over the State of Iowa with 4 km spatial resolution (100 x 150 grid cells) and 41 vertical layers up to 100 mb. In Chapter 3, we used SYNMAP land cover with only one crop type. The simulation period was June to August 2008. In the later chapters, a bigger model domain was studied to include more observations. We simulated the CO_2 biosphere fluxes and atmospheric concentrations over the Midwest with 4 km spatial resolution (280 x 300 grid cells) and 41 vertical layers up to 100 mb.

The transport model requires meteorological data for simulating shortwave downward radiation and surface temperature. Here, North American Regional Reanalysis (NARR) meteorological data, 30km x 30km resolution were used. Vegetation indices (EVI/LSWI) were calculated from MODIS surface reflectance using VPRM preprocessor

program. Prior VPRM parameters were derived from Ameriflux data for each vegetation type (provided by Christoph Gerbig). Initial and boundary conditions for total CO_2 were interpolated from Carbon Tracker, 3-hourly data, 1x1 degree resolution. VULCAN, hourly data for year 2002, 0.1 x 0.1 degree resolution CO_2 fossil fuel emission were incorporated into the WRF transport to generate CO_2 concentration contributed by fossil fuel emissions. The simulated shortwave radiation and surface temperature were input to VPRM along with VPRM parameters and vegetation indices to calculate NEE fluxes which are the sum of GEE (negative) and ecosystem respiration (positive) fluxes. The generated biosphere fluxes and VULCAN CO_2 anthropogenic fluxes were added to transport routines to generate total CO_2 concentration, and CO_2 concentrations contributed by biosphere fluxes and fossil fuel emissions. The schematic diagram of WRF-VPRM model is illustrated in Figure 2.2.

For Chapter 4 to Chapter 7, the CDL land cover with multi-crop classifications along with optimized VPRM parameters were used to drive biosphere flux estimates over the Midwest at 4 km resolution. We simulated CO_2 fluxes and concentrations summer 2008. The anthropogenic emission and initial and boundary conditions were the same as used in the transport studies for consistency.

2.8 CO_2 Observations

2.8.1 NOAA Tall Towers

Data from two NOAA/GMD tall towers located at West Branch, Iowa (WBI tower) and at Park Fall, Wisconsin (LEF tower) were used for model evaluation. The tall towers were established as part of North American Carbon Program (NACP) to provide high temporal continuous measurement of CO and CO_2 concentration and flask sampling of other atmospheric trace gases. Air samplings were taken at 30m, 99m, and 379m at WBI and 11 m, 30 m, 76 m, 122 m, 244 m, and 396 m at WLEF. Locations of the two tall towers are shown in Table 2.1.

2.8.2 Ring2 Towers

Five Ring2 tall towers (Table 2.1) were established as part of the Mid Continent Intensive (MCI) Campaign (http://www.nacarbon.org/nacp/mci_about.htm) to provide high-accuracy CO_2 measurements for top-down data assimilation studies of carbon fluxes in the Midwest, USA. CO_2 were collected continuously at two tower levels (30m and 110-140m above ground) from April 2007 to October 2009. The data are available at http://www.ring2.psu.edu/.

2.8.3 Ameriflux Data

Ameriflux networks provide a long-term continuous record of exchange of carbon fluxes and surface energy balance components from various vegetation types using eddy covariance technique. Ameriflux NEE fluxes, PAR, and temperature were utilized in this research for VPRM parameter optimization purpose as well as model evaluations. Ameriflux data can be obtained at http://ameriflux.ornl.gov/.

2.9 Carbon Tracker

NOAA's carbon dioxide data assimilation system, Carbon Tracker (Peters et al., 2007), provides assimilated 1x1 degree carbon dioxide biosphere fluxes and mixing ratios which were used as initial and boundary conditions for the WRF-VPRM model. CT uses the Ensemble Kalman filter technique for assimilation tool TM5 model as the transport model. Carbon Tracker utilized the Carnegie-Ames Stanford Approach (CASA) to estimate a priori biosphere fluxes. Observed atmospheric carbon dioxide concentrations from NOAA tall tower network informed the assimilation.
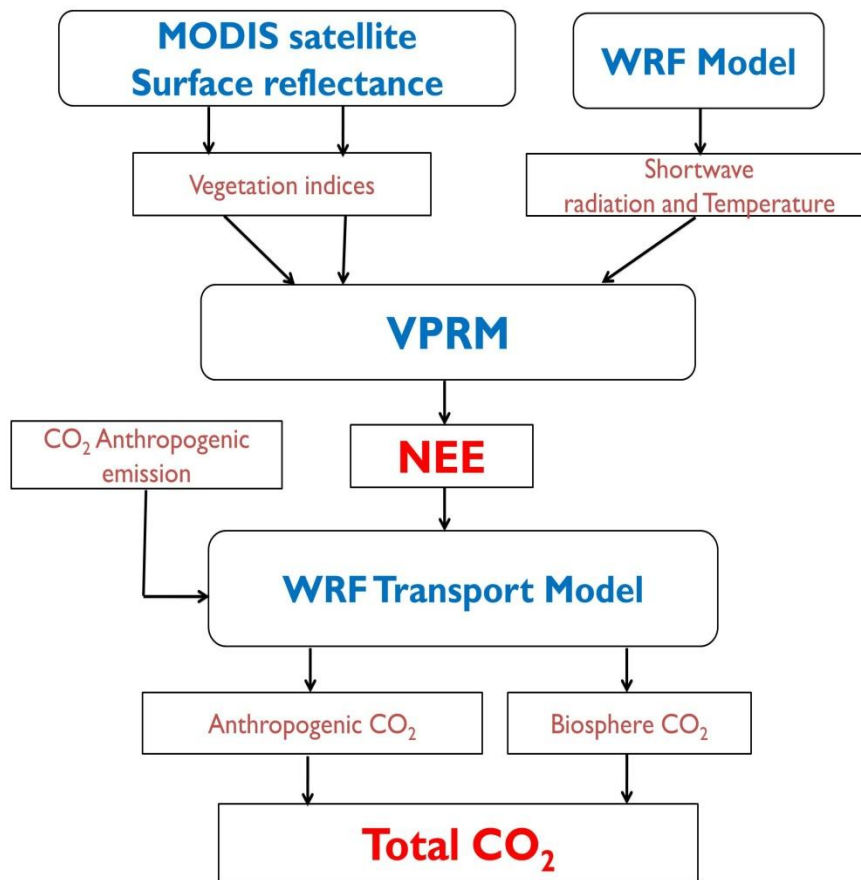
Figure 2.2 Schematic diagram of WRF-VPRM model.

Table 2.1 Locations of CO_2 tall towers used in the study.

Tall towers	State	Latitude	Longitude	Sampling height (m agl)
NOAA tall towers				
WBI	Iowa	38.2650 °N	91.3530 °W	31, 99, 379
WLEF	Wisconsin	45.9451 °N	90.2732 °W	11, 30, 76, 122, 244, 396
Ring2 towers				
Kewanee	Illinois	41.2762 °N	89.9724 °W	30, 140
Centerville	Iowa	40.7919 °N	92.8775 °W	30, 110
Mead	Nebraska	41.1386 °N	96.4559 °W	30, 120
Round Lake	Minnesota	43.5263 °N	95.4137 °W	30, 110
Galesville	Wisconsin	44.0910 °N	91.3382 °W	30, 140

CHAPTER 3 INFLUENCE OF METEOROLOGICAL TRANSPORT

CONFIGURATIONS ON WRF-VPRM CO_2 SIMULATIONS

3.1 Introduction

Despite the previous studies by Denning et al. (2003), Nicholls et al. (2004), Ahmadov et al. (2007), and Ahmadov et al. (2009), mesoscale modeling of CO_2 in the boundary layer remains challenging. The regional studies (Ahmadov et al., 2007; Ahmadov et al., 2009) for CO_2 simulation in France during the CarboEurope Regional Experiment Strategy (CERES) campaign during 16 May - 15 June , 2005 using the WRF-VPRM model showed that the model could capture the observed diurnal variability quite well. However, it failed to resolve high concentrations of CO_2 during early morning (underestimated by about 10 ppm) when respired CO_2 is retained in the nocturnal boundary layer. Ahmadov et al. 2007 indicated that WRF-VPRM model-observation discrepancies are caused by WRF model inaccuracies.

PBL scheme parameterizations in WRF play an important role in the transport of mass, moisture, and energy and in turn, the prediction of tracer concentrations. The PBL parameterization controls the impact of subgrid-scale turbulent motions on grid scale variables. The two PBL schemes in WRF-VPRM version 3.0.1.1 which can be used for CO_2 simulation are the Mellor-Yamada-Janjic (MYJ) scheme (Janjic et al., 1990) and the Yonsei University (YSU) scheme (Hong et al., 2006; Hong et al., 2010). The MYJ scheme (one-and-a-half order TKE closure) is a local mixing scheme, where the turbulent fluxes are estimated from the mean atmospheric variables and/or their gradients at that point, from the lowest to the highest vertical level. In other words, the vertical mixing is confined to adjacent grid cells. It estimates the eddy diffusion coefficient using calculated turbulent kinetic energy (TKE). However, turbulent fluxes are dominated by large eddies (long distance transport) in convective conditions, conditions when a local scheme is least valid. YSU is considered a non-local mixing scheme where mass can be transferred

from any layer directly to any other layer in the entire model column. In stable boundary conditions, YSU applies an enhanced vertical diffusion (Hong et al., 2010) which is based on the bulk Richardson number between the surface layer and the top of the boundary layer.

In this chapter, we compared the effects of MYJ and YSU PBL schemes on transport CO_2 by comparing observed CO_2 from WBI tall tower and the simulated concentrations. We also studied effects of vertical layers on CO_2 simulation. Two numbers of vertical layers were chosen i.e., 31 layers and 41 layers. The results of the PBL studies and vertical layer studies are shown in sections 3.3 and 3.4, respectively.

3.2 Methodology

3.2.1 Model Configuration

The estimates of CO_2 concentrations and fluxes are highly dependent on the quality of the metrological prediction. Here, MYJ and YSU planetary boundary layer schemes in WRF-VPRM model were evaluated during July 2008. Effects of vertical layers on WRF-VPRM were also investigated. We simulated CO_2 fluxes and concentrations over the model domain using 4 km horizontal resolution with different model configurations i.e. using MYJ PBL schemes, using YSU PBL schemes, using 31 vertical layers and using 41 vertical layers. Meteorological surface observations in the domain were used in evaluations of simulated meteorological variables (wind speed, wind direction, temperature, and humidity). CO_2 observations from WBI tall tower were used for comparison. The model domain for the PBL sensitivity study and vertical layer study is the State of Iowa. SYNMAP land cover was utilized as the model input as well as VULCAN anthropogenic CO_2 emissions. Carbon Tracker was utilized as initial and boundary conditions. The details for setting up and running WRF-VPRM can be found in Chapter 2 (section 2.7). The other model configurations for the simulations are listed in Table 3.1.

Table 3.1 WRF-VPRM model configurations for the effects of PBL schemes and vertical
layer studies.

Features	Options
Domain description	The State of Iowa, 150x100 grid cells 4km resolution, 41 vertical layers.
Meteorological data	North American Regional Reanalysis (NARR), 3-hourly, 32 km resolution
Microphysics	WSM 5-class scheme
Longwave Radiation	Rapid Radiative Transfer Model (RRTM)
Shortwave Radiation	Dudhai scheme
Cumulus option	Kain-Fritsch (new Eta) scheme
Surface layer option	Monin-Obukhov (Janjic Eta) scheme
Land surface option	unified Noah land-surface model
Effects of PBL schemes	1) YonSei University (YSU) 2) Mellor –Yamada-Janjic (Eta) TKE scheme (MYJ)
Effects of vertical layers	31 vertical layers 41 vertical layers

3.2.2 Evaluation using METSTAT

The meteorological variables predicted for July 2008 were evaluated using the

METSTAT program (developed by ENVIRON group, www.environcorp.com). It

compares the WRF model output with surface observation data and provides statistical

evaluation for wind speed and wind direction, temperature, and humidity. The

observation data used for comparison were the ds472.0 surface observational data set

published by NCAR. The model values were compared against observations in the State

of Iowa domain (~56 sites). The statistics used for comparison are mean value, gross

error, average bias, root mean square error (RMSE, equation 3.1) and Index of

Agreement (IOA, equation 3.2) (Willmont et al., 1981).

$$RMSE = \left[\frac{1}{IJ}\Sigma_{j=1}^{J}\Sigma_{i=1}^{I}\left(P_j^i - O_j^i\right)^2\right]^{1/2} \tag{3.1}$$

Index of Agreement using the approach of Willmont et al. (1981). The higher the

IOA the better correlation of model results with observation.

$$IOA = 1 - \left[\frac{IJ \cdot RMSE^2}{\Sigma_{j=1}^{J}\Sigma_{i=1}^{I}\left(\left|P_j^i - M_o\right| + \left|O_j^i - M_o\right|\right)^2}\right] \tag{3.2}$$

We also used the statistical benchmarks proposed by Emery et al. (2001) to

identify the number of days (July 1st – July 30th, 2008) in each simulation that do not

satisfy the benchmarks. The statistical benchmarks used for bias, root mean square error

(RMSE) and index of agreement (IOA) are listed in Table 3.2.

Table 3.2 Statistical Benchmarks (Emery et al., 2001).

Variables	Statistical Benchmarks
Wind speed	RMSE ≤ 2 m/s Bias $\leq \pm 0.5$ m/s IOA ≥ 0.6
Wind direction	Gross Error ≤ 30 degree Bias $\leq \pm 10$ degree
Temperature	Gross Error ≤ 30 degree Bias $\leq \pm 10$ degree IOA ≥ 0.8
Humidity	Gross Error ≤ 2 g/kg Bias $\leq \pm 1$ g/kg IOA ≥ 0.6

<u>3.3 Effects of PBL Schemes on CO$_2$ Simulations</u>

3.3.1 Wind Speed and Wind Direction

Figure 3.1 and 3.2 show time series and diurnal plots of hourly 10-m wind speed averaged over all sites in the domain. During daytime (0800 to 1600 CST), YSU yielded better results than the MYJ scheme. At nighttime, MYJ which use local mixing achieved higher correlation with observations compared to YSU, which often overestimated wind speed at night.
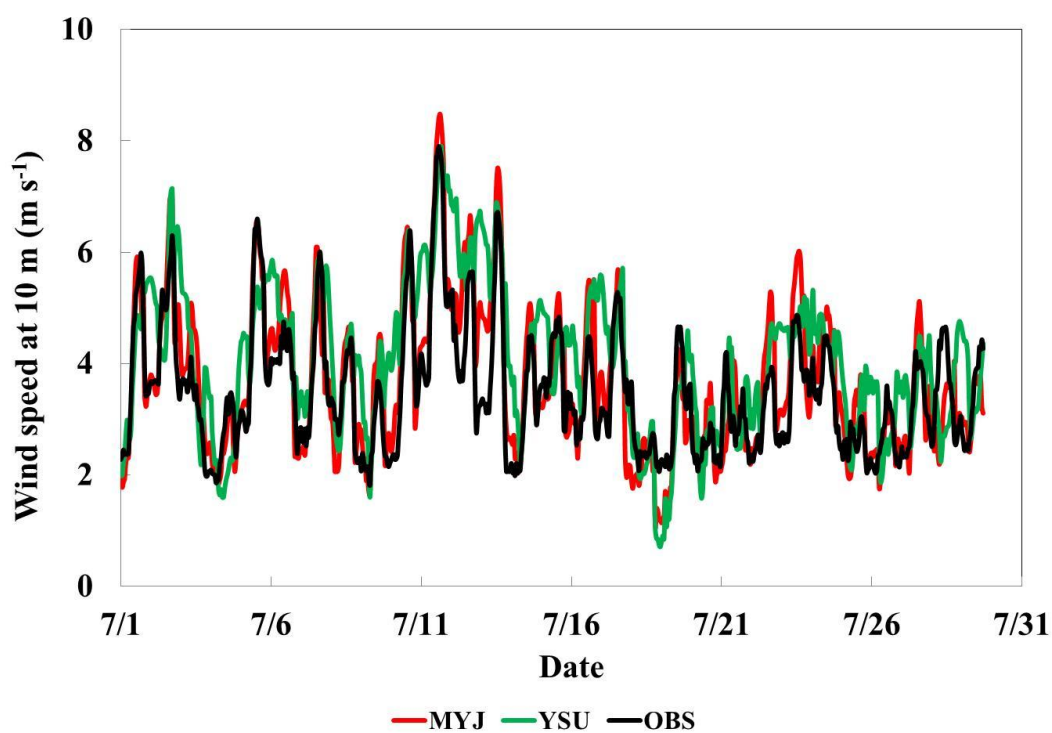
Figure 3.1 Hourly wind speed of meteorological observation sites over the Iowa domains in July 2008
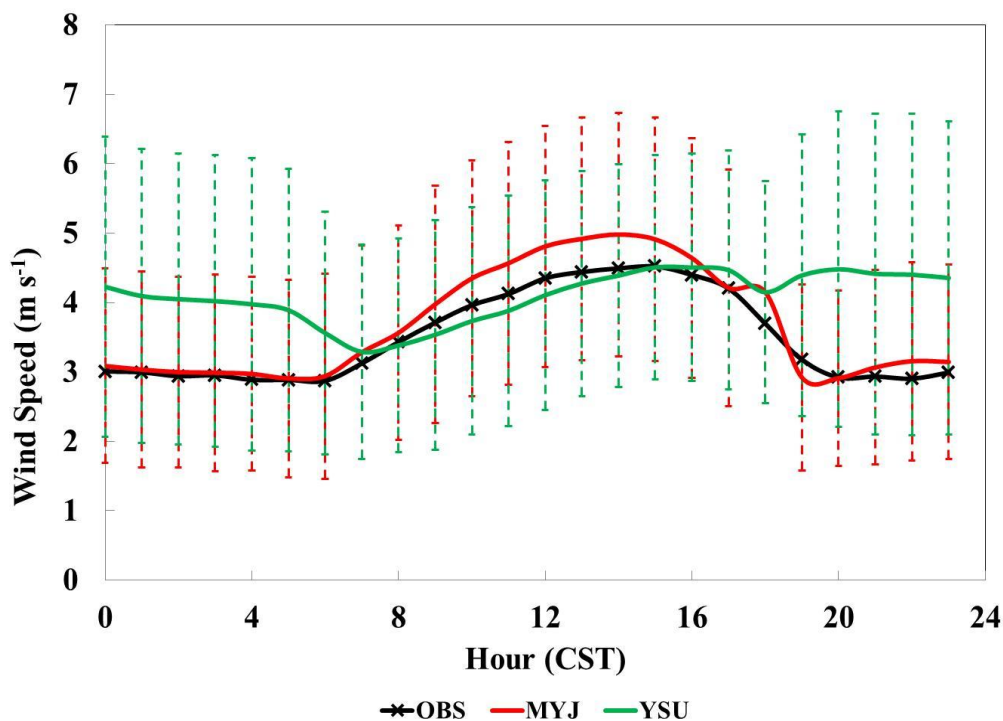
Figure 3.2 Diurnal variation of wind speed (error bars show average RMSE of all sites at each hour from July 1st to July 28th 2008)

Table 3.3 shows the monthly averages of model mean, RMSE, and IOA of wind speed, temperature, and humidity compared to meteorological surface observational sites over the State of Iowa in July 2008. YSU scheme shows higher average daily wind speed bias and RMSE (lower IOA) than the MYJ scheme. YSU has the highest number of days that do not meet the wind speed and wind direction benchmarks (Table 3.4). MYJ showed better performance than YSU in predicting wind speed and wind direction. However, both PBL schemes overestimated wind speed during most days.

3.3.2 Temperature

For prediction of temperature, both PBL schemes followed the diurnal variations of observations quite well. Both MYJ and YSU tend to predict warmer surface values

compared to observations during daytime with the highest warm bias using YSU. MYJ follows observations the best during daytime. MYJ underestimated nighttime temperatures (Table 3.3 and Table 3.4), while YSU followed the nighttime temperatures quite well. For the daily average values, YSU overestimated temperatures in most days. MYJ had about the same numbers of days of overestimation/underestimation.

Shin and Hong (2011) compared five PBL schemes during the CASES-99 field campaign from 1200 UTC 23 October to 1200 UTC 24 October 1999 in Leon, Kansas, USA. They reported that YSU produced warmer daytime surface temperatures by approximately 3.5 K and 1 K, respectively, while MYJ and BouLac (local schemes) nearly followed the observations. For T2, the closet to the observations was YSU. The largest daytime temperature gradient was observed in the YSU scheme. The authors suggested that although none of the PBL schemes yielded satisfactory results in stable conditions, local TKE closure schemes showed better performance. However, Hu et al. (2010) reported that the YSU scheme had less bias than the MYJ scheme (during July-September 2005 in Southeast Texas). The three-month mean 2-m temperatures showed that YSU estimated higher afternoon and nighttime temperatures than the MYJ scheme. The differences in vertical mixing strength and entrainment of air from above the PBL are the main differences between the schemes.

3.3.3 Humidity

Both MYJ and YSU schemes over predict daytime humidity; MYJ had more overprediction than YSU (Figure 3.5 and Figure 3.6). For nighttime humidity, both schemes follow the observations better than during daytime. MYJ has the higher numbers of days that did not follow the statistical benchmarks than YSU (Table 3.4).

3.3.4 Comparison of PBL Heights at WBI Tower

Figure 3.7 shows the time-series of PBL heights from model simulations and from observations. The observed values are derived from potential temperature and relative

humidity profiles from the balloon launches (constructed by Ken Davis group at Penn State University) at the tower. The PBL heights derived from CO_2 concentrations, using the times when the CO_2 concentrations at the bottom two layers were well mixed (i.e. had the same concentrations) and the times that all three layers were well mixed, are also shown.

During daytime, MYJ estimates the lowest PBL heights. YSU is a non-local scheme which predicts higher PBL heights than MYJ (local scheme) due to its stronger mixing strength (Hu et al., 2010). The times of well-mixed CO_2 concentrations suggest that the nighttime PBL heights at the tower are lower than 100 m since CO_2 at the bottom two layers are quite different. The boundary layer heights (well-mixed conditions) usually reach 100 m and 379 m around 8 am and 10 am, respectively. MYJ tends to estimate very low nighttime boundary layer heights (sometime reaching zero). YSU often gives higher nighttime PBL heights since it applies enhanced vertical diffusion (Hong et al., 2010) for stable conditions, unlike MYJ which applies a local closure method.

Table 3.3 Monthly averages of Mean, RMSE and IOA of MYJ and YSU PBL schemes in July 2008

PBL Schemes	Wind Speed			Temperature			Humidity		
	Mean	RMSE	IOA	Mean	RMSE	IOA	Mean	RMSE	IOA
Obs	3.54	-	1	23.2	-	1	13.3	-	1
MYJ	3.73	1.61	0.66	23.1	2.42	0.91	14.7	2.52	0.68
YSU	4.12	1.92	0.55	23.9	2.43	0.91	14.1	2.15	0.71

Table 3.4 Numbers of days not follow the statistical benchmarks in Emery et al., 2001.

PBL Schemes	Wind Speed			Wind Direction		Temperature			Humidity		
	RMSE	Bias	IOA	Gross Error	Bias	Gross Error	Bias	IOA	Gross Error	Bias	IOA
MYJ	4	8	9	16	3	9	20	0	14	20	7
YSU	11	17	23	19	13	8	23	1	2	11	5
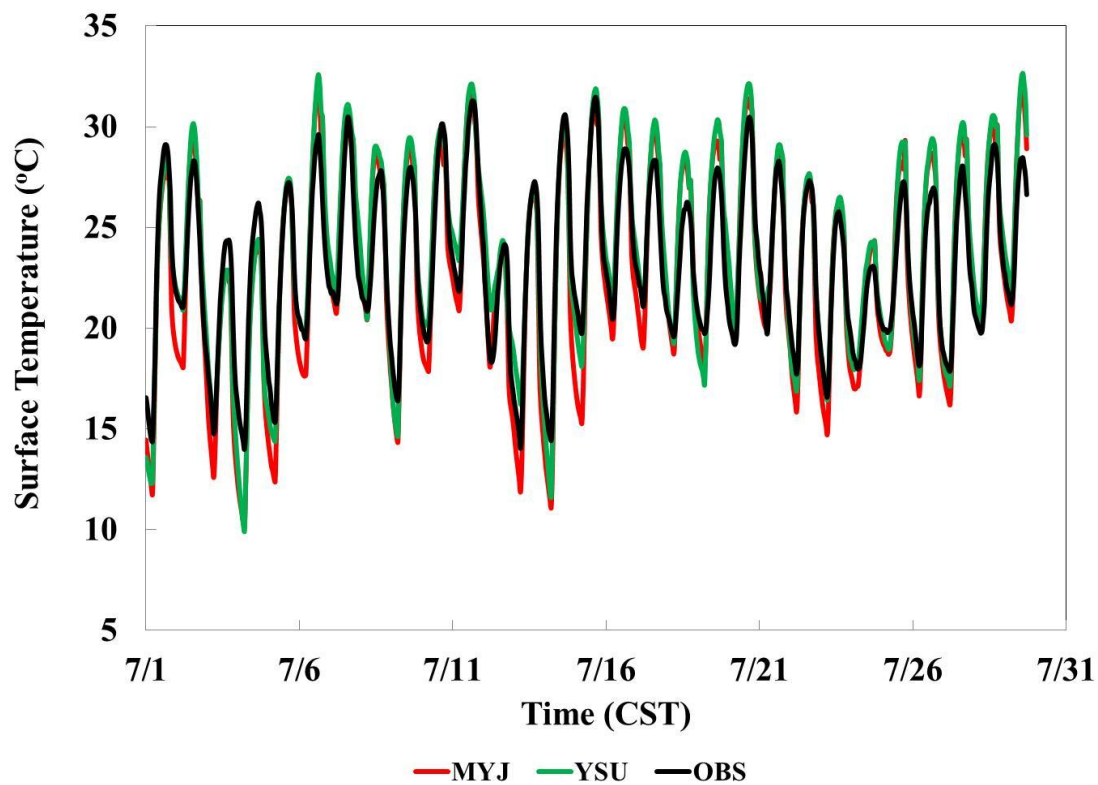
Figure 3.3 Hourly temperature of meteorological observation sites over the Iowa domains in July 2008
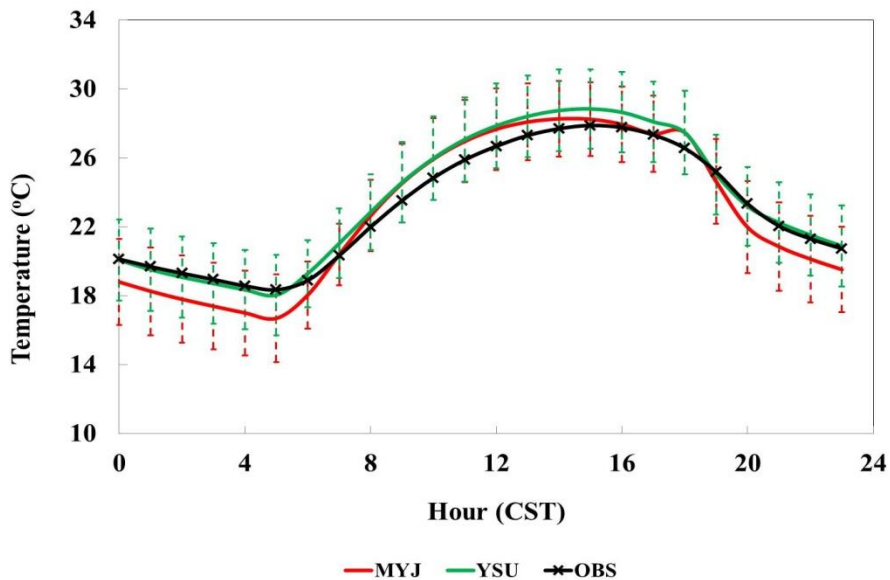
Figure 3.4 Diurnal variation of temperature (Error bars show average RMSE of all sites at each hour from July 1st to July 28th 2008)
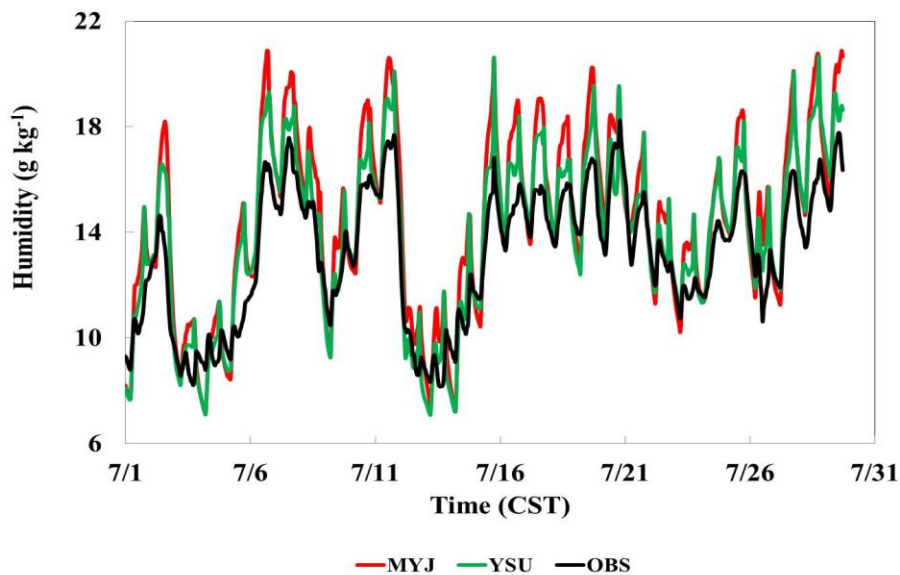
Figure 3.5 Hourly humidity of meteorological observation sites over the Iowa domains in July 2008
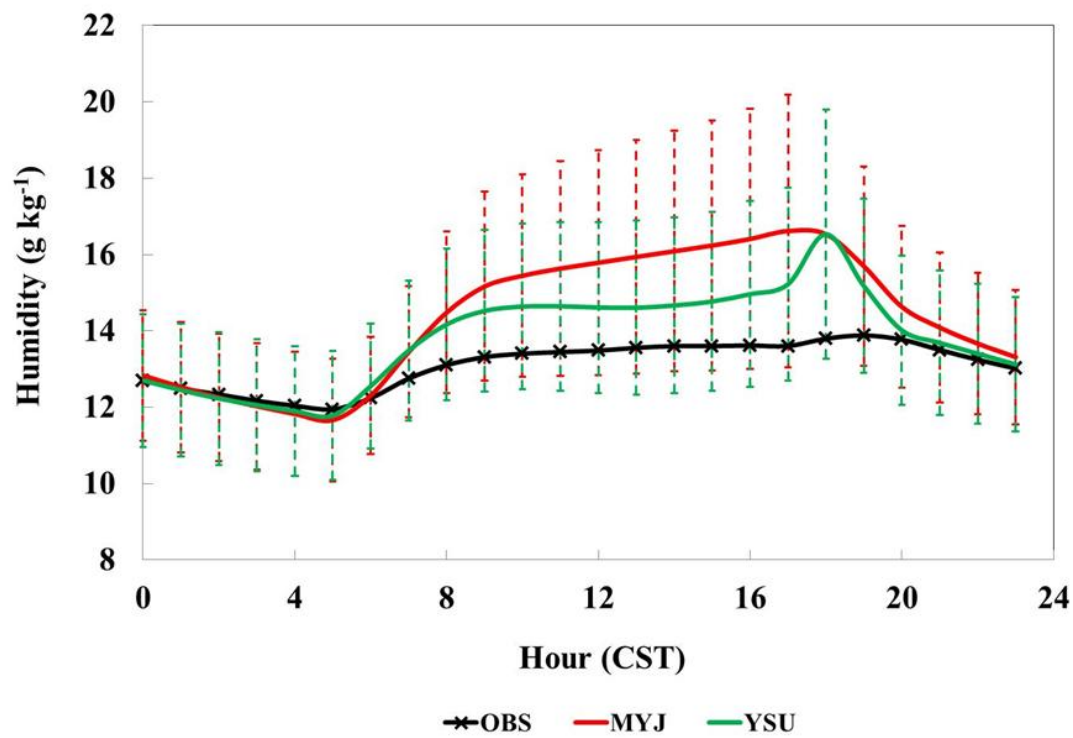
Figure 3.6 Diurnal variation of humidity (Error bars show average RMSE of all sites at each hour from July 1st to July 28th 2008)
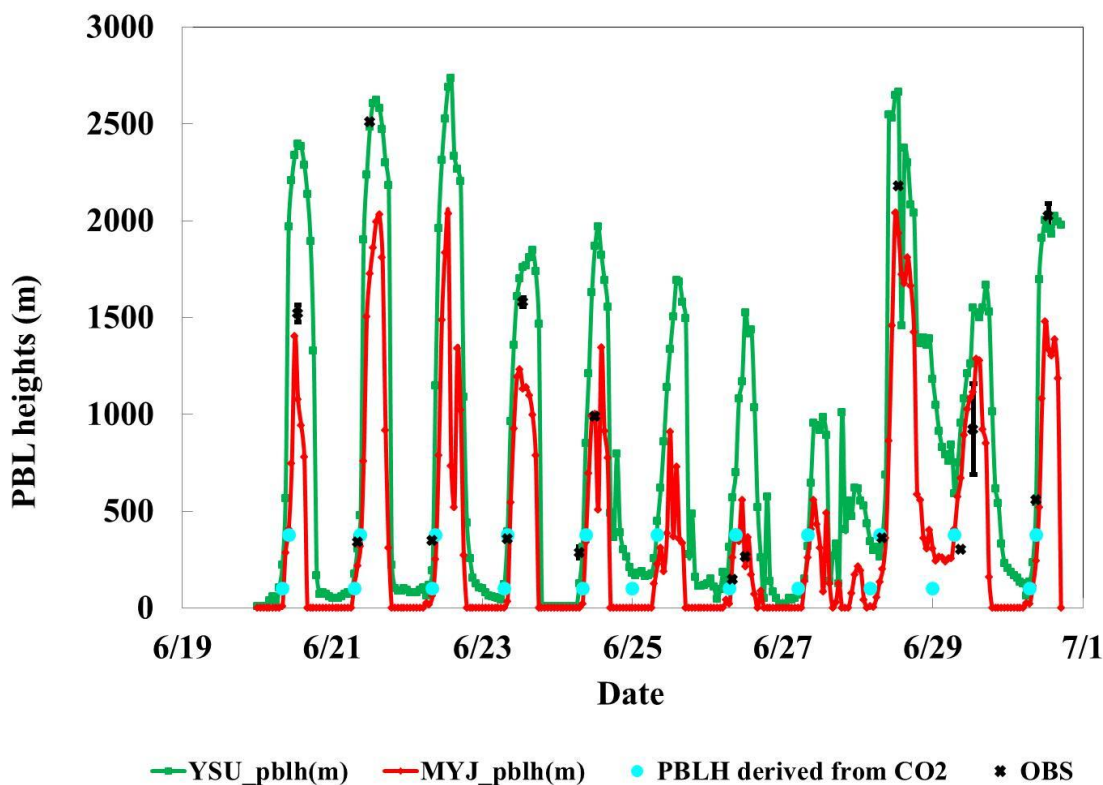
Figure 3.7 Time-series plots of PBL height at WBI tower from June 20th to July 1st 2008

3.3.5 Comparison Simulated CO_2 Concentrations with WBI
Tall Tower Observations

Figure 3.8 to Figure 3.10 show the comparison of CO_2 concentrations and Figure 3.11 to Figure 3.13 show diurnal variations using MYJ and YSU together with observations from the WBI tower at 30m, 99m, and 379m above ground. Peak CO_2 concentrations are observed in the early morning when the PBL height is low and the air becomes stable which prevents the plants' respired CO_2 from mixing with the air above the boundary layer. The lowest CO_2 concentrations are observed in the afternoon when the highest photosynthesis rate occurs and the PBL heights are the highest. During daytime, both PBL schemes can capture the drawdown due to plant uptake quite well

since the boundary layer heights are usually higher than the tower. At night, both schemes sometime underestimate total CO_2 concentrations at 30 m. The under prediction suggests that the PBL may be too high or the calculated respiration fluxes may be too low. YSU in general estimates lower CO_2 concentrations at night than MYJ due to higher PBL heights.

Figure 3.14 shows CO_2 monthly average RMSE (July 2008) at the tower levels. YSU shows better performance than MYJ for both daytime and nighttime, especially at 30 m and 99 m tower levels. The errors become smaller at the higher levels and the average RMSE of both nighttime and daytime reach about 6.5 ppm for all levels at the highest tower level (379 m). Hypothesis for this is that the CO_2 concentrations at the highest level are mainly influenced by the boundary condition and not by the surface fluxes.
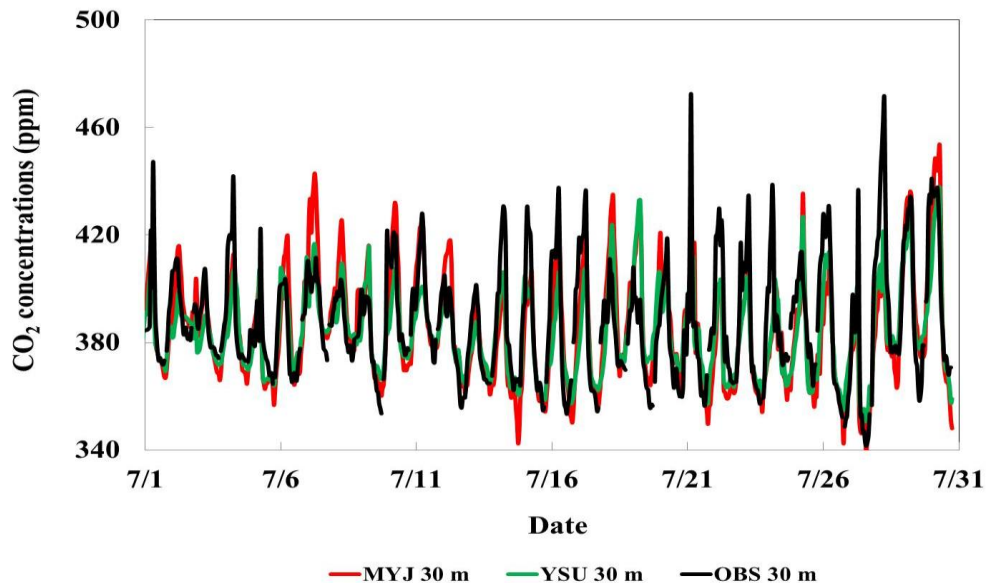
Figure 3.8 CO_2 concentrations using MYJ and YSU PBL schemes at WBI tower at 30m in July 2008
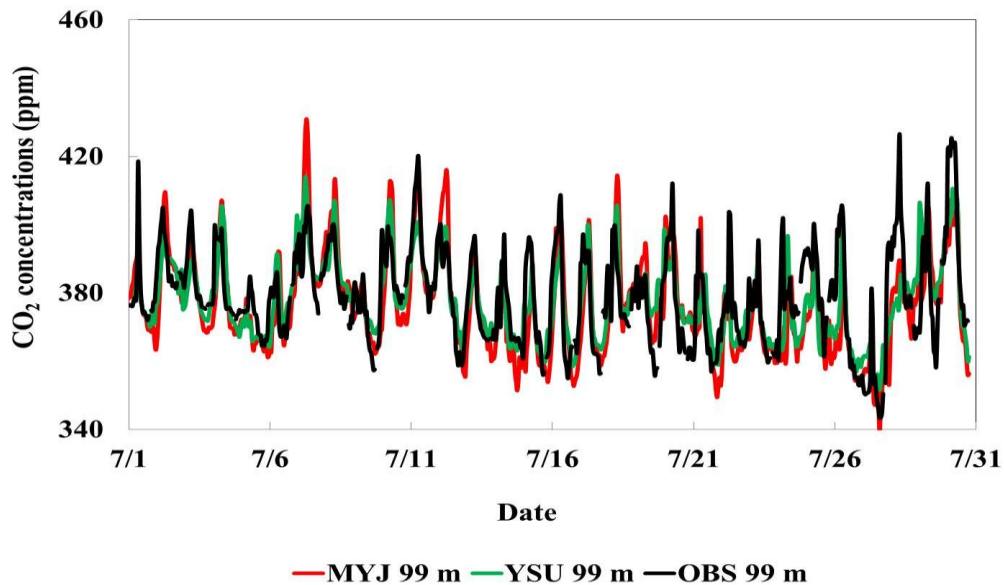
Figure 3.9 CO_2 concentrations using MYJ and YSU PBL schemes at WBI tower at 99 m
in July 2008
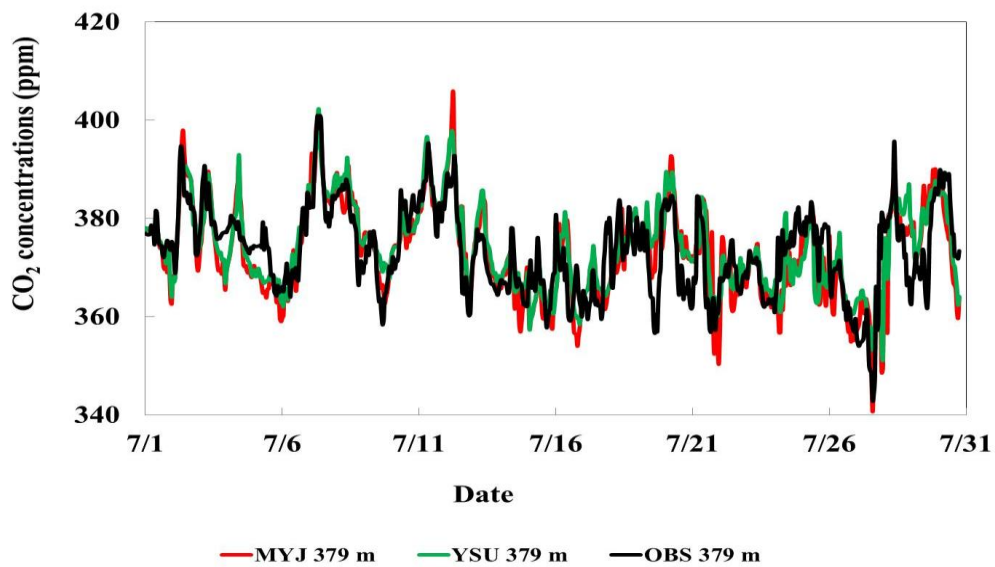
Figure 3.10 CO_2 concentrations using MYJ and YSU PBL schemes at WBI tower at 379
m in July 2008

Figure 3.11 Mean CO_2 diurnal variation using MYJ and YSU PBL schemes at WBI tower in July 2008 at 30 m
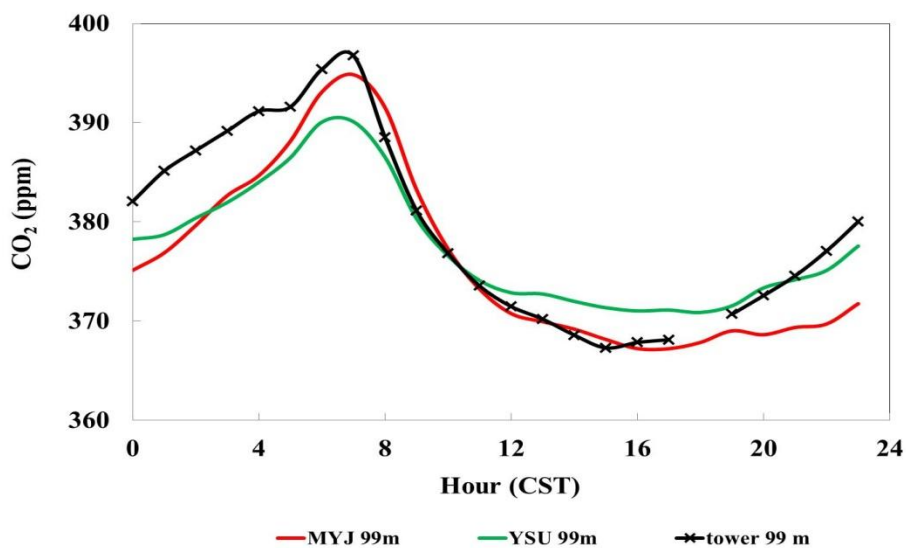
Figure 3.12 Mean CO_2 diurnal variation using MYJ and YSU PBL schemes at WBI tower in July 2008 at 99 m

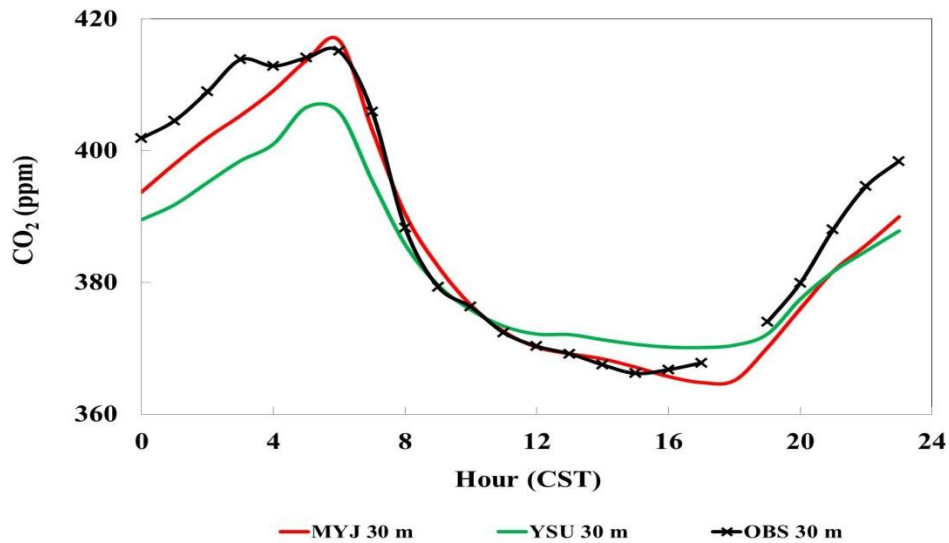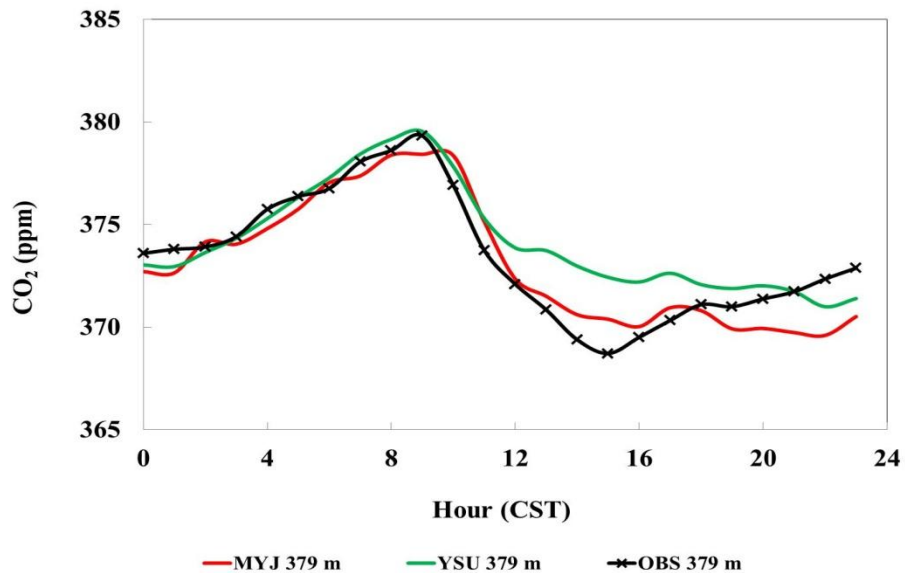Figure 3.13 Mean CO_2 diurnal variation using MYJ and YSU PBL schemes at WBI
tower in July 2008 at 379 m
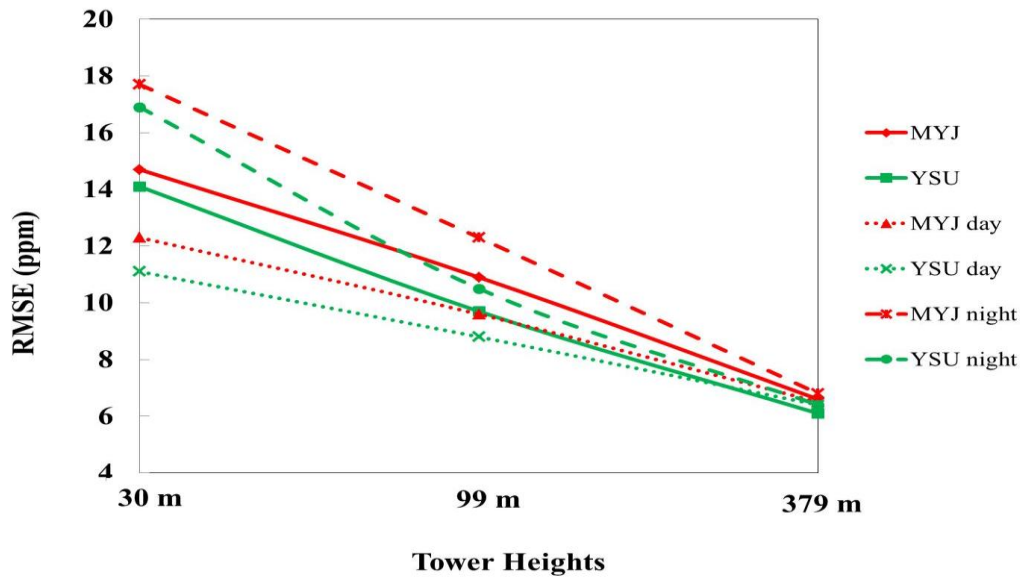
Figure 3.14 RMSE of CO_2 concentration at WBI tower using MYJ and YSU PBL
schemes

3.4 Effects of Vertical Resolution

We compared CO_2 simulations using two different numbers of vertical layers: 31 layers (with 9 layers below 1.5 km) and 41 layers (with 18 layers below 1.5 km) up to 100 mb (~16 km). The heights at the center of the lowest grids were 28 m and 8 m for the 31 and 41 vertical layers, respectively. Figure 3.15 shows CO_2 concentration plots of observations at WBI (at 30m above ground sampling) in July 2008 against the model results using 31 and 41 layer simulations. The results of both cases are comparable in most days. The results of 41 vertical layer simulation show slight improvement at the 30m level (Figure 3.16 and Table 3.5) with lower RMSE (14.2 ppm) and higher IOA (0.85) compared to using 31 vertical layers (RMSE 15.3 ppm and IOA 0.82). The differences of the 41 and 31 vertical layers were less significant at the 99m and 379m levels. Statistical analysis of the CO_2 concentrations was performed for both daytime (from 10am-5pm CST) and nighttime (from 10pm – 5am CST). The RMSE at 30m and 99m levels were higher at night. At the 379m level, CO_2 concentrations are less influenced by the photosynthesis and respiration fluxes and boundary layer transport compared to the lower levels, which results in lower RMSE and higher IOA at the 379m level. The average daytime and nighttime RMSE at the 379m level were close (~6.4 ppm for 41 vertical layers and 6.3 ppm for 31 vertical layers). This suggests that the biases from the boundary conditions and/or regional transport of anthropogenic emissions contributed 1/3 to 1/2 of the bias. This finding is in agreement with the PBL heights which showed the RMSE of approximately 6.5 ppm at the highest tower level (379 m).

Predictions of T2 from both 31 and 41 vertical layer simulations are close, with mean absolute differences less than 0.5 ^{o}C. As a result, comparable values of respiration are predicted (mean absolute difference of 0.13 μmol m^{-2} s^{-1}). The 41 layer simulation sometime predicts lower shortwave radiation compared to using 31 layers which causes lower values of GEE in some days. The 41 layer setting generally gives slightly lower nighttime PBL heights but higher midday values.
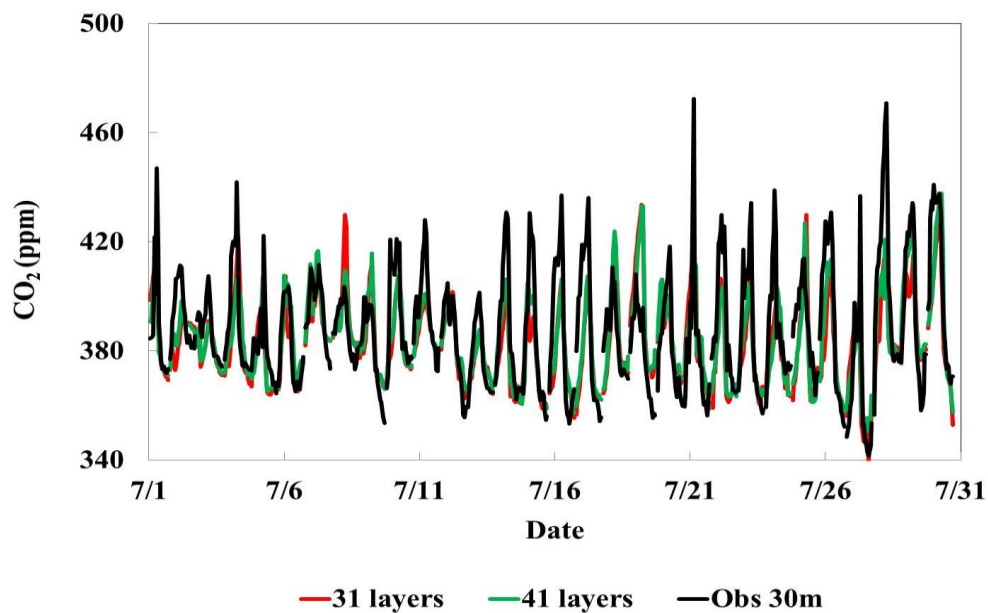
Figure 3.15 Timeseries of CO_2 at WBI (at 30m) in July 2008 with 31 and 41 vertical layers
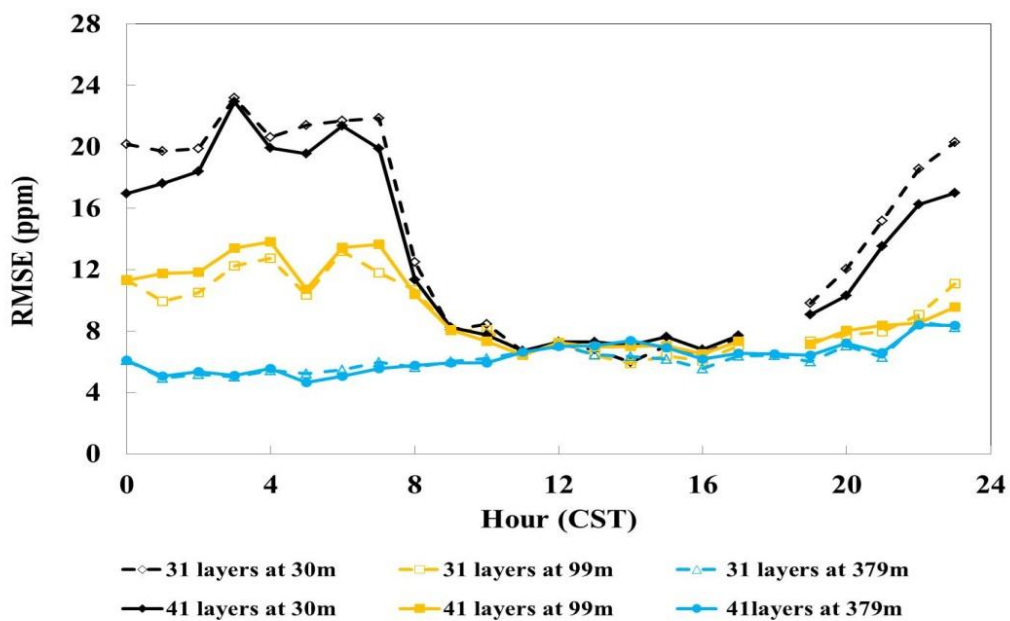
Figure 3.16 Hourly RMSE of CO_2 at WBI in July 2008 with 31 and 41 vertical layers

Table 3.5 Statistical analysis of CO_2 at WBI in July 2008 with 31 and 41 vertical layers

	30m		99m		379m	
	31 layers	41 layers	31 layers	41 layers	31 layers	41 layers
RMSE	15.5	14.2	9.3	9.7	6.3	6.4
Daytime RMSE (10am – 5pm)	7.1	7.3	6.7	7.0	6.4	6.7
Nighttime RMSE (10pm – 5am)	20.5	18.7	11.0	11.5	6.2	6.2
IOA	0.82	0.85	0.86	0.84	0.87	0.86
Daytime IOA	0.84	0.83	0.85	0.83	0.86	0.83
Nighttime IOA	0.57	0.63	0.79	0.78	0.86	0.86
Bias error	-5.03	-3.70	-1.09	-1.13	0.56	0.93
Gross error	11.36	10.42	7.18	7.29	4.87	4.89

Figure 3.17 shows monthly average vertical profiles of CO_2 with 31 and 41 vertical layers at WBI at 5 am, 10 am, and 5pm in July 2008 from surface layer up to 2 km. The CO_2 vertical profiles above 2 km were quite close when using 31 versus 41 vertical layers. During daytime and late afternoon (10 am and 5pm), the vertical profiles concentrations when using 31 and 41 vertical layers were less than 0.5 ppm different even below 500 m. However, in the early morning (5 am), CO_2 concentrations at the first layer of the 41 vertical layer simulation were much higher (~ 15 ppm difference) than the 31 layer one because of the lower height from the ground, ~8 m compared to 28 m. The 8 meter level has higher effects from nighttime respiration and emissions.
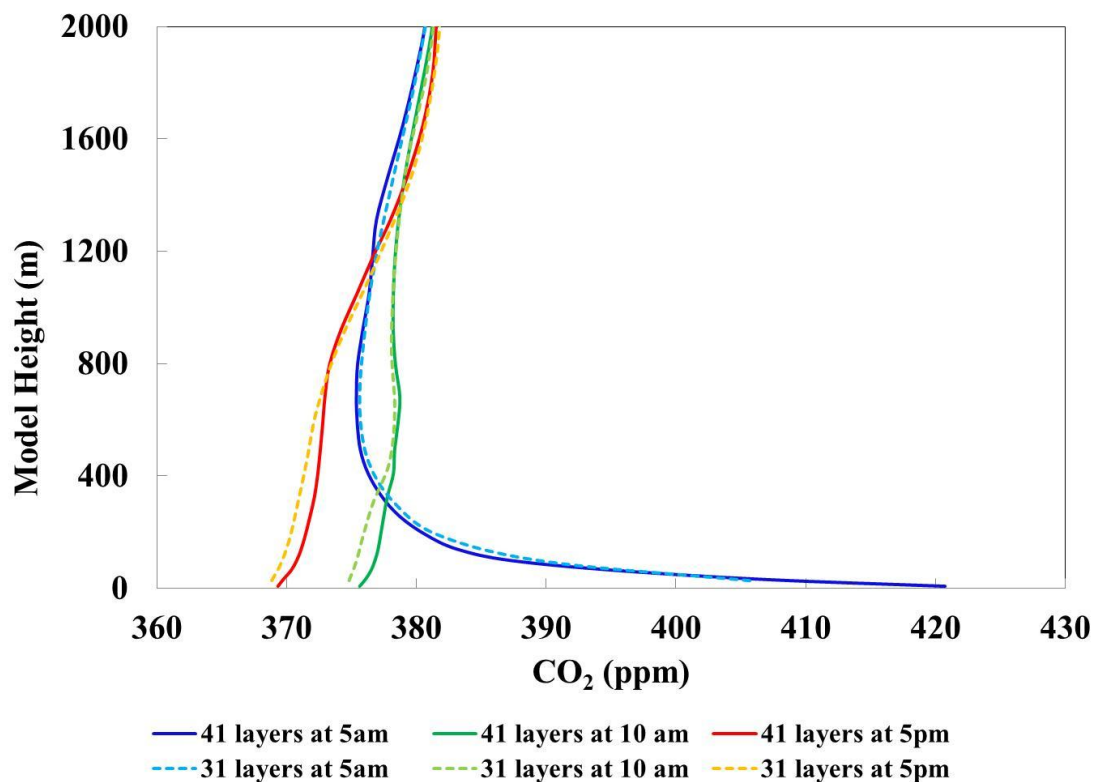
Figure 3.17 CO_2 monthly average vertical profiles at WBI in July 2008

3.5 Effect of Horizontal Resolution

The high horizontal resolution (4 km x 4 km) WRF-VPRM produces flux maps at much higher resolution than Carbon Tracker (120 km resolution). The spatial variation of the average NEE fluxes from WRF-VPRM and Carbon Tracker for June, July and August 2008 are illustrated in Figure 3.18 (a) to (f). The VPRM average net NEE fluxes over the State of Iowa in June, July, and August 2008 are -0.7, -5.8, and -6.3 $\mu mol/m^2$, respectively, while the Carbon Tracker estimates are -1.2, -4.9, and -3.9 $\mu mol/m^2$, respectively. The differences of the monthly average net fluxes were significant, 71%, 18%, and 62% in June, July, and August, respective.

With the higher horizontal resolution, the WRF-VPRM better discriminates between vegetation types and their corresponding fluxes. For instance, two nearby flux towers (Brook Field site 10 and 11) located in Ames, Iowa show different CO_2 fluxes when estimated by WRF-VPRM (Figure 3.19 (a) and (b)) but not by Carbon Tracker. The high nighttime respiration fluxes of Carbon Tracker (Figure 3.19 (c)) also contributed to overestimations of carbon dioxide mixing ratios as seen in Figure 3.19 (d).

3.6 Conclusions

Based on METSTAT evaluation of wind speed, temperature, and humidity for all surface observation sites in the domain, MYJ showed better results in predicting of wind speed and wind direction than YSU, while YSU yielded better results in predicting humidity. Both schemes showed comparable results for surface temperature with high IOA. YSU shows better performance in predicting CO_2 concentrations in both daytime and nighttime than MYJ at all tower levels. The CO_2 errors of both schemes became smaller at the higher levels and all level CO_2 RMSE became smallest (~6.5 ppm) at the highest tower level for both nighttime and daytime. This may suggest that some biases in CO_2 concentrations may come from the boundary conditions or background, and not by the surface fluxes.

As expected, increased numbers of vertical layer played larger impact during nighttime and early morning especially at the 30 m tower level. The effects were insignificant at 99 m and 379 m.

WRF-VPRM with higher horizontal resolution could capture more details of the biosphere flux estimates. The differences of the monthly average net fluxes between WRF-VPRM and Carbon Tracker were significant. The high nighttime respiration fluxes of Carbon Tracker also contributed to overestimations of carbon dioxide mixing ratios at WBI tower.

(a) Average VPRM NEE in June 2008

(- 0.7 μmol/m^{2}s)

(b) Average CT NEE in June 2008

(- 1.2 μmol/m^{2}s)

(c) Average VPRM NEE of July 2008

(-5.8 μmol/m^{2}s)

(d) Average CT NEE of July 2008

(-4.9 μmol/m^{2}s)

(e) Average VPRM NEE of August 2008

(-6.3 μmol/m^{2}s)

(f) Average CT NEE of August 2008

(-3.9 μmol/m^{2}s)
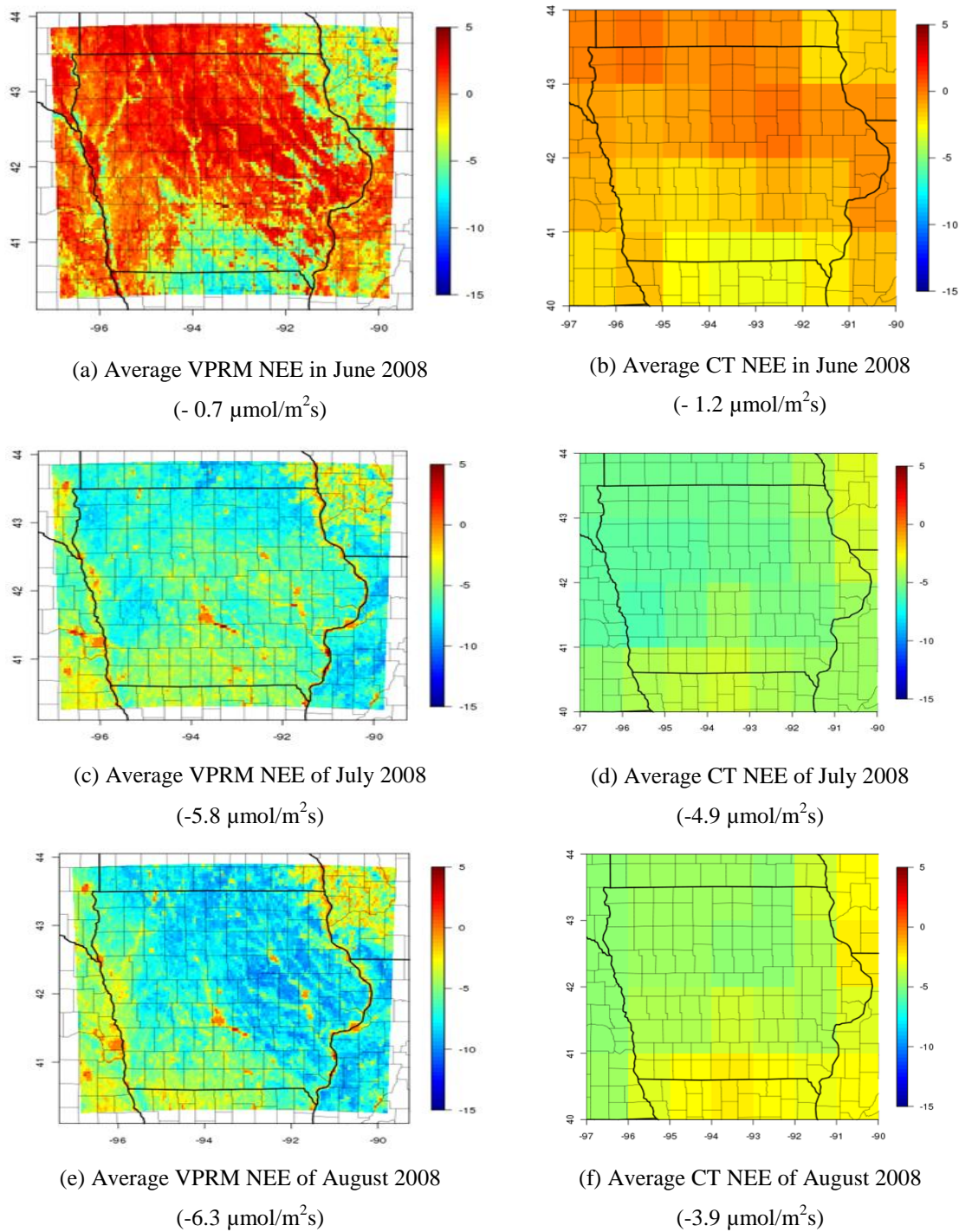
Figure 3.18 Monthly average biosphere CO_2 fluxes of WRF-VPRM and Carbon Tracker
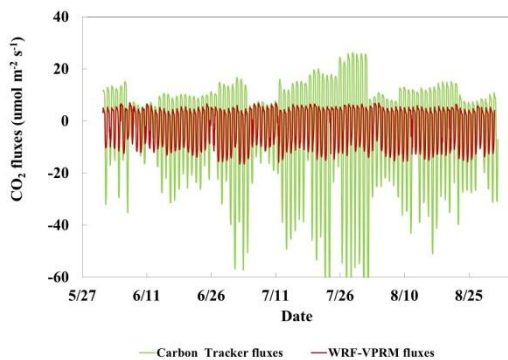
(a) CO$_2$ fluxes at Brook Field site 10, Ames, Iowa
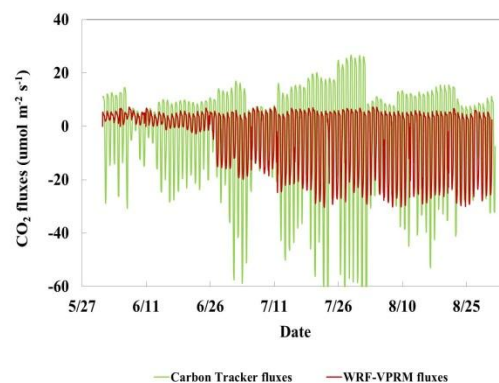
(June-August, 2008)

(b) CO$_2$ fluxes at Brook Field site 10, Ames, Iowa

(June-August, 2008)
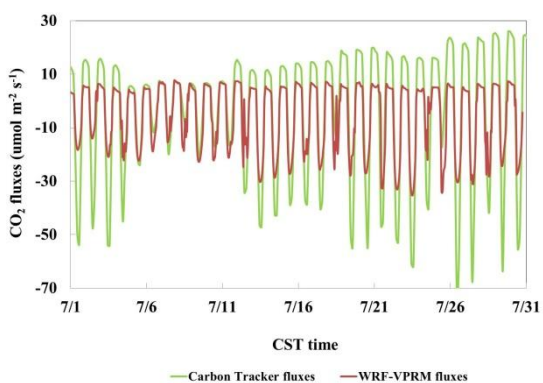
(c) CO$_2$ fluxes at West Branch Iowa
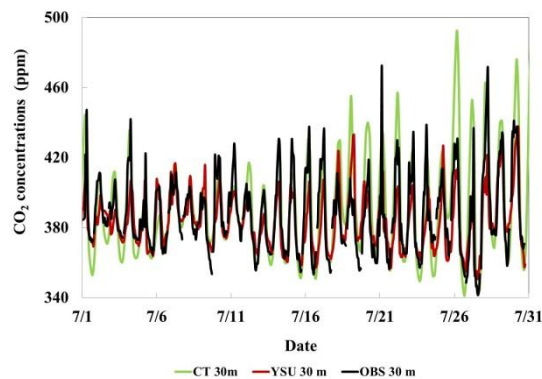
(July, 2008)

(d) CO$_2$ concentrations at West Branch Iowa

(July, 2008)

Figure 3.19 WRF-VPRM and Carbon Tracker CO$_2$ fluxes and mixing ratios at Brook Field site 10, Brook Field site 10, and WBI in summer 2008

CHAPTER 4 VPRM PARAMETER OPTIMIZATION AGAINST

AMERIFLUX CO_2 FLUX TOWERS (BOTTOM-UP APPROACH)

4.1 Introduction

Since the biosphere is quite diverse, challenges of bottom-up model estimates in general include low temporal and spatial resolutions which lead to aggregation error, quality of land cover products and limitation of biosphere model parameters which lead to representation errors. This chapter focuses on improving the bottom-up model estimates of CO_2 biosphere fluxes by optimizing VPRM parameters for corn and soybean separately. The VPRM biosphere model estimates Net Ecosystem Exchange (NEE), photosynthesis (GEE), and respiration (R) based on meteorology, vegetation indices, and biophysical properties of plants.

$$NEE = -GEE + R \tag{4.1}$$

$$GEE = \lambda \times T_{scale} \, x \, P_{scale} \times W_{scale} \times EVI \times \frac{1}{(1 + PAR/PAR_0)} \times PAR \tag{4.2}$$

$$R = \alpha \times T + \beta \tag{4.3}$$

VPRM parameters, light use efficiency (λ), PAR_0, α and β in GEE and Respiration equations can be derived from eddy flux towers. λ, PAR0, α, and β vary depending on vegetation types, regions, time period, photosynthesis pathways (e.g. C3 and C4 plants), etc. Corn which is a C4 plant has a higher CO_2 uptake compared to a C3 plants like soybean due to a more efficient photosynthesis pathway. Prueger et al. (2004) reported that seasonal uptake of corn (~490 g/m^2 to over 650 g/m^2) was nearly twice that of soybean (~200 g/m^2 to 300 g/m^2). The study also showed that the peak CO2 concentration over corn (around 3 am 16 July 2002 CST) was significantly higher than

soybean, ~515 ppm versus ~475 ppm. This suggests that using a single set the model parameters for all crops can lead to significant errors in the biosphere flux estimates.

To my knowledge, only one article has published VPRM parameter values. Mahadevan et. al. (2008) optimized VPRM parameters for corn and soybean (λ, PAR0, α, and β) using Ameriflux data in USA and Canada during the years 2000 to 2004. However, the optimization was not specific to growing season time period. We anticipate that the model can better capture the growing season uptake and emitted CO_2 peaks through optimizing VPRM parameters for specific regions and time periods, e.g., during the growing season of 2008 and month by month during the growing season in the Midwest region. Figure 4.1 shows the domain of VPRM parameters optimization in the Midwest. The optimization program requires observed PAR, temperature, and NEE from the Ameriflux sites (shown in green squares) as well as vegetation indices data from MODIS.

4.2 Ameriflux Data used in the Optimization

The Ameriflux network provides a long-term continuous record of exchange of carbon fluxes and surface energy balance components from various vegetation types include tundra, grassland, agricultural crops, tropical forests and temperate coniferous and deciduous forests. The raw data are collected by Ameriflux site measurement teams. Then, the data are submitted to the Carbon Dioxide Information Analysis Center (CDIAC) for further processing. Level 2 Ameriflux data are the products that were checked and formatted by CDIAC. There are eight Ameriflux sites with Level 2 data in the study area in 2008 (Table 4.1), two sites each for corn, soybean, deciduous, and grassland. Seven of them were used in the optimization since one of the grassland sites, Brooking site, had inadequate amount of data during the time of this study.

The Ameriflux data used in the optimization included air temperature (^{o}C) measured just above the canopy, PAR (*u*mol PPFD m^{-2} s^{-1}) the incoming

photosynthetically active radiation (i.e., radiation in the 0.4 to 0.7 micrometer waveband)
measured above the canopy, and NEE which includes subcanopy CO_2 storage (includes
the entire column from the ground to the height of the eddy covariance system). FC
($u$mol m^{-2} s^{-1}), the rate of vertical transfer of CO_2 (not corrected for storage or advection)
as calculated from measurements above the canopy, was utilized when NEE was not
available. The data gap filling was done by CDIAC as described in Falge et al., 2002. We
utilized gap filled data in the optimization if available. NEE data were further filtered
using u* (friction velocity) before feeding to the optimization routine as described below.
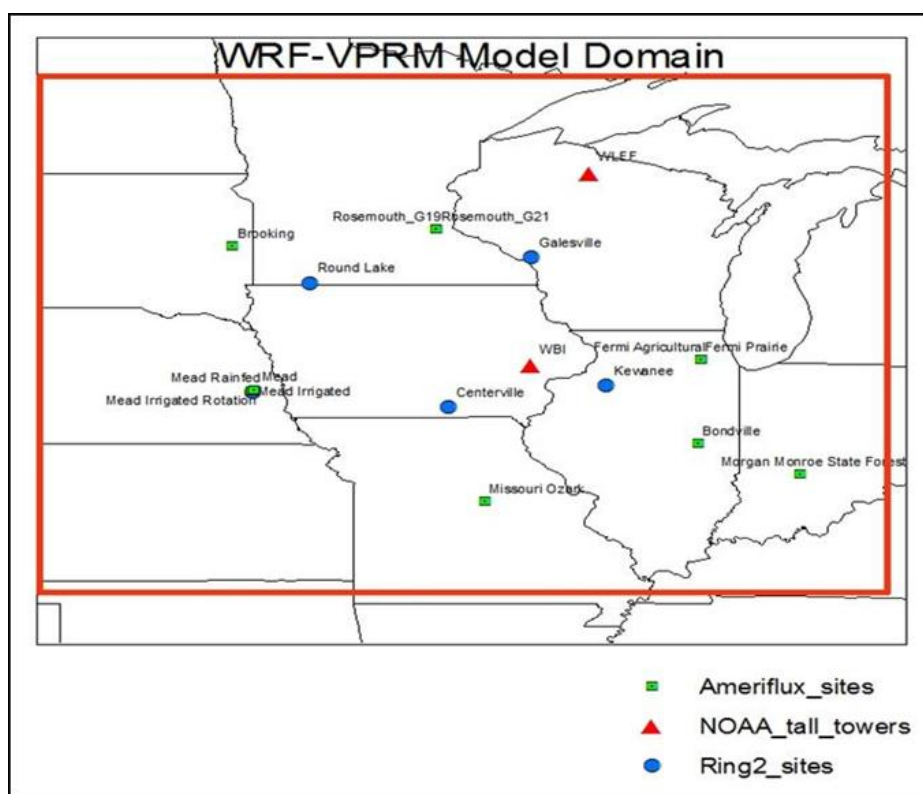
Figure 4.1 The model domain of VPRM parameters optimization in the Midwest using
Ameriflux tower data.

Table 4.1 Ameriflux sites (with Level 2 data in 2008) used for VPRM parameters optimization

Sites	States	site ID	longitude	latitude	Veg. types	Tower Height (m)	Canopy Height (m)	Data types
1. Fermi Agricultural	IL	USIB1	-88.2227	41.8593	corn	4.05	na	30-min (gap filled)
2. Fermi Prairie	IL	USIB2	-88.2410	41.8406	grass	3.76	na	30-min (gap filled)
3. Brooking	SD	USBkg	-96.8362	44.3453	grass	4	0.2-0.4	30-min w/ gap
4. Mead Irrigated	NE	USNe1	-96.4766	41.1651	corn	6	2.9	1-hr (gap filled)
5. Mead Irrigated Rotation	NE	USNe2	-96.4701	41.1649	soybean	6	1.8	1-hr (gap filled)
6. Mead Rainfed	NE	USNe3	-96.4396	41.1797	soybean	6	na	1-hr (gap filled)
7. Missouri Ozark	MO	USMOz	-92.2000	38.7441	deciduous	30	24.2	30-min (with gap)
8. Morgan Monroe State Forest	IN	USMMS	-86.4131	39.3232	deciduous	48	27	1-hr (gap filled)

4.3 Methodology

4.3.1 Reclassifying Land Cover Map

In the previous chapter, SYNMAP was utilized as land cover data for the VPRM model. SYNMAP land cover product has high spatial resolution at 1 km. However, it did not discriminate between different types of crops including corn and soybean, which are the major vegetation types in the Midwest. Corn and soybean have significantly different rates of carbon dioxide uptake and respiration due to their different photosynthesis pathways. Therefore, separating corn and soybean is expected to yield better estimates of CO_2 biosphere fluxes which in turn should improve CO_2 concentration predictions. Thus, in this chapter, we utilized the Crop Data Layer (CDL) land cover product for the year 2008 (processed by L. Olsen at Oak Ridge National Laboratory). The vegetation types of CDL land cover were classified based on the National Agricultural Statistics Service (NASS) Crop Data Layer, which also separated corn from soybean areas. To incorporate

this land cover into the VPRM model, we reclassified 55 vegetation types of CDL product to 12 VPRM vegetation types as follows (1) Trees evergreen, (2) Trees deciduous, (3) Trees mixed, (4) Trees and shrubs, (5) Tree and grasses, (6) C3 crops, (7) Soybean, (8) C4 Crop, (9) Corn, (10) Mixed C3/C4 crops, (11) Grasses, and (12) Barren, urban and built-up, permanent snow and ice.

The comparison of 8 VPRM classifications SYNMAP land cover with single crop and the 12 VPRM classifications CDL land cover with multi-crops is shown in Figure 4.2 and Figure 4.3, respectively. SYNMAP shows more crop areas compared to CDL land cover product (58.1% vs 34.8%), while CDL shows higher deciduous (20.8% vs 7.9%) and grassland (26.6% vs 15.6%) areas.
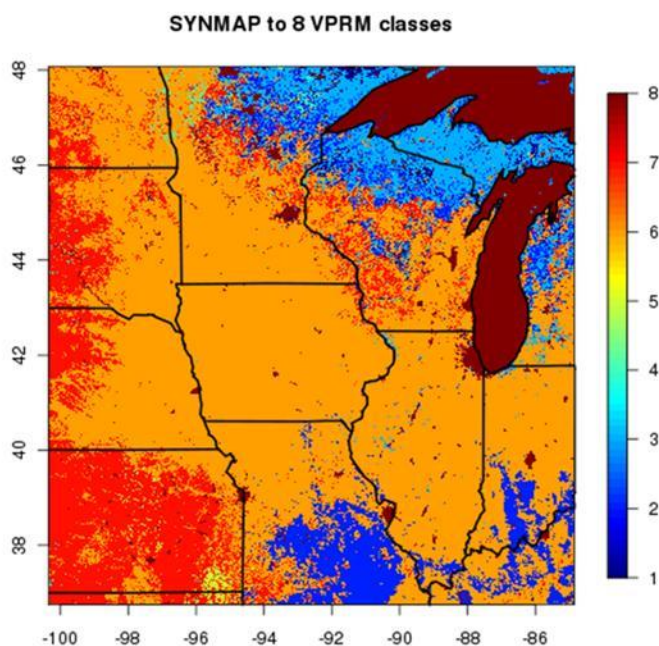
Figure 4.2 SYNMAP land cover classified to 8 VPRM classes: 1. Trees evergreen, 2. Trees deciduous (dark blue ~7.9%), 3. Trees mixed (light blue ~6.5%), 4. Trees and shrubs, 5. Tree and grasses, 6. Crops (orange ~58.1%), 7. Grasses (red ~15.6%), and 8 Barren, urban and built-up, permanent snow and ice (dark brown ~10.1%).

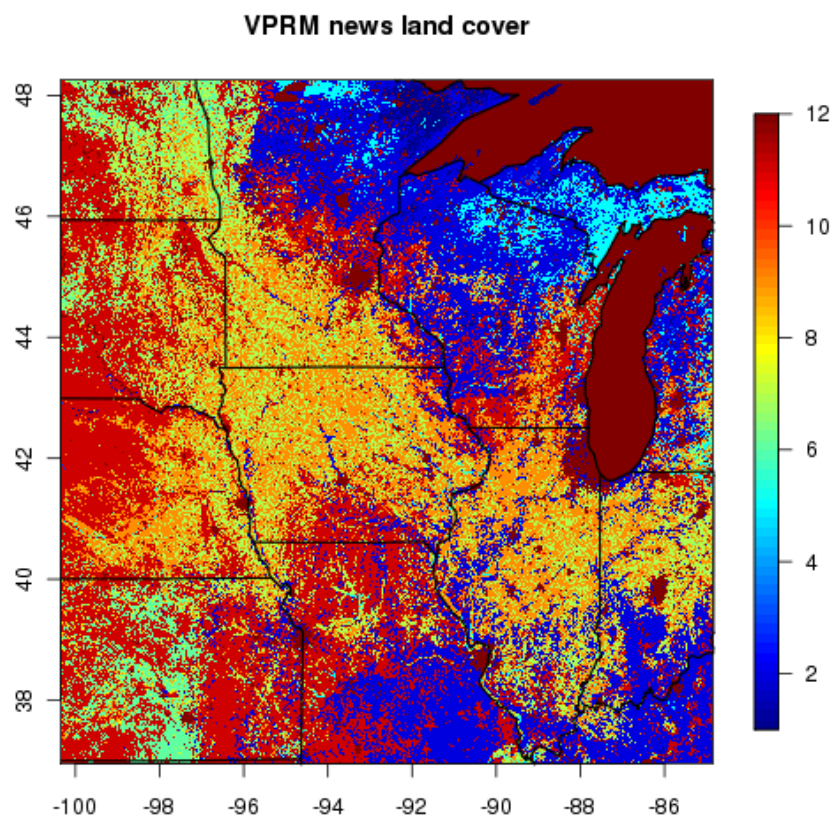Figure 4.3 CDL land cover classified to 12 VPRM classes: 1. Trees evergreen (1.2%), 2. Trees deciduous (dark blue ~ 20.8%), 3. Trees mixed (0.1%), 4. Trees and shrubs, 5. Tree and grasses (2.9%), 6. C3 crops (4.3%), 7. Soybean (orange ~13%), 8. C4 Crop (0.3%), 9. Corn (green ~17.2%), 10. Mixed C3/C4 crops (0.1%), 11. Grasses (brown ~26.6%), and 12. Barren, urban and built-up, permanent snow and ice (dark brown ~13.5%).

4.3.2 Input Data

Input data required in the optimization routine included land cover data, observations of PAR, temperature, and NEE at the Ameriflux sites, and prior VPRM parameters (see Table 4.2, with values provided by Christoph Gerbig). The prior parameters did not differentiate C3 crops, soybean, C4 crops, corn, and mixed C3/C4 crops. All crop types were treated as a sigle crop and therefore the one set of parameters was applied for all crops. Figure 4.4 (a), (b), (c), and (d) show observed NEE/FC at Ameriflux deciduous, soybean, corn, and grassland sites, respectively. Measured FC was utilized when NEE data were not available.

Table 4.2 Prior VPRM parameters.

Vegetation types	λ (μmol CO_2/ μmol PPFD)	PAR_0 (μmol PPFD m^{-2} s^{-1})	α (μmol CO_2 m^{-2} s^{-1} /^oC)	β (μmol CO_2 m^{-2} s^{-1})	T_{min} (^oC)	T_{max} (^oC)	T_{opt} (^oC)
1) Evergreen	0.12460	522	0.3301	0	0	40	20
2) Deciduous	0.08645	648	0.3258	0	0	40	20
3) Mixed Forest	0.12775	412	0.3422	0	0	40	20
4) Shrubland	0.04368	726	0.0239	0	2	40	20
5) Savanna	0.05705	1364	0.0049	0	2	40	20
6) C3 crops	0.07665	1514	0.2680	0	5	40	22
7) Soybean	0.07665	1514	0.2680	0	5	40	22
8) C4 crops	0.07665	1514	0.2680	0	5	40	22
9) Corn	0.07665	1514	0.2680	0	5	40	22
10) Mixed C3/C4 crops	0.07665	1514	0.2680	0	5	40	22
11) Grassland	0.06668	314	0.0269	0	2	40	18
12) Others	0	0	0	0	0	0	0

Note: The prior VPRM parameters were provided by Christoph Gerbig.
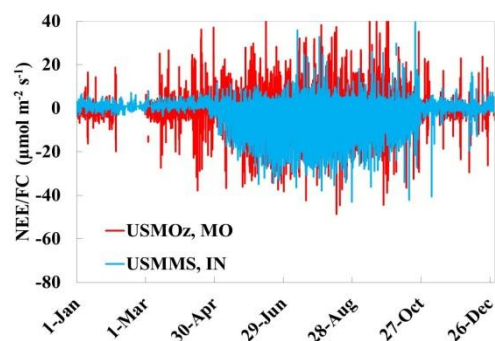
(a) At deciduous sites
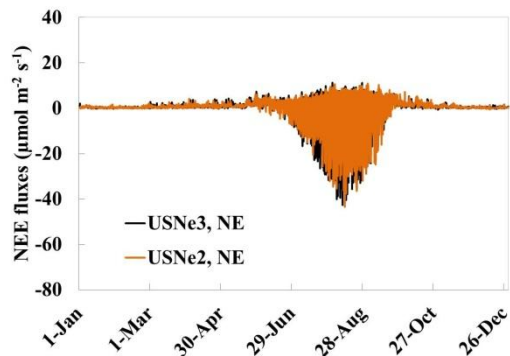
(b) At soybean sites
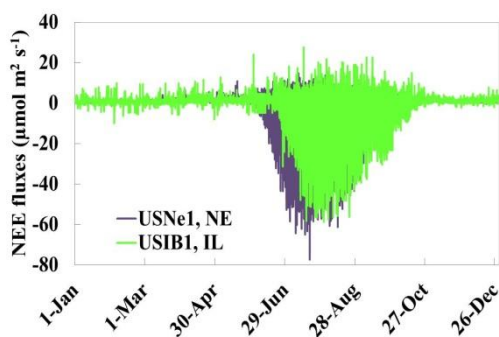
(c) At corn sites
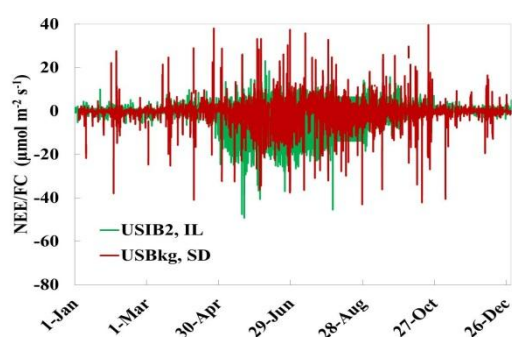
(d) At grassland sites

Figure 4.4 Observed NEE/FC at Ameriflux deciduous, soybean, corn and grassland sites in the study area in 2008

The optimization program also required EVI and LSWI at each site. We used EVI and LSWI derived from MODIS surface reflectance at 8 day intervals, and 500 m resolution. The indices were smoothed using the VPRM preprocessor program, then extracted and interpolated to 30 min or hourly to match with observed NEE data at each site. Figure 4.5 illustrates EVI values at Ameriflux deciduous, soybean, corn, and grassland sites.
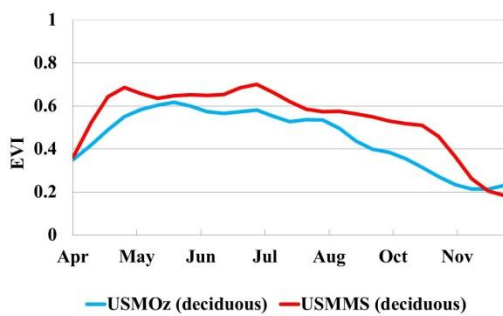
(a) Deciduous sites
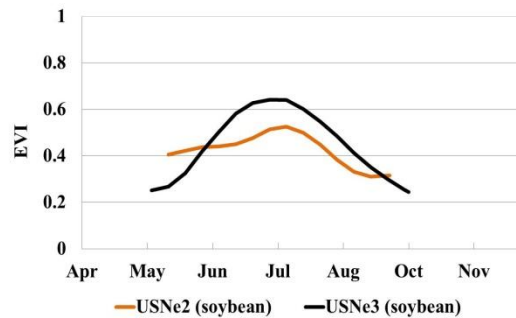
(b) Soybean sites
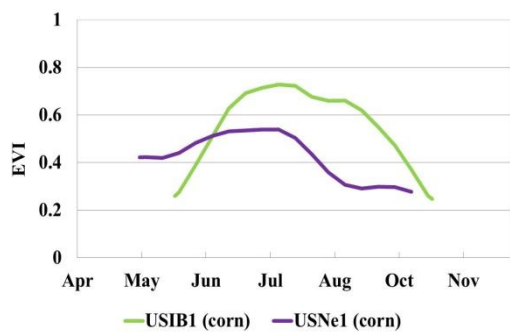
(c) Corn sites
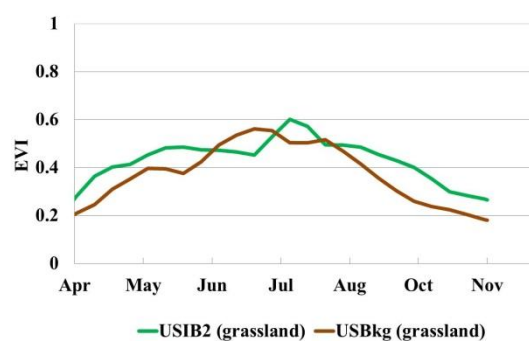
(d) Grassland sites

Figure 4.5 EVI at Ameriflux deciduous, soybean, corn, and grassland sites.

4.3.3 Optimization Procedures

A Gauss-Newton nonlinear (weighted) least square algorithm was applied to optimize the VPRM parameters. This technique was also used for VPRM parameter optimization in Mahadevan et al., 2008. The optimization program was written in the programming language R provided by Christoph Gerbig. First, the program calculated GEE, respiration, and NEE fluxes based on VPRM equations using provided input data at each site and prior model parameters for each vegetation type. Measured NEE with friction velocity (u*) less than 0.1 were eliminated before feeding to the optimization program. Then, predicted NEE was fitted against measured NEE and the optimization program tried to minimize the sum of square of errors between the predicted and measured NEE. Three optimization approaches were applied as follows.

Approach 1: Optimize both GEE and respiration simultaneously for the whole growing season.

Approach 2: Use growing season nighttime NEE to optimize for α first. Then, α was used to calculate respiration and subtract respiration from measured NEE (to obtain measured GEE). Finally, the measured GEE was used to optimize for λ and PAR_0. In this approach, β is set to zero.

Approach 3: Monthly optimization. Used the same procedures as Approach 2 but performing month by month optimization.

4.4 Optimization Results and Discussion

Prior VPRM parameters of corn, soybean, deciduous, and grassland were optimized against observed Ameriflux NEE data for the growing season of 2008 in the Midwest, USA. The GEE and respiration parameters were fed to the optimization program simultaneously (Approach 1), the results yielded too high beta and a very low alpha. When the alpha and beta respiration were substituted back in to the respiration equation, as a result, the variations of the model respiration were very small compared to

the observed nighttime NEE (dark respiration) values. Therefore, we only show the results obtained from Approach 2.

4.4.1 Optimization for Corn

The optimized VPRM parameters at Ameriflux corn sites Fermi Agricultural (USIB1) and Mead Irrigated (USNe1) in the Midwest for the 2008 growing season are shown in Table 4.3. Some of the optimized parameters at USNe1 are higher than at USIB1. This may be caused by the lower values of EVI at USNe1 during July and August compared to USIB1 (Figure 4.5), which may be due to contaminations of EVI of corn by other vegetation types with lower EVI values. The low value of EVI resulted in higher values of λ and PAR_0, since the optimization model tried to force the estimated NEE to yield the observed NEE values.

Figure 4.6 (a) and (c) show the average Root Mean Square Error (RMSE) of NEE for the different optimization approaches at the Ameriflux corn sites from June to October 2008 and Figure 4.6 (b) and (d) show average RMSE of diurnal variations at the sites. The black, green, and red lines represent the average RMSE when using prior, growing season optimized, and monthly optimized VPRM parameters, respectively. Monthly optimized parameters provide the lowest RMSE especially at the beginning of the growing season in June. As expected, optimized parameters yield better RMSE compared to using the original values. Figure 4.7 illustrates the average diurnal variations in June and August at USNe1 when using growing season and monthly optimized parameters. This figure indicates that the model can capture the flux diurnal variations quite well, both at the beginning (June) and at the peak (August) of the growing season using monthly optimized parameters. When using growing season parameters, on the other hand, the model overestimated the fluxes at the beginning of the growing season in June and could not capture the peak CO_2 uptake in August.

Table 4.3 Optimized VPRM parameters for corn using observed NEE from Ameriflux sites during growing season 2008.

Approaches	Sites	Period	λ (μmol CO_2/ μmol PPFD)	PAR_0 (μmol PPFD m^{-2} s^{-1})	α (μmol CO_2 m^{-2} s^{-1}/$^\circ$C)	β (μmol CO_2 m^{-2} s^{-1})
Prior	-	-	0.0767	1514	0.268	0
Mahadevan et al., 2008	-	2003	0.075	11250	0.209	0.2
Growing season	USIB1	Growing season	0.0801	2186	0.3661	0
optimization	USNe1	Growing season	0.1079	2485	0.3874	0
		Average	**0.094**	**2336**	**0.3768**	**0**
Monthly optimization	USIB1	June 15th – 30th	0.0928	554	0.1914	0
	USNe1	June 15th – 30th	0.0825	2532	0.3208	0
		Average	**0.088**	**1543**	**0.2561**	**0**
	USIB1	July	0.0817	2135	0.3254	0
	USNe1	July	0.1054	5280	0.399	0
		Average	**0.0936**	**3708**	**0.3622**	**0**
	USIB1	August	0.0725	3407	0.4657	0
	USNe1	August	0.1055	4529	0.4	0
		Average	**0.089**	**3968**	**0.4329**	**0**
	USIB1	September	0.1341	732	0.4015	0
	USNe1	September	0.1365	1510	0.3188	0
		Average	**0.1353**	**1121**	**0.7203**	**0**
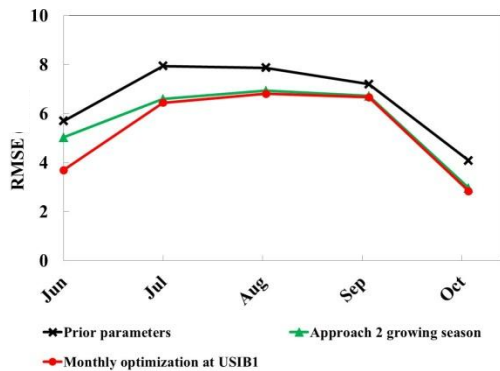
(a) Average RMSE at USIB1
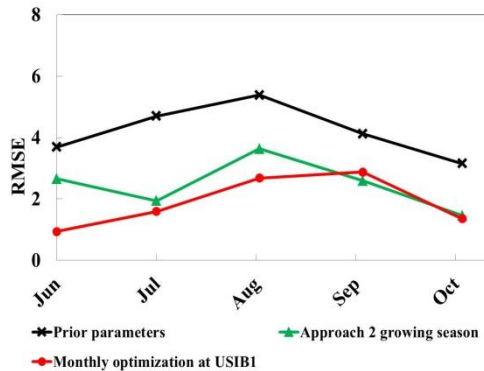
(b) Average diurnal RMSE at USIB1
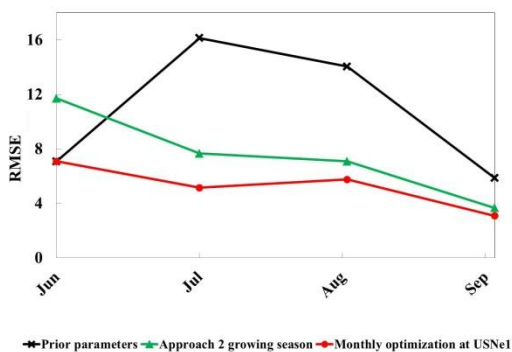
(c) Average RMSE at USNe1

(d) Average diurnal RMSE at USNe1

Figure 4.6 Average RMSE and diurnal RMSE at Ameriflux corn sites when using prior, growing season, and monthly optimized VPRM parameters.
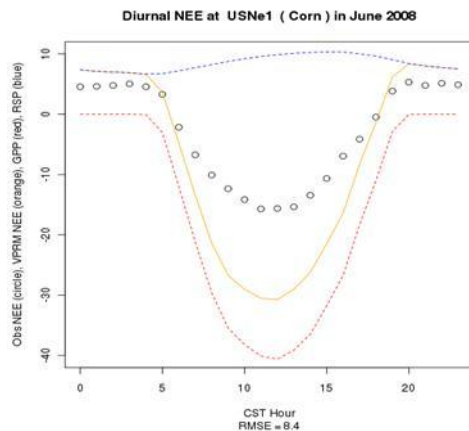
(a) Growing season optimization, June diurnal
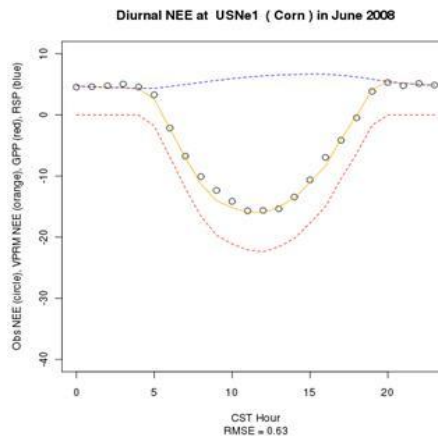
(b) Monthly optimization, June diurnal
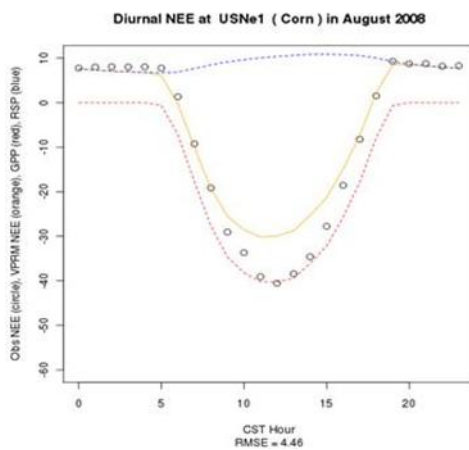
(c) Growing season optimization, August diurnal

(d) Monthly optimization, August diurnal

Figure 4.7 Diurnal NEE plots when using growing season and monthly optimization
VPRM parameters at USNe1 (Circle: Obs NEE, Orange line: VPRM NEE,
Red line: GPP, Blue line: Respiration).

4.4.2 Optimization for Soybean

Table 4.4 illustrates the optimized VPRM parameters at the Ameriflux soybean sites Mead Irrigated Rotation (USNe2) and Mead Rainfed (USNe3) in the Midwest in the 2008 growing season. RMSE of NEE of prior (black), growing season optimized (green), and monthly optimized (red) VPRM parameters from June to September 2008 at soybean sites are depicted in Figure 4.8 (a) and (c) and the average diurnal RMSE in Figure 4.8 (b) and (d). As shown, monthly optimized parameters yield considerably lower average RMSE and diurnal average than growing season optimized parameters, especially at the beginning (June) and at peak (August) of the growing season.

The average diurnal plots (Figure 4.9) at soybean sites are similar to the corn sites; the model with growing season optimized parameters overestimated the NEE fluxes in June but underestimated the peak flux uptakes in August. The model can better capture the peak uptakes of CO_2 when using monthly optimized parameter as seen from significant reduction of average diurnal RMSE from 7.2 ppm to 0.47 ppm in June and from 5.54 ppm to 1.04 ppm in August.

4.4.3 Optimization for Grassland and Deciduous Forest

The optimized VPRM parameters at the Ameriflux grassland site Fermi Prairie (USIB2) and deciduous sites Missouri Ozark (USMOz) and Morgan Monroe State Forest (USMMS) in the Midwest in 2008 are shown in Table 4.5. Growing season optimization was used for grassland and deciduous forest since the growth rates are gradual and extend for a long period as seen in the observed NEE plots in Figure 4.4. The RMSE of grassland was improved significantly in June and July when using growing season optimized parameters (Figure 4.10 (a)). Since grasslands can be very diverse from region to region, the optimized parameters can be quite different from site to site as seen in the differences of the prior, Mahadevan et al. 's, and the growing season optimized

parameters. The RMSE of deciduous forest using optimized parameters slightly improved when compared to using the prior values (Figure 4.10 (b)).
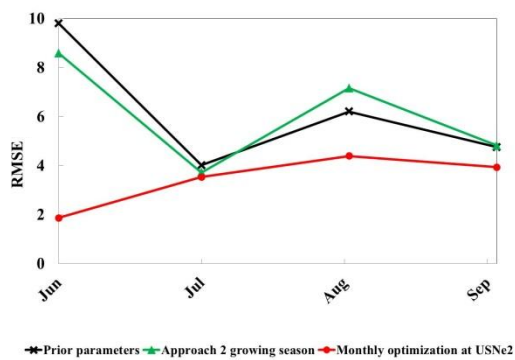
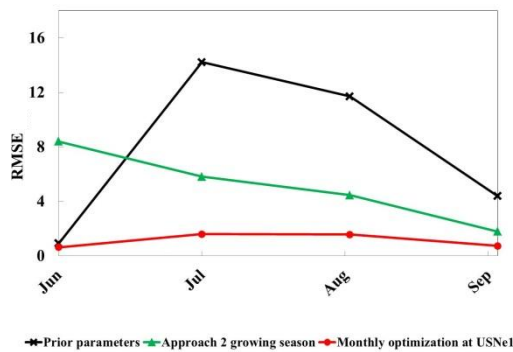

(a) Average RMSE at USNe2
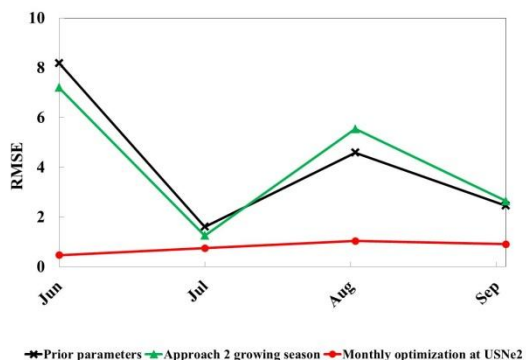
(b) Average diurnal RMSE at USNe2
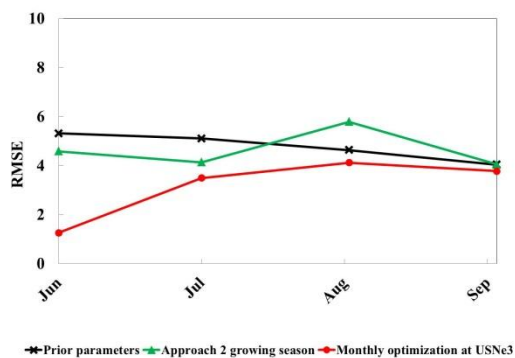
(c) Average RMSE at USNe3
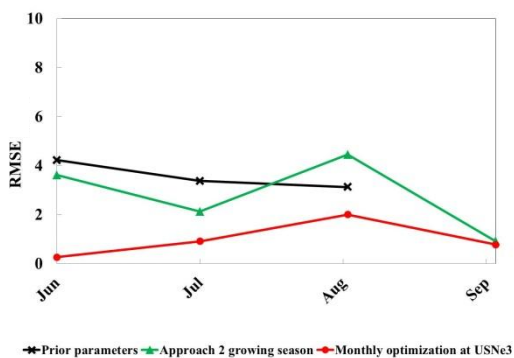
(d) Average diurnal RMSE at USNe3

Figure 4.8 Average RMSE and diurnal RMSE at Ameriflux soybean sites when using prior, growing season, and monthly optimized VPRM parameters.
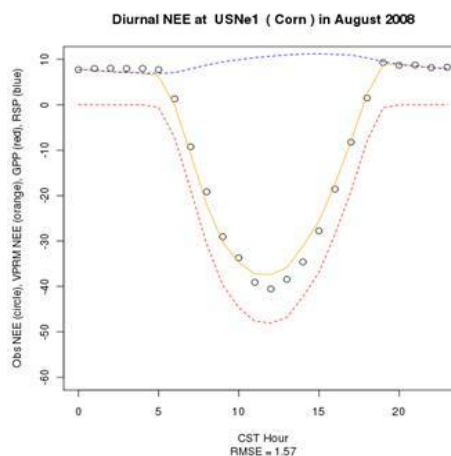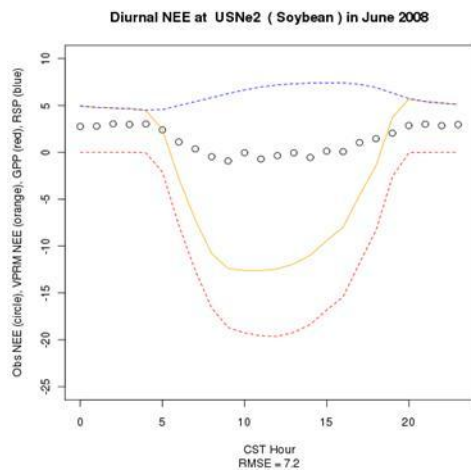
(a) Growing season optimization, June diurnal
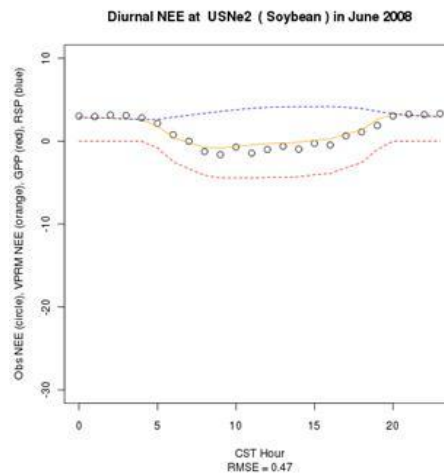
(b) Monthly optimization, June diurnal
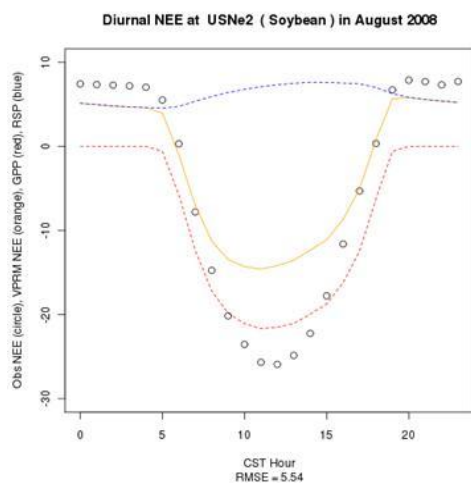
(c) Growing season optimization, August diurnal
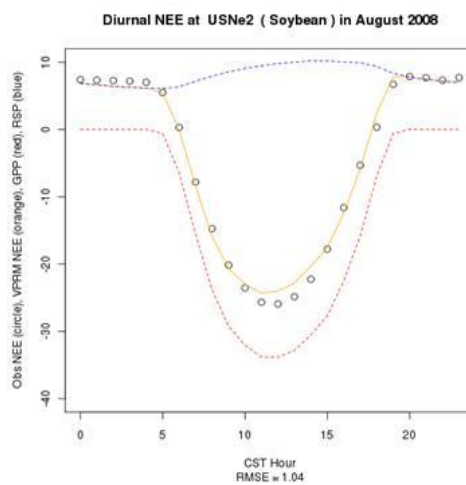
(d) Monthly optimization, August diurnal

Figure 4.9 Diurnal NEE plots when using growing season and monthly optimization VPRM parameters at USNe2 (Circle: Obs NEE, Orange line: VPRM NEE, Red line: GPP, Blue line: Respiration).

Table 4.4 Optimized VPRM parameters for soybean using observed NEE from Ameriflux sites during growing season 2008.

Approaches	Sites	Period	λ (μmol CO_2/ μmol PPFD)	PAR_0 (μmol PPFD m^{-2} s^{-1})	α (μmol CO_2 m^{-2} s^{-1}/$^{\circ}$C)	β (μmol CO_2 m^{-2} s^{-1})
Prior	-	-	0.07665	1514	0.2686	0
Mahadevan et al., 2008	-	2002	0.064	2051	0.209	0.2
Growing season optimization	USNe2	Growing season	0.0991	830	0.2782	0
	USNe3	Growing season	0.0759	1252	0.2566	0
		Average	**0.0875**	**1041**	**0.2674**	**0**
Monthly optimization	USNe2	June	0.03839	401	0.1596	0
	USNe3	June	0.03783	584	0.1618	0
		Average	**0.0381**	**493**	**0.1607**	**0**
	USNe2	July	0.0762	1045	0.2177	0
	USNe3	July	0.0755	948	0.2477	0
		Average	**0.0759**	**997**	**0.2327**	**0**
	USNe2	August	0.0984	1881	0.3724	0
	USNe3	August	0.0746	2173	0.3513	0
		Average	**0.0865**	**2027**	**0.3619**	**0**
	USNe2	September	0.2534	363	0.3985	0
	USNe3	September	0.18	365	0.2971	0
		Average	**0.2167**	**364**	**0.3478**	**0**

Note: growing season optimization used data from June 1st to Oct 06th 2008

Table 4.5 Optimized VPRM parameters for grassland and deciduous forest using observed NEE from at Ameriflux sites in 2008.

Approaches	Sites	Period	λ (μmol CO_2/ μmol PPFD)	PAR_0 (μmol PPFD m^{-2} s^{-1})	α (μmol CO_2 m^{-2} s^{-1}/$^{\circ}C$)	β (μmol CO_2 m^{-2} s^{-1})
Grassland Prior	-	-	0.0667	314	0.0269	0
Mahadevan et al., 2008	-	2001-2003	0.213	542	0.028	0.72
Growing season optimization	USIB2	**Growing season**	**0.0745**	**1422**	**0.2523**	**0**
Deciduous Prior	-	-	0.08645	648	0.3258	0
Mahadevan et al., 2008	-	2000-2003	0.127	570	0.271	0.25
Growing season optimization	USMOz	Growing season	0.1023	664	0.2756	0
	USMMS	Growing season	0.0624	1115	0.2121	0
		Average	**0.0824**	**890**	**0.2439**	**0**

Note: growing season optimization used data from April 1st to Oct 31st 2008

(a) Average RMSE at USIB2

(b) Average RMSE at USMOz
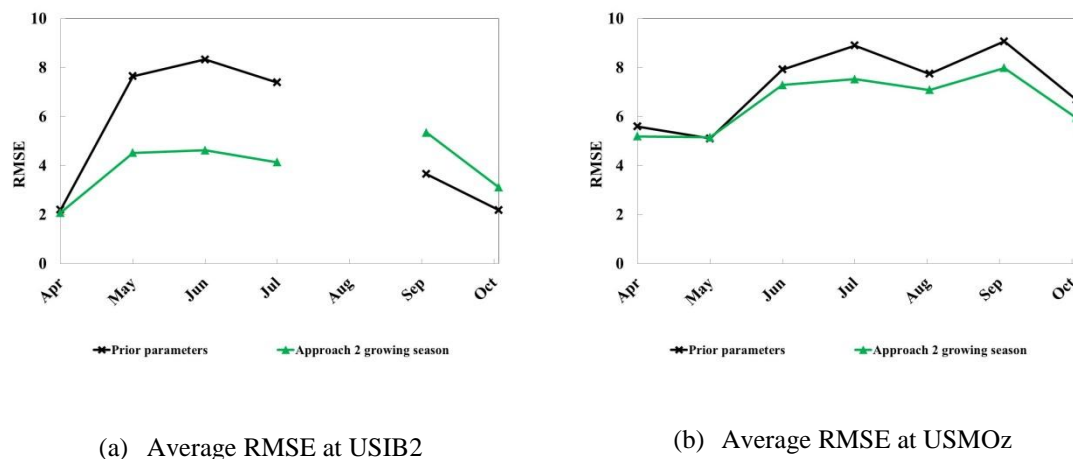
Figure 4.10 Average RMSE at Ameriflux grassland and deciduous sites when using prior
and optimized parameters.

4.6 Conclusions

In this chapter, the VPRM bottom-up model estimates of CO_2 biosphere fluxes were improved, by separately optimizing VPRM parameters for corn and soybean using two approaches, growing season and monthly optimization. Since the growth rate of corn and soybean are quite abrupt, we anticipated that monthly optimization would give significantly better correlation with observations, and this was shown to be the case. In growing season optimization, first, we optimized for alpha respiration using night time NEE (dark respiration). Then we subtracted dark respiration from observed NEE to obtain observed GEE for λ and PAR_0 optimization. The same optimization method was applied to monthly optimization but using month by month data instead of the whole growing season at once.

Using growing season optimized VPRM parameters for corn and soybean, the model usually overestimated NEE at the beginning of the growing (June) NEE but could not capture the high uptake at the peak time of plant growth in August. With monthly optimized parameters, on the other hand, the model could capture NEE at the beginning of the season and the peak uptakes in July or August quite well. The improvement when

using monthly optimization compared to growing season is not significant for deciduous forest.

CHAPTER 5 EFFECT OF SEPARATING CORN AND SOYBEAN

5.1 Introduction

As described in Chapter 4, the VPRM model parameters and land cover map greatly influence the biosphere flux estimate since photosynthesis and respiration rates of vegetation types differ from one another. Corn (C4 crop) and soybean (C3 crop) specifically show significant carbon uptake (Prueger et al., 2004) and peak carbon dioxide concentrations. The more representative (e.g. for specific vegetation types, regions, time periods) the biosphere model parameters, the better accuracy the flux estimates.

Land cover is another important issue affecting the accuracy of the flux estimate. In the Midwest study domain, SYNMAP land cover shows approximately 58.1% of crops, while CDL land cover consists of approximately 34.9% of crops (corn 17.2%, soybean 13%, C3 crops 4.3%, C4 crops 0.3% and Mixed C3/C4 crops 0.1%). The two land cover also reported significant different areas of deciduous forest and grassland. CDL shows higher deciduous (20.8% vs 7.9%) and grassland (26.6% vs 15.6%) areas. More detail land cover information could lead to better accuracy in biosphere flux estimates.

To improve the biosphere flux and CO_2 concentrations estimates, in this Chapter, we utilized VPRM parameters which were optimized against the Ameriflux flux tower NEE data (Chapter 4) and the more detailed land cover map (CDL land cover) which separates corn from soybean and other crops. We anticipated significant differences in the estimates in the simulations when corn and soybean were separated and with the monthly optimized parameters. The simulations were constructed at 4 km horizontal resolution over the Midwest region (280 by 300 grid cells). Atmospheric CO_2 concentrations at WBI and Ring2 tall towers were used for comparisons.

5.2 Model Configurations

To compare the effects of corn and soybean versus a single crop, we constructed the following simulations. The first simulation, we ran the model with a single crop using original VPRM parameters from C. Gerbig for crops and other vegetation types, except deciduous and grassland which the growing season optimized values in the Midwest 2008 were used. The other simulation, we separated corn and soybean and used monthly optimized VPRM parameters for August 2008 for corn and soybean and growing season optimized VPRM parameters for grassland and deciduous. The VPRM parameters used in the simulations are listed in Table 5.1 and the model transport configurations are in Table 5.2. Table 5.3 shows percent land cover at the tower 4 by 4 km pixel at the tall towers

5.3 Results and Discussion

The multi-crop simulation (separating corn and soybean from other crops) yielded significantly higher carbon dioxide uptake and higher respiration than the simulation with a single crop (Figure 5.1). The higher CO_2 uptake fluxes in the multi-crop simulation resulted in an underestimation of the concentrations at the WBI tower at all three tower levels (30 m, 99 m, and 379 m) as shown in Figure 5.2 to 5.4. When compared to CO_2 observations at the WBI tower, the single-crop run yielded closer CO_2 predictions during the daytime since the drawdowns of CO_2 were not as high as in multi-crop run. The results may imply the overestimations of VPRM photosynthesis parameters of corn, soybean, deciduous or grassland since these vegetation types are dominate in the study area, and/or the uncertainties in other model inputs such as land cover.

The multi-crop simulation yielded higher nighttime respiration fluxes (Figure 5.1) compared to the single crop run. The higher nighttime respirations in the multi-crop run increased the nighttime CO_2 concentrations at WBI at 30 m tower level (Figure 5.2) and are closer to the observations. However, the model nighttime the CO_2 peak

concentrations were still generally lower than observations at all tower levels at the WBI tower. The daily delta CO_2 concentrations (maximum minus minimum CO_2 concentration of each day) of the single-crop and multi-crop simulations were plotted against daily delta observations at WBI tower 30 m level in August 2008 (Figure 5.5). As seen in the figure, the delta max-min is better captured by the multi-crop fluxes compared to the single-crop. The same improvement was also observed at WBI tower at 99 m and 379 m, Round Lake, Mead, Kewanee, Centerville towers at both levels, and Galesville tower at 30 m. This suggests the need to try to reduce the uncertainties from other parts of the model.

Table 5.1 Prior and optimized VPRM parameters used in the simulations with single crop and multi-crops.

Vegetation types	Single crop simulation				Vegetation types	Separating corn and soybean			
	λ	A	β	PAR0		λ	α	β	PAR0
1) Evergreen Forest	0.1246	0.3301	0	522	1) Evergreen	0.12460	0.3301	0	522
2) Deciduous Forest	0.0704	0.255	0.25	1168	2) Deciduous	0.0704	0.255	0.25	1168
3) Mixed Forest	0.1278	0.3422	0	412	3) Mixed Forest	0.12775	0.3422	0	412
4) Shrubland	0.0437	0.0239	0	726	4) Shrubland	0.04368	0.0239	0	726
5) Savanna	0.0571	0.0049	0	1364	5) Savanna	0.05705	0.0049	0	1364
6) Crops	0.0767	0.2680	0	1514	6) C3 crops	0.07665	0.2680	0	1514
					7) Soybean[1]	0.0865	0.3619	0.2	2027
					8) C4 crops	0.07665	0.2680	0	1514
					9) Corn[1]	0.0890	0.4329	0.82	3968
					10) Mixed C3/C4 crops	0.07665	0.2680	0	1514
6) Grassland[1]	0.0725	0.2467	0.72	867.2	11) Grassland	0.0725	0.2467	0.72	867.2
7) Others	0	0	0	0	12) Others	0	0	0	0

Note: [1] Corn and soybean parameters are monthly optimized for August 2008,

[2] Beta respiration of deciduous, grassland, soybean, and corn are taken from Mahadevan et al., 2008

Table 5.2 WRF-VPRM model configurations

Features	Model configurations
Domain descriptions	**The Midwest region, USA, 280x 300 grids, 4km horizontal resolution**, 41 vertical layers.
Meteorological data	North American Regional Reanalysis (NARR), 3-hourly, 32 km resolution
Physics options	WSM 5-class scheme, RRTM longwave, Dudhai shortwave, Kain-Fritsch (new Eta) scheme cumulus option
Land surface option	unified Noah land-surface model
PBL schemes	YonSei University (YSU)

Table 5.3 Land cover at the tower location (4x4 km pixel).

Sites/ Vegetation Classes	Deciduous (%)	Soybean (%)	Corn (%)	Grassland (%)	Others (%)
NOAA tall towers - WBI, IA - LEF, WI	0.9 6.6	16.1 -	37.3 -	45.6 -	- Evergreen (1.3), Tree and grass i.e. woody wetland (92.1)
Ring2 towers					
- Kewanee, IL	7.2	-	18.1	26.5	Urban/built-up/water (48.2)
- Centerville, IA	3.6	-	-	90.4	Tree and grass i.e. woody wetland (1.8), Urban/water (4.3)
- Mead, NE	-	5.7	22.1	72.1	-
- Round Lake, MN	-	36.4	54	-	Urban/built-up/water (9.6)
- Galesville, WI	30.9	-	22	26.8	Tree and grass i.e. woody wetland (20.3)
Ameriflux towers					
- USNe1, NE	-	5.7	22.1	72.1	-
- USNe2, NE	-	5.7	22.1	72.1	-
- USNe3, NE	-	23.4	25.8	42.1	C3 crops (8.6)
- USIB1, IL	1.6	2.7	7	4.5	Urban/built-up/water (84.4)
- USIB2, IL	4.5	7.9	13.5	28.9	Urban/built-up/water (45.1)
- USMOz, MO	84.1	-	-	15.9	-
- USMMS, MN	100	-	-	-	-
- USBkg, SD	-	22	16.1	59.2	C3 crop (2.7)

Figure 5.1 Biosphere fluxes from single and multi-crops simulation at WBI tower, IA in August 2008.

Figure 5.2 CO$_2$ concentrations from single and multi-crops simulation at WBI tower, IA at 30 m in August 2008.
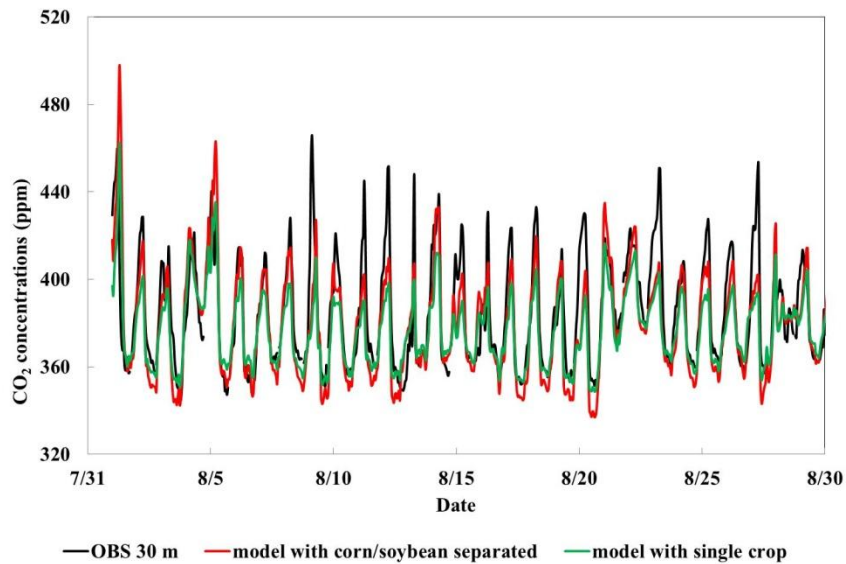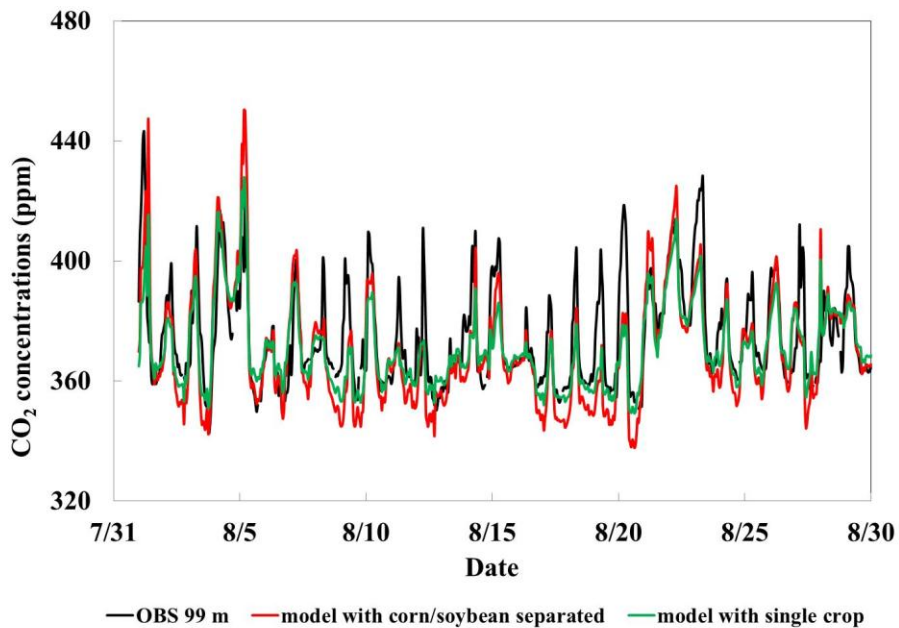

Figure 5.3 CO$_2$ concentrations from single and multi-crops simulation at WBI tower, IA at 99 m in August 2008.
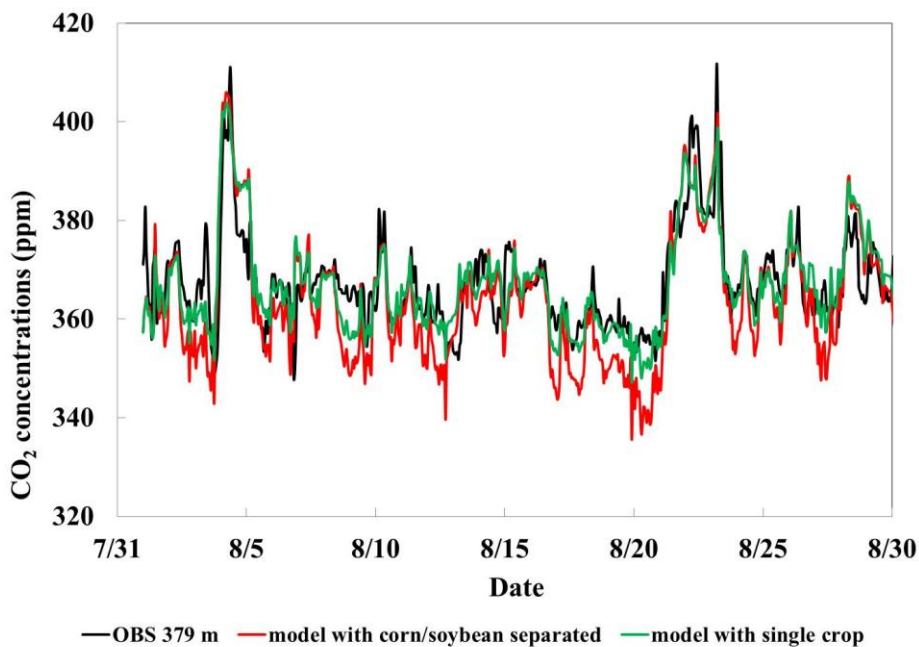
Figure 5.4 CO$_2$ concentrations from single and multi-crops simulation at WBI tower, IA at 379 m in August 2008.
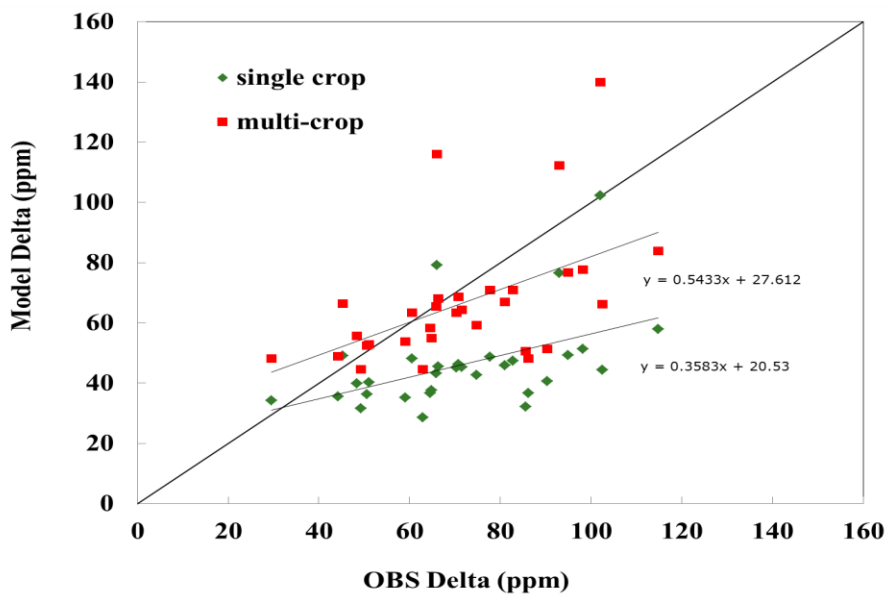

Figure 5.5 Daily delta CO$_2$ (daily maximum – daily minimum) of single-crop and multi-crop against observations at WBI tower at 30 m level in August 2008

Figure 5.6 shows the comparisons of predicted NEE at Kewanee tower in Illinoi when using single-crop and multi-crop simulations. The multi-crop run predicted significantly higher NEE uptakes compared to the single-crop run and higher respiration fluxes (Figure 5.6). The increased CO_2 uptakes at the Kewanee tower resulted in the underprediction of daytime carbon dioxide mixing ratios at the two tower levels, 30 m (Figure 5.7) and 140 m (Figure 5.8) above ground. The increase in nighttime NEE also increased the peak nighttime CO_2 concentrations, especially at the lowest tower level. The plots of biosphere fluxes and CO_2 concentrations of single-crop and multi-crop simulations at other tower locations are presented in Appendix B. The average CO_2 vertical profiles at WBI tower of the single-crop and multi-crop simulations at 3 am and 3 pm are shown in Figure 5.9. As seen, the vertical profiles show significant differences when corn and soybean were separated. The influences of the fluxes are as high as 2.5 km.

The average daytime (10 am – 5pm CST) and nighttime (10 pm – 5 am CST) RMSE of CO_2 at the tall towers with single-crop and multi-crop simulations are listed in Table 5.4. As shown below, the over predicted carbon uptakes caused the underestimation of CO_2 during the day when using the multi-crop simulation, which yielded higher RMSE compared to the single crop simulation at all towers and all levels. However, the increased respiration fluxes have improved the nighttime CO_2 mixing ratio estimates at WBI, Kewanee, Round Lake, and Galesville towers at 30 m levels.

5.4 Conclusions

The VPRM parameters of corn, soybean, deciduous and grassland optimized against Ameriflux NEE data from Chapter 4 were used in the multi-crop simulation, which separated corn and soybean from other crops, to compare against the single-crop simulation. The results at WBI tower in Iowa and Kewanee tower in Illinois showed that the daytime CO_2 uptakes significantly increased at the two sites which resulted in the

underestimations of daytime concentrations due to too high CO_2 drawdown. However, the higher nighttime NEE (respiration) have improved the nighttime CO_2 estimates at WBI, Kewanee, Round Lake, and Galesville towers at the 30 m levels.
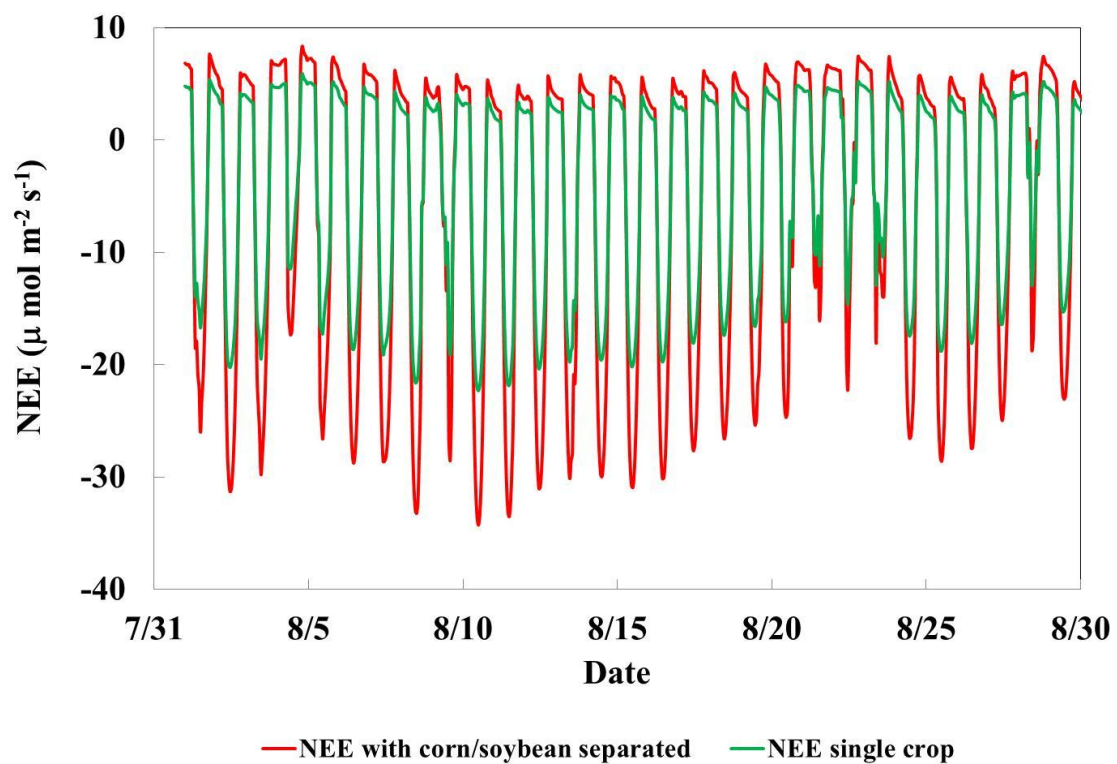
Figure 5.6 Biosphere fluxes and CO_2 concentrations from single and multi-crops simulation at Kewanee tower, IL in August 2008.
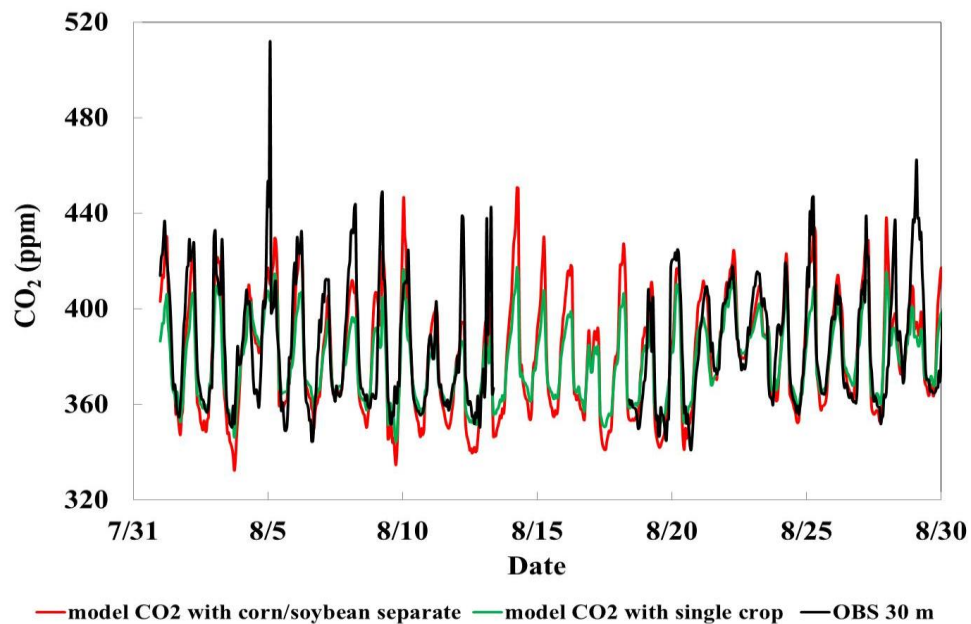
Figure 5.7 CO_2 concentrations from single and multi-crops simulation at Kewanee tower at 30 m in August 2008.
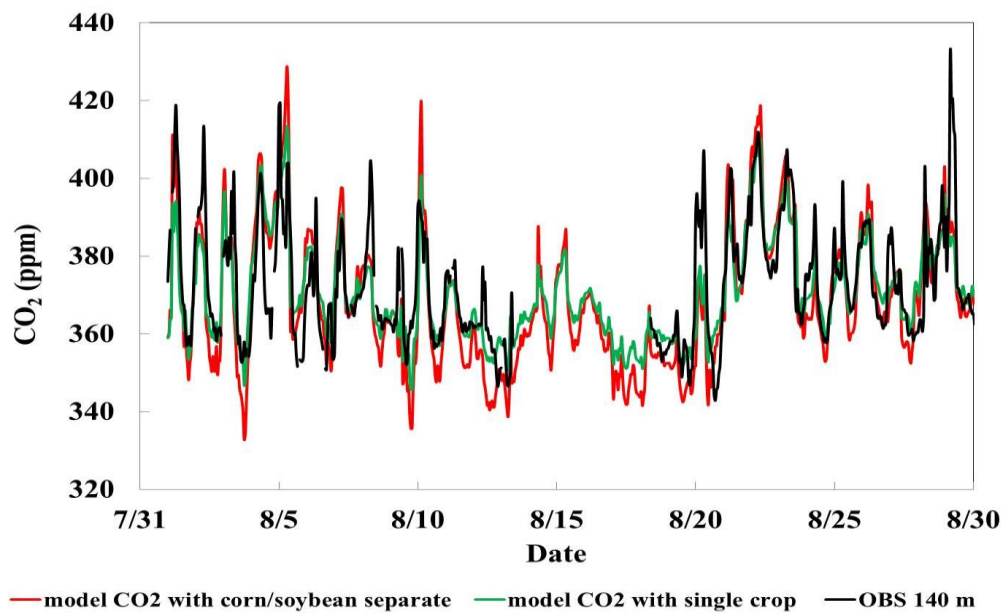
Figure 5.8 CO_2 concentrations from single and multi-crops simulation at Kewanee tower, IL at 140 m in August 2008.
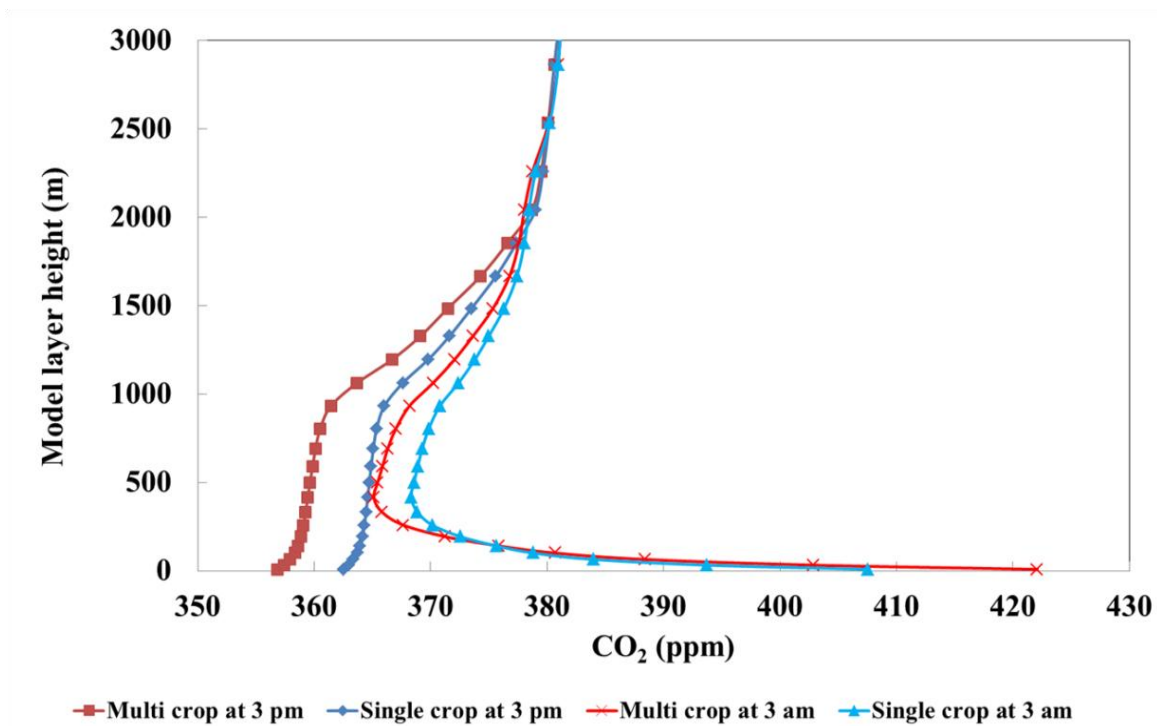
Figure 5.9 Average vertical profile of the single-crop and multi-crop simulations at WBI tower, IA in August 2008.

Table 5.4 Average daytime and nighttime RMSE of CO_2 at the tall towers with single-crop and multi-crops (separate corn and soybean) simulations.

Sites	RMSE daytime (ppm)		RMSE nighttime (ppm)	
	Single-crop	Multi-crops	Single-crop	Multi-crops
WBI 30 m	6.25	9.22	21.6	**19.09**
WBI 99 m	5.89	9.05	14.46	15.47
WBI 379 m	5.36	8.22	6.59	8.90
Kewanee 30 m	8.39	9.46	24.35	**22.78**
Kewanee 140 m	7.86	9.61	9.96	11.34
Centerville 30 m	7.60	7.93	20.39	21.20
Centerville m	10.09	9.73	10.92	11.67
Mead 30 m	7.61	7.17	17.16	23.86
Mead 122 m	10.34	10.12	14.05	15.02
Round Lake 30 m	7.98	8.70	19.60	**19.03**
Round Lake 110 m	7.63	8.76	10.87	12.71
Galesville 30 m	7.05	8.60	19.16	**18.78**
Galesville 122 m	6.39	8.01	6.54	9.29

CHAPTER 6 VPRM PARAMETER OPTIMIZATION USING

ATMOSPHERIC INVERSION (TOP-DOWN) APPROACH

6.1 Introduction

In Chapter 4, the VPRM parameters (λ, PAR_0, α, and β) of corn, soybean, deciduous, and grassland were optimized against Ameriflux NEE data in the Midwest region to improve the model biosphere flux and CO_2 mixing ratio estimates (the bottom-up approach). Although we anticipated that the simulation with optimized parameters (against more specific crops, region, and time period) and with separation of corn and soybean from other crops (multi-crops) would provide more accurate biosphere fluxes and mixing ratios of carbon dioxide at the tall towers, the multi-crops simulation seemed to over predict daytime CO_2 uptake by plants photosynthesis, thus, underestimated CO_2 concentrations during the daytime. One reason for this may be that the bottom-up optimized VPRM parameters may not accurately represent the same vegetation type in the large domain due to limitation in the numbers of Ameriflux sites as well as the diversity of the biosphere. In this Chapter, we intend to improve the model estimates by utilizing tall tower CO_2 concentrations and a generalized Bayesian inversion method to retrieve the VPRM parameters (the top-down approach) of corn, soybean, deciduous, and grassland.

The biosphere fluxes directly affect carbon dioxide concentrations. Therefore, observed CO_2 mixing ratios can be used to estimate the biosphere flux through atmospheric inversion (Enting et al., 2002). Since the changes of the estimated fluxes are caused by the VPRM model parameters, inversion approaches can also be used to obtain VPRM parameters. In this chapter, a top-down approach using a generalized Bayesian inversion was applied to retrieve the posterior VPRM parameters. The optimized parameters derived from Ameriflux towers obtained from Chapter 4 were used as prior

parameters. It is the first time application for the WRF-VPRM parameter optimizations using this inversion approach.

6.2 Methodology

In equation 6.1, J(x) is known as the cost function. It represents the distance of the state vector to the background and observations. The inversion for the new parameters (x) was accomplished by minimizing the cost function by applying the Limited memory Broyden-Fletcher-Goldfarb-Shanno (L-BFGS) algorithm (Zhu et al., 1997).

$$J(x) = \frac{1}{2} E (x - x_b)^T B^{-1} (x - x_b) + \frac{1}{2} [H(x) - y]^T R^{-1} [H(x) - y] \qquad (6.1)$$

where B is the VPRM parameters covariance matrix and R is the observation error covariance matrix. E is the values of the weight given to the prior. The larger the value the more the optimization trusts the prior, the smaller the value the more trust given to the observations. X_b is a vector of the a priori VPRM parameters used in the base simulation which were obtained from optimizing VPRM parameters against Ameriflux NEE data as described in Chapter 4. The variable x is the vector of the unknown VPRM parameters we inverted for and y is a vector of CO_2 observations and R are the observational errors. H is a matrix which represents the sensitivity of the VPRM parameter to the observed CO_2 concentrations (observation operator).

$$H = (Cp - Cb)/(Sp - Sb) \qquad (6.2)$$

It can be estimated from a series of model simulations as shown in equation 6.2, as a function of perturbed concentrations (C_p), base concentrations (C_b), perturbed parameters (S_p) and base parameters (S_b). The perturb parameters (S_p) are the changes of a VPRM parameter of each vegetation type and the perturb concentrations (C_p) are

atmospheric CO_2 concentrations extracted from the simulation using perturbed parameters. Here, we refer to the perturbation simulations as sensitivity simulations since they quantify the sensitivity of carbon dioxide concentration to each parameter. Sensitivity simulations were done for each VPRM parameter (PAR_0, λ, α, and β) by increasing their values by 20% in each vegetation type (deciduous, soybean, corn, and grassland). Perturbations were done one at a time for a total of 16 simulations. The base simulation values (C_b), i.e. the background CO_2 concentrations, were extracted from the simulation using the previously optimized VPRM parameters. The 20% perturbation allowed us to observe reasonable changes in the sensitivity simulations.

Top-down inversions were done for two domains. The study domains of the VPRM parameters inversion were the State of Iowa and the Midwestern, USA. For the State of Iowa domain, atmospheric CO_2 concentrations at WBI tall tower during the first week of August 2008 were utilized as observation (y) in the optimization routine. At the tower, the continuous measurement is taken at 30 m, 99 m, and 379 m above ground. CO_2 data at all three levels were fed to the optimization routine. For the Midwest domain, the CO_2 data at WBI and five Ring 2 towers were utilized in the assimilation. At Ring 2 tall towers, the data were taken at 30 m and $100 - 140$ m above ground. The data at all levels were fed to the optimization routine. The results of the optimization in the State of Iowa and the Midwest are shown in 6.3 and 6.4, respectively. The one week was chosen to reduce the computational time. The inversion with longer time periods will be carried out and compared with the results obtained from the one week period in the later studies.

6.3 Inversion of VPRM Parameters in the State of Iowa

6.3.1 Sensitivity of CO_2 Concentrations to VPRM Parameters

The sensitivity of CO_2 concentrations to VPRM parameters was determined by the differences of the mixing ratios predicted by a sensitivity simulation and the base

(using perturb parameters) simulation ($CO_{2,p} - CO_{2,b}$) or delta CO_2 at a tall tower location. Figure 6.1 shows delta CO_2 at WBI at 30 m when increasing λ of deciduous, soybean, corn, and grassland by 20%. In each simulation, only one parameter of each vegetation type was modified. Negative values indicate higher uptake of CO_2 by photosynthesis in the sensitivity simulation compared to the base simulation. Positive values indicate higher respiration in the sensitivity simulations compared to the base simulation.

For photosynthesis parameters, the results indicate that increasing λ of corn affects the concentrations the most with maximum uptake of 6.6 ppm (Table 6.1) followed by soybean and grassland (2.6 ppm and 2.4 ppm, respectively). Increasing λ of deciduous vegetation insignificantly affects the concentrations due to the small area of deciduous land cover in the domain. Changes in PAR_0 slightly affected the concentrations (Figure 6.2) compared to changes in λ; the change in λ of corn is about 5 times more sensitive than PAR_0.

Table 6.1 Sensitivity of carbon dioxide concentrations to VPRM GEE parameters

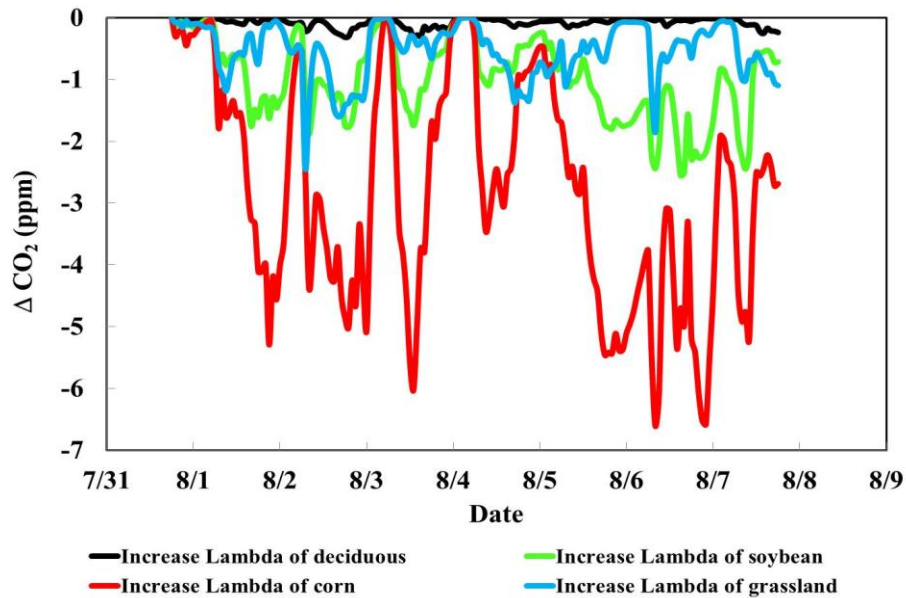| Vegetation types	λ			PAR_0			Changes of CO_2 from λ compared to PAR_0 (times)
	Prior	After 20% increased	Max. CO_2 changes (ppm)	Prior	After 20% increased	Max. CO_2 changes (ppm)	
Deciduous	0.0725	0.087	-0.3	867.2	1040.6	-0.2	1.5
Soybean	0.0984	0.1181	-2.6	1881	2257.2	-0.8	3.3
Corn	0.089	0.1068	-6.6	3968	4761.6	-1.3	5.1
Grassland	0.075	0.09	-2.4	1168	1401.6	-0.8	3.0

Figure 6.1 Delta CO_2 ($CO_{2,p} - CO_{2,b}$) at WBI at 30 m when increasing λ by 20%.
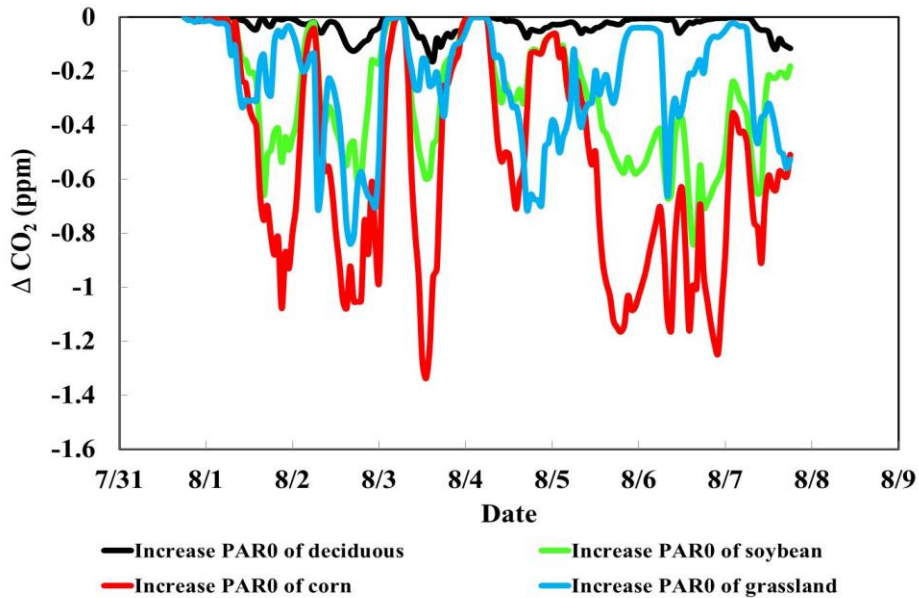

Figure 6.2 Delta CO_2 ($CO_{2,p} - CO_{2,b}$) at WBI at 30 m when increasing PAR_0 by 20%.

CO$_2$ concentrations are very sensitive to the respiration parameter α with a maximum increase of 10.2 ppm of CO$_2$ for corn (Table 6.2). Corn respiration parameters show the highest change in CO$_2$ concentrations compared to the base values followed by grassland (4.7 ppm), soybean (4.4 ppm), and deciduous (0.6 ppm) land cover (Figure 6.3). Increasing β slightly affected the concentrations compared to changes in α (Figure 6.4).

Table 6.2 Sensitivity of carbon dioxide concentration to VPRM respiration parameters

Vegetation types	A			β			Changes of CO$_2$ from α compared to β (times)
	Prior	After 20% increase	Max. CO$_2$ changes (ppm)	Prior[1]	After 20% increased	Max. CO$_2$ changes (ppm)	
Deciduous	0.2467	0.296	0.6	0.25	0.3	0.03	20
Soybean	0.3724	0.4469	4.4	0.2	0.24	0.1	44
Corn	0.4329	0.5195	10.2	0.82	0.984	0.8	12.75
Grassland	0.255	0.306	4.7	0.72	0.864	0.6	7.8

Note: [1]from Mahadevan et al., 2008

6.3.2 Inverted VPRM Parameters in the State of Iowa

Domain

Comparisons of prior and posterior VPRM parameters for deciduous, soybean, corn, and grassland using the atmospheric inversion technique are shown in Table 6.3. The results shows that the prior parameters which were derived from Ameriflux tower seem to overestimate photosynthesis parameters (PAR$_0$ and λ) for corn when compared

to the inverted parameters. The inverted Alpha respiration for corn and soybean are significantly lower than the prior values, but higher for grassland. The overestimations of PAR_0 and λ may cause the significant drawdown of carbon dioxide concentrations at several tall tower sites as shown in the previous chapter.

The CO_2 concentrations at WBI tower at 30 m simulated with the posterior parameters are presented in Figure 6.5. The improvement when using posterior parameters was not significant. This may be due to the limited background information (only WBI site) was fed into the inversion.
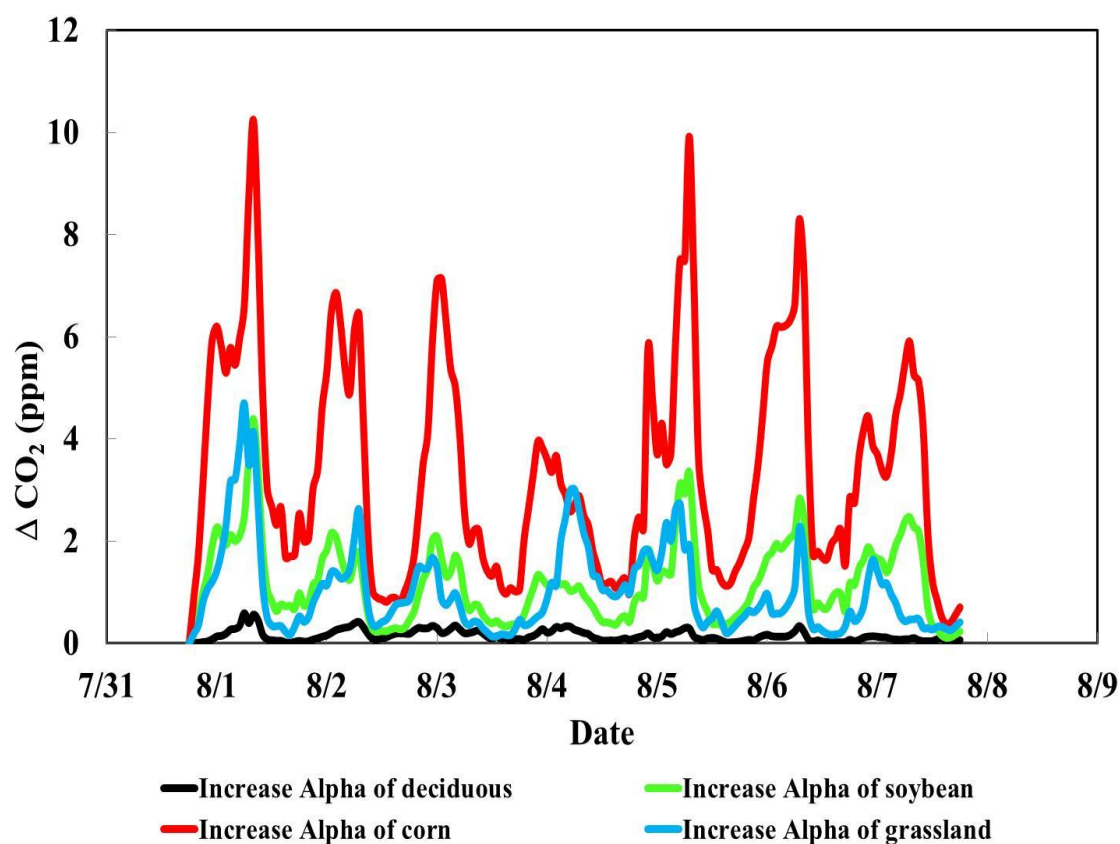

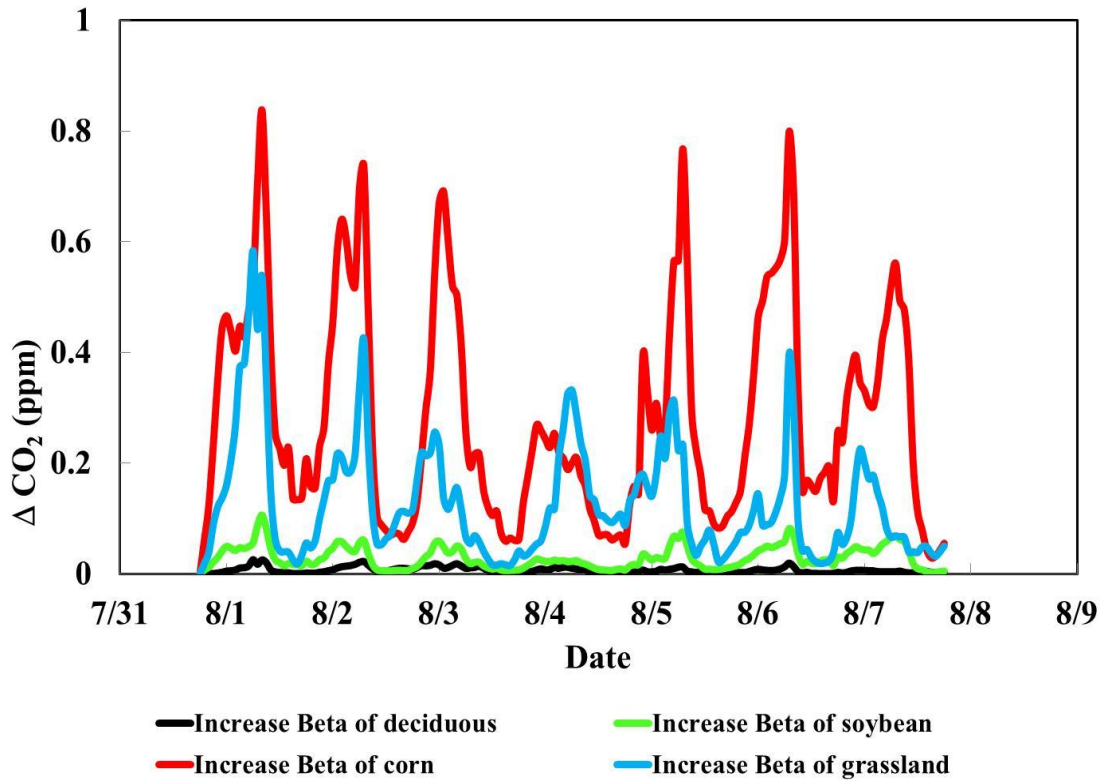Figure 6.3 Delta CO_2 ($CO_{2,p} - CO_{2,b}$) at WBI at 30 m when increasing α by 20%.

Figure 6.4 Delta CO_2 ($CO_{2,p} - CO_{2,b}$) at WBI at 30 m when increasing β by 20%.
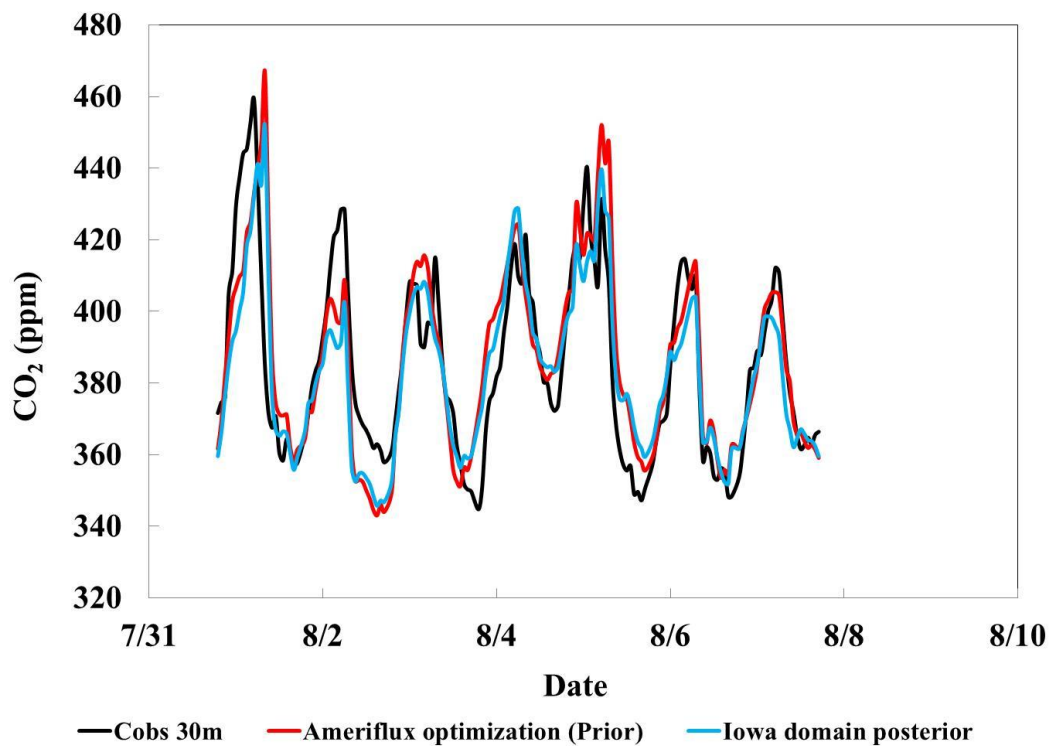
Figure 6.5 The simulation results with Iowa posterior VPRM parameters at WBI tower, IA at 30 m in August 2008

Table 6.3 Comparisons of prior and inverted VPRM parameters in Iowa domain

Vegetation types	PAR0		λ		α		β	
	Prior	Posterior	Prior	Posterior	Prior	Posterior	Prior	Posterior
Deciduous	1168	2336	0.070	0.048	0.255	0.387	0.25	0.5
Soybean	2027	1013.5	0.087	0.172	0.362	0.181	0.20	0.29
Corn	3968	1984	0.089	0.045	0.433	0.236	0.82	1.64
Grassland	867	1286.4	0.073	0.117	0.247	0.408	0.72	1.44

6.3.3 Effect of Initial and Boundary Conditions

We also tested the sensitivity of the calculations to the influences of initial and boundary conditions (IC/BC). To investigate the effect of IC/BC, the boundary conditions were added as another VPRM parameter. To perform the assimilation, Carbon Tracker CO_2 mixing ratios used as IC/BC were increased by 20%. Then the simulation with increased IC/BC was used as a based simulation. The inversion method was applied to obtain the factor that the base values should be reduced. The optimization routine was implemented with different E (i.e. the values of the weight given to the prior) values. As shown in Figure 6.6, the reduction factors of IC/BC of approximately 0.2 were obtained Delta CO_2 (model CO_2 values- observations) with 20% increase of boundary condition and after the optimization shows significant reduction of biases (Figure 6.7). This implies that the inversion method functions properly.
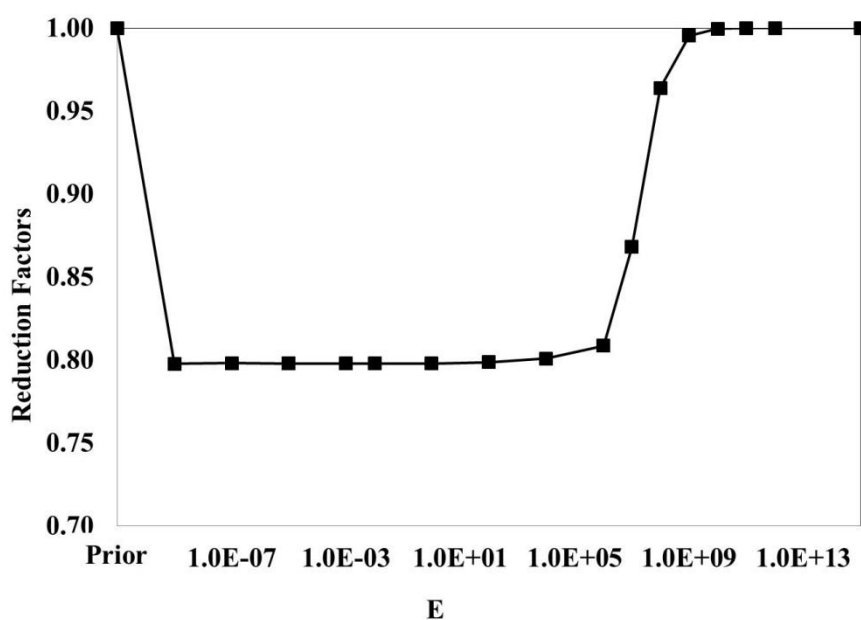

Figure 6.6 Factors of IC/BC reduction at different E (weight of the model and observation) values obtained from 3Dvar optimization routine.
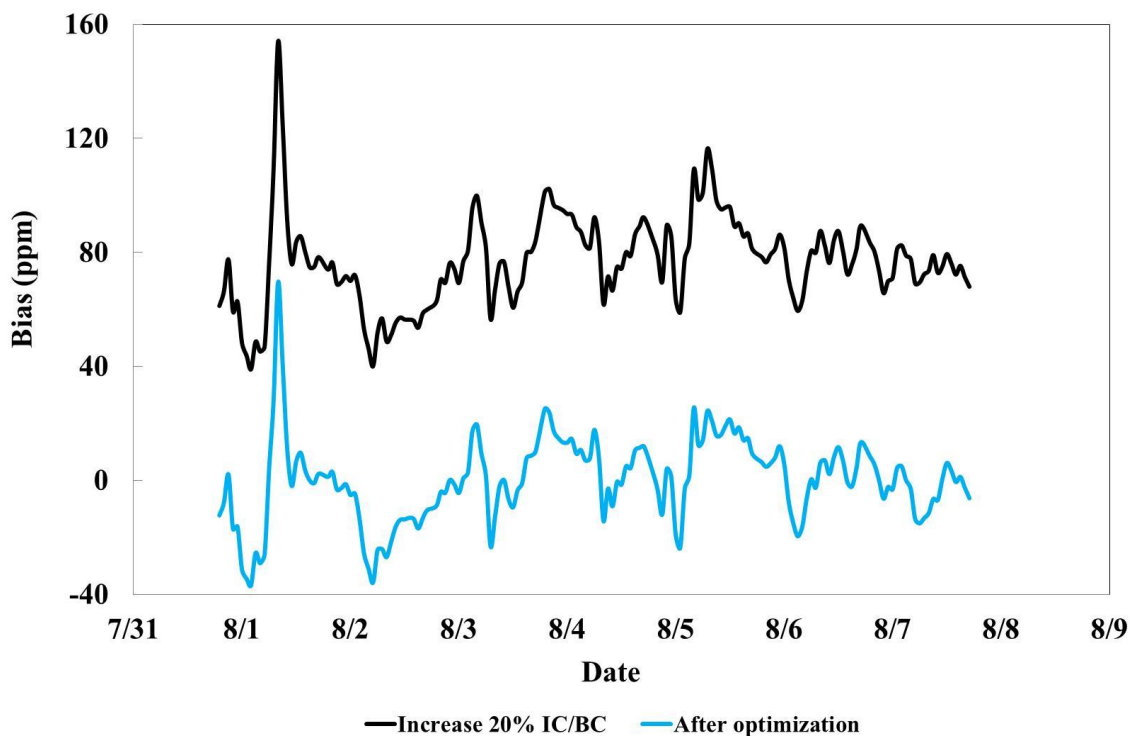
Figure 6.7 CO_2 concentration biases with increased 20% IC/BC and after the optimization at WBI tower at 30 m

6.4 Inversion of VPRM Parameters in the Midwestern,

USA

6.4.1 Inverted VPRM Parameters in the Midwest Domain

In this part, atmospheric CO_2 concentrations from six tall towers in the Midwest region were utilized in the inversion to obtain the posterior VPRM parameters. The generalized inversion method reduced the average RMSE by approximately 5.6 ppm, from 26.5 ppm (base run with prior (Ameriflux optimized) parameters) to 21.9 ppm as shown in Figure 6.8. The optimized VPRM parameters obtained from the inversion in the Midwest domain are listed in Table 6.4 and Figure 6.9 to Figure 6.12.
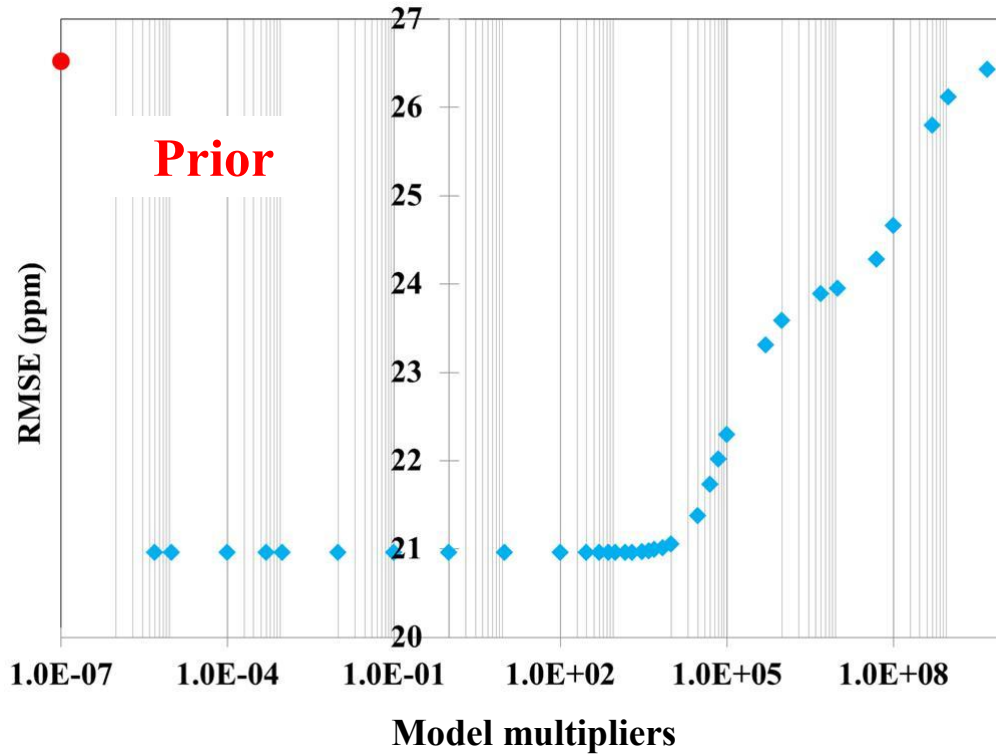
Figure 6.8 RMSE of the optimization results at different E (weight of the model and observation)

Table 6.4 The posterior VPRM parameters obtained from the 3Dvar optimization.

Vegetation types	PAR0	λ	α	β
Deciduous	2336	0.0352	0.2213	0.35
Soybean	4054	0.1406	0.4431	0.21
Corn	1984	0.0445	0.2387	0.82
Grassland	870	0.0363	0.1234	0.72

Figure 6.9 to Figure 6.11 depict PAR_0, λ, and α parameters of Ameriflux optimized parameters (Prior), and the posterior parameters of inversion in the State of Iowa and the Midwest. For the Midwest domain, the top-down estimates yield higher values of PAR_0, λ, and α for soybean, but lower values for corn compared to the prior values. The posterior β parameters were quite close to the prior parameters. Comparing the State of Iowa and the Midwest domain inversions, the results suggest significant differences in PAR0 values of soybean, λ of grassland, α of deciduous forest, soybean, and grassland, and β of corn and grassland.
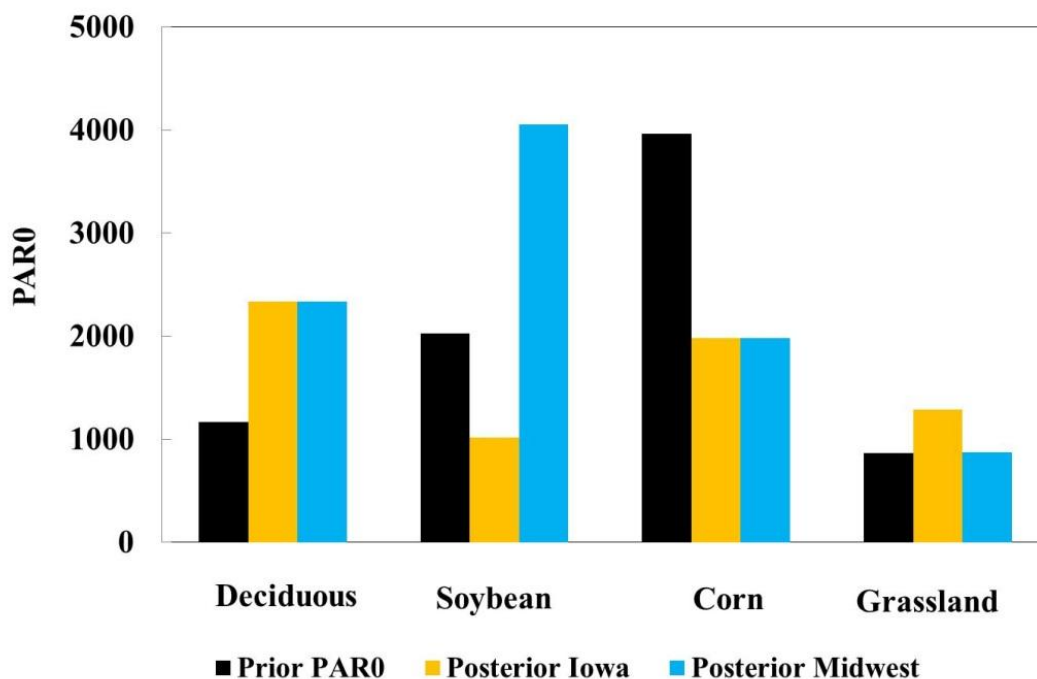

Figure 6.9 Prior and posterior PAR_0 of Deciduous, Soybean, Corn, and Grassland
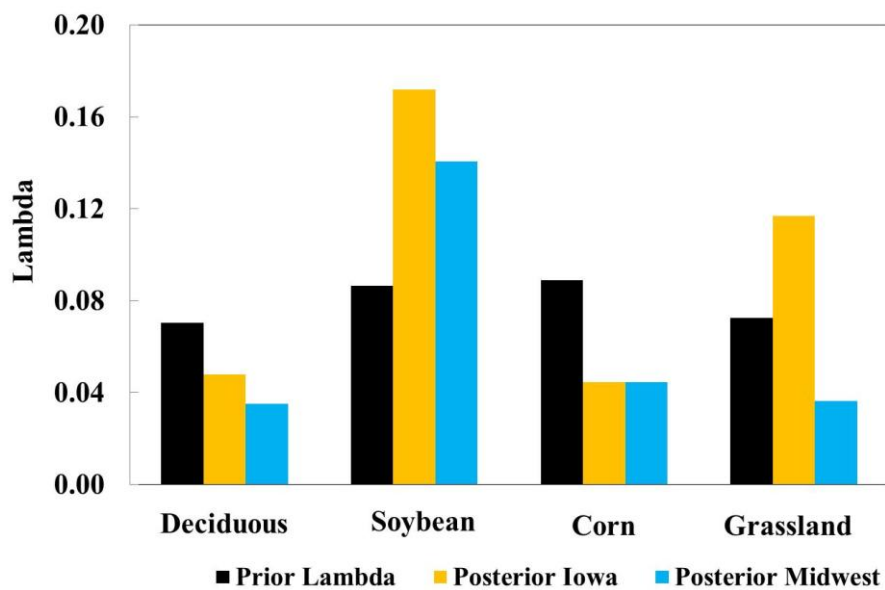
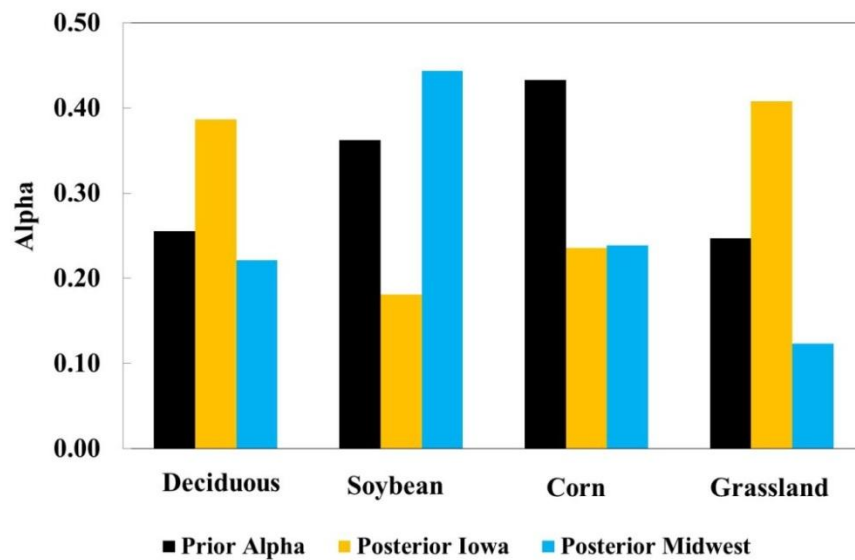Figure 6.10 Prior and posterior λ of Deciduous, Soybean, Corn, and Grassland

Figure 6.11 Prior and posterior α of Deciduous, Soybean, Corn, and Grassland
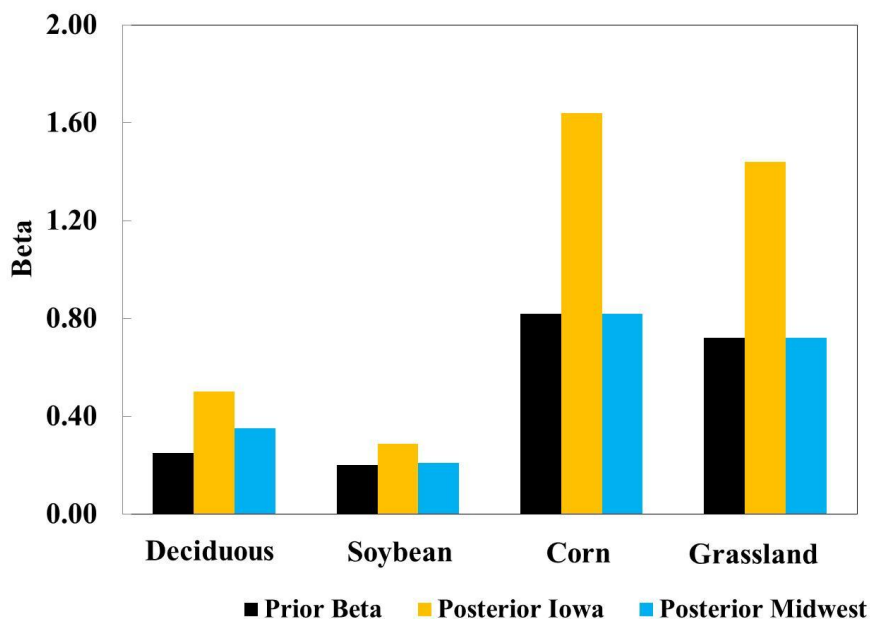
Figure 6.12 Prior and posterior β of Deciduous, Soybean, Corn, and Grassland

6.4.2 The Simulation with Posterior Parameters

The posterior VPRM parameters were used to simulate CO_2 biosphere fluxes and concentrations in the Midwest region. The NEE results of the simulation were compared to the simulation with Ameriflux optimized VPRM parameters. As seen in Figure 6.13 at the WBI tower and Figure 6.14 at the Galesville tower, the inverted parameters yielded lower CO_2 drawdown during daytime at both towers. The nighttime respiration values at both towers were also lower when using the inverted VPRM parameters in the simulation.

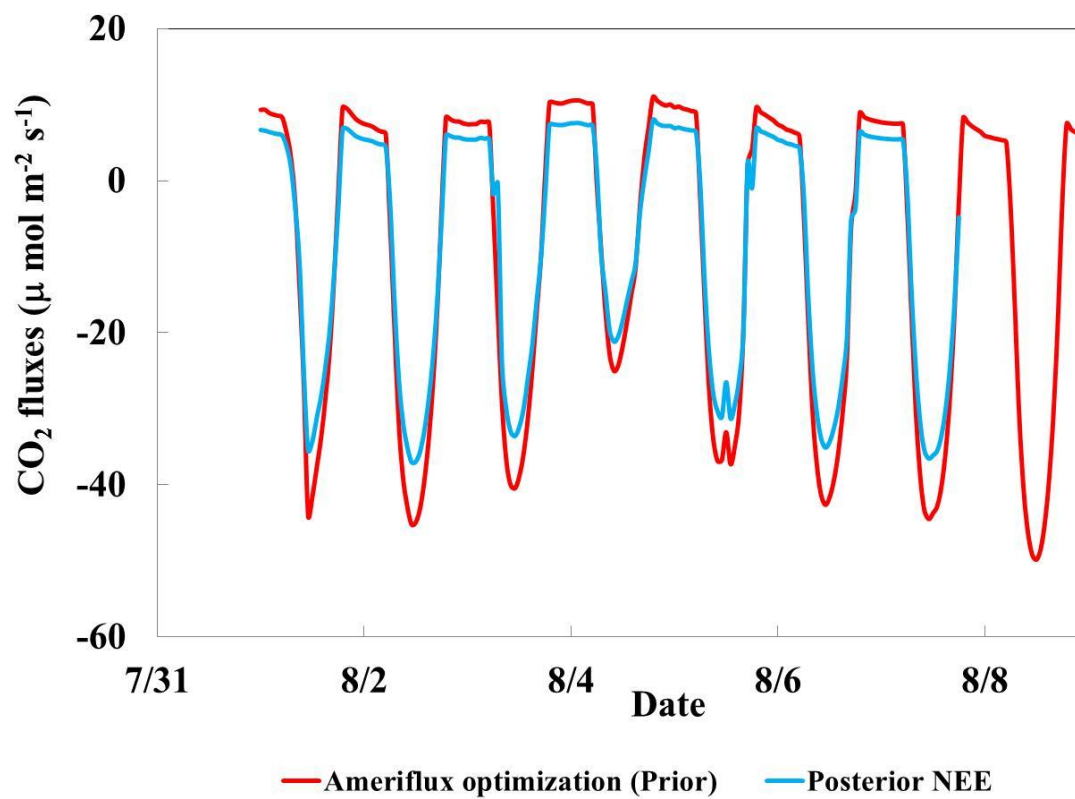Figure 6.13 Comparison of NEE when using Ameriflux optimized (Prior) and Inverted VPRM parameters at WBI tower, IA in August 2008
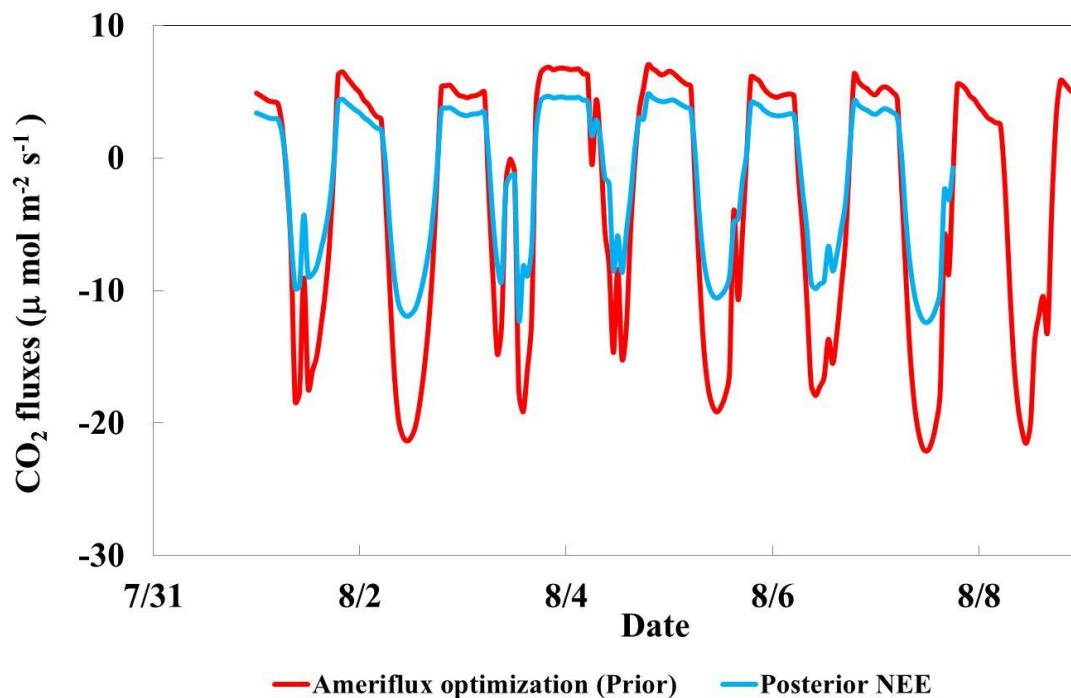
Figure 6.14 Comparison of NEE when using Ameriflux optimized (Prior) and Inverted
VPRM parameters at Galesville tower, WI in August 2008

The decreases in CO_2 drawdown result in an increase in the daytime predicted

CO_2 concentrations, which are closer to the observations (Figure 6.15 and Figure 6.16).

The daytime RMSE at WBI, Centerville, and Galesville sites at 30 m level reduced when

using the top-down parameters (Table 6.5). The top-down parameters also caused lower

nighttime CO_2 concentrations due to lower respiration fluxes, which decreased the

nighttime CO_2 concentrations significantly in some days and caused the nighttime

concentrations to be further from the observations compared to when using the Ameriflux

optimized parameters.
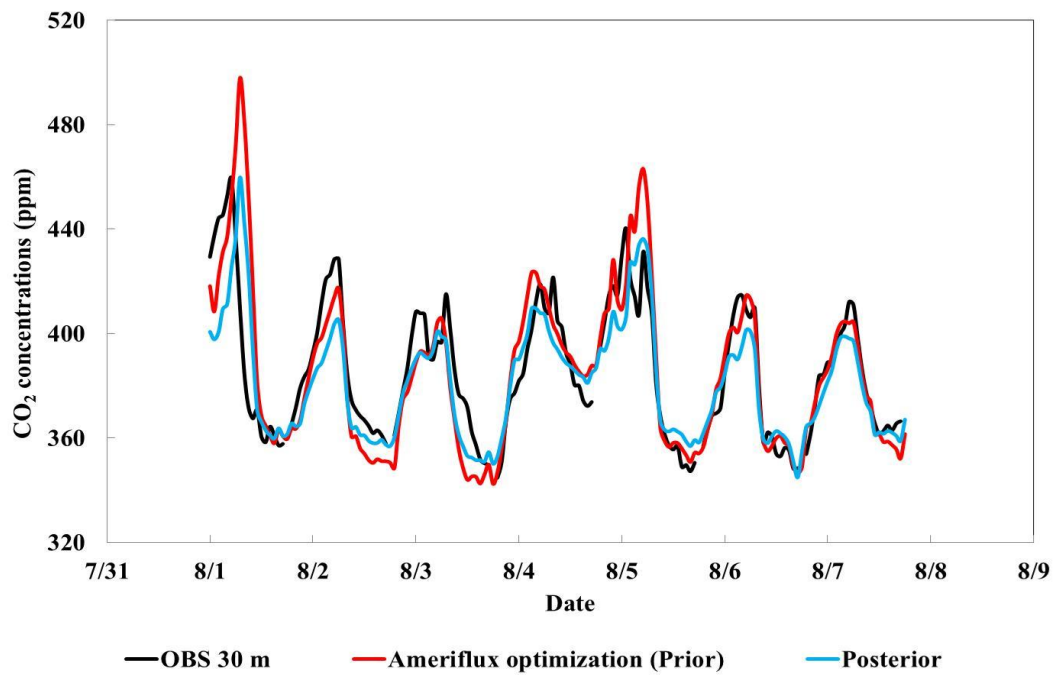
Figure 6.15 The simulation result with posterior VPRM parameters at WBI tower, IA at
30 m in August 2008
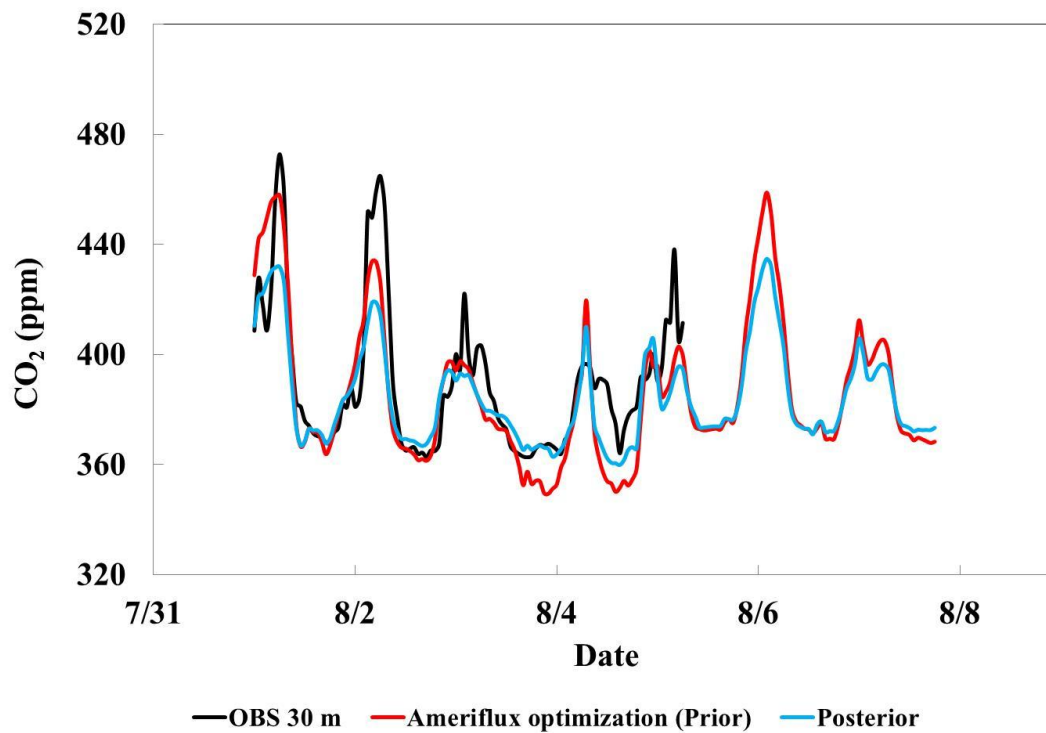
Figure 6.16 The simulation result with posterior VPRM parameters at Galesville tower 30 m in August 2008

Table 6.5 CO_2 daytime RMSE when using Ameriflux optimization (Prior) and Posterior parameters

Tall tower sites	Daytime RMSE	
	Ameriflux optimization (Prior)	Posterior
WBI, IA	11.6	7.8
Kewanee, IL	5.9	7.0
Centerville, IA	8.8	8.7
Galesville, WI	14.0	10.2

Figure 6.17 to Figure 6.19 show NEE hourly averaged flux (from August 1st, 2012 – August 7th, 2012) at 12 pm CST when using the original VPRM parameters (from C. Gerbig) with single crop, using Ameriflux optimized parameters with multi-crop, and invert VPRM parameters with multi-crop, respectively. Figure 6.20 to Figure 6.22 show the hourly averaged NEE flux (from August 1st, 2012 – August 7th, 2012) with three different VPRM parameter sets at 12 am CST. During midday (12 pm), the top-down VPRM parameters yielded higher NEE fluxes than the original parameters, but lower than the Ameriflux optimized parameters. At night (12 am), the top-down VPRM parameters also yielded higher respiration fluxes than the original parameters, but lower than the Ameriflux optimized parameters.

6.5 Conclusion

The inversion study in the State of Iowa showed that carbon dioxide concentrations at the WBI tall tower are very sensitive to changing α and λ of corn which the maximum changes of CO_2 concentration of 10.2 ppm and 6.6 ppm, respectively. β showed the least effect compared the other VPRM parameters. Initial and boundary condition seems to have insignificant effect on the parameter optimization results.

The results from the inversion study in the Midwest suggested the overestimation of PAR_0, λ, and α of corn which were derived from Ameriflux data ("Prior parameters"). The inversion method yielded significantly higher PAR_0, λ, and α for soybean compared to the Ameriflux optimized (Prior) parameters. The simulation with inverted parameters decreased the CO_2 drawdown which increased the daytime predicted CO_2 concentrations to be closer to observations.

Figure 6.17 NEE flux hourly average (from August 1st, 2012 – August 7th, 2012) at 12 pm CST when using original VPRM parameters (from C. Gerbig) and single crop.

Figure 6.18 NEE flux hourly average (from August 1st, 2012 – August 7th, 2012) at 12 pm CST when using Ameriflux optimized VPRM parameters and multi-crop.

VPRM NEE hourly average at 12 CST

Figure 6.19 NEE flux hourly average (from August 1st, 2012 – August 7th, 2012) at 12 pm CST when using invert VPRM parameters and multi-crop.
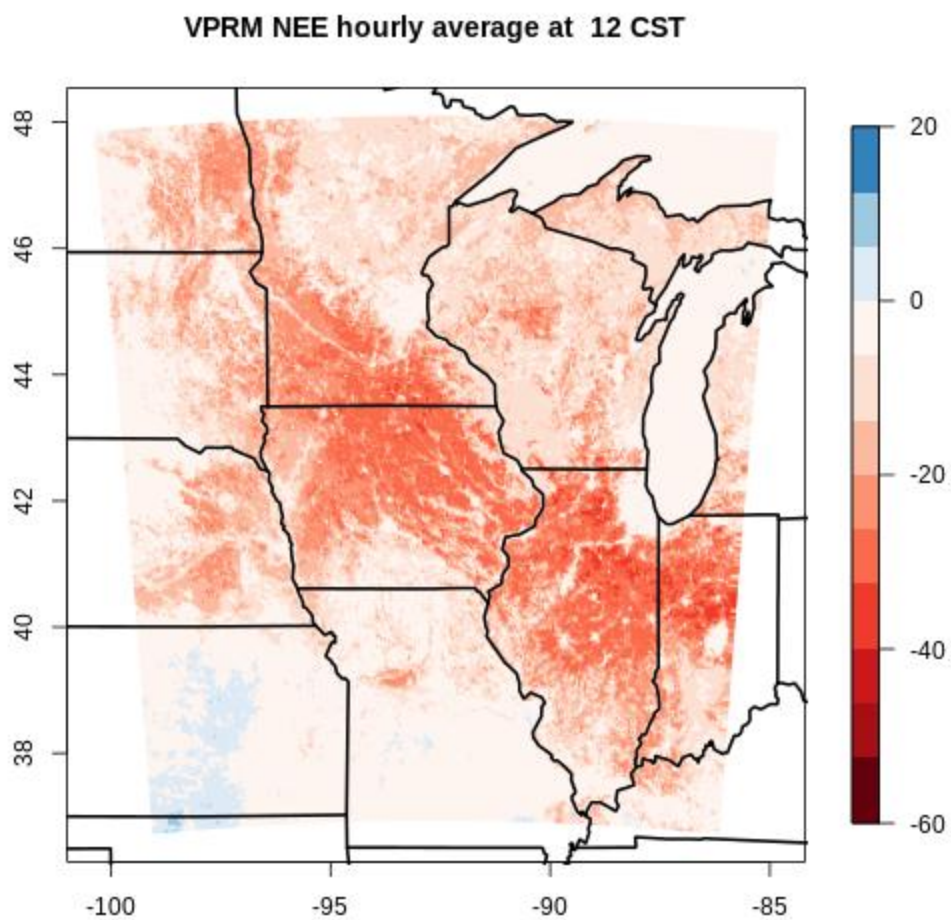
Figure 6.20 NEE flux hourly average (from August 1st, 2012 – August 7th, 2012) at 12 am CST when using original VPRM parameters (from C. Gerbig) and single crop.
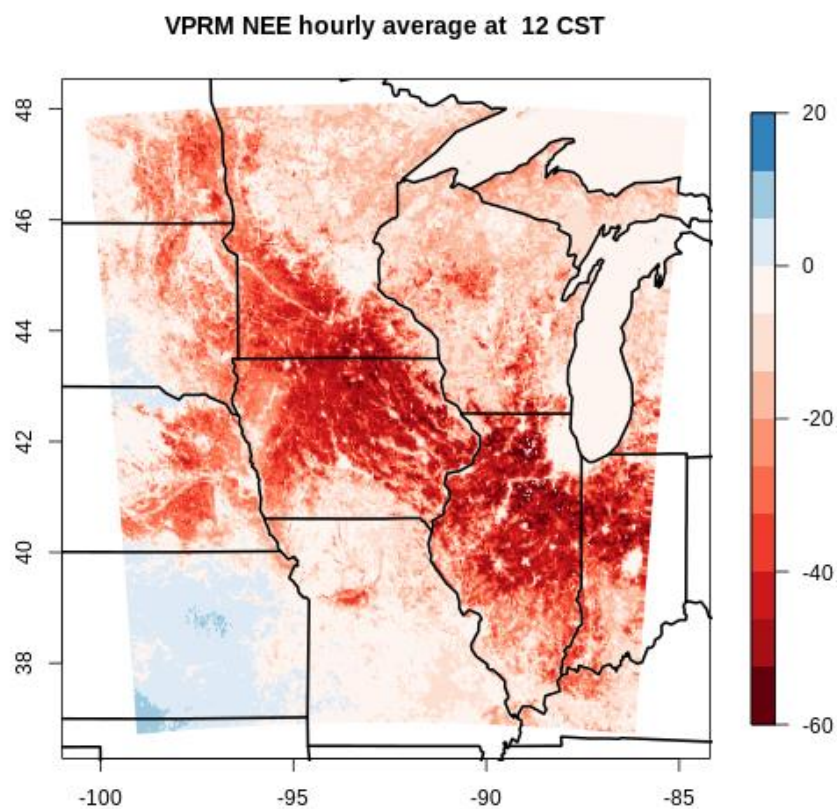
Figure 6.21 NEE flux hourly average (from August 1st, 2012 – August 7th, 2012) at 12 am CST when using Ameriflux optimized VPRM parameters and multi-crop.
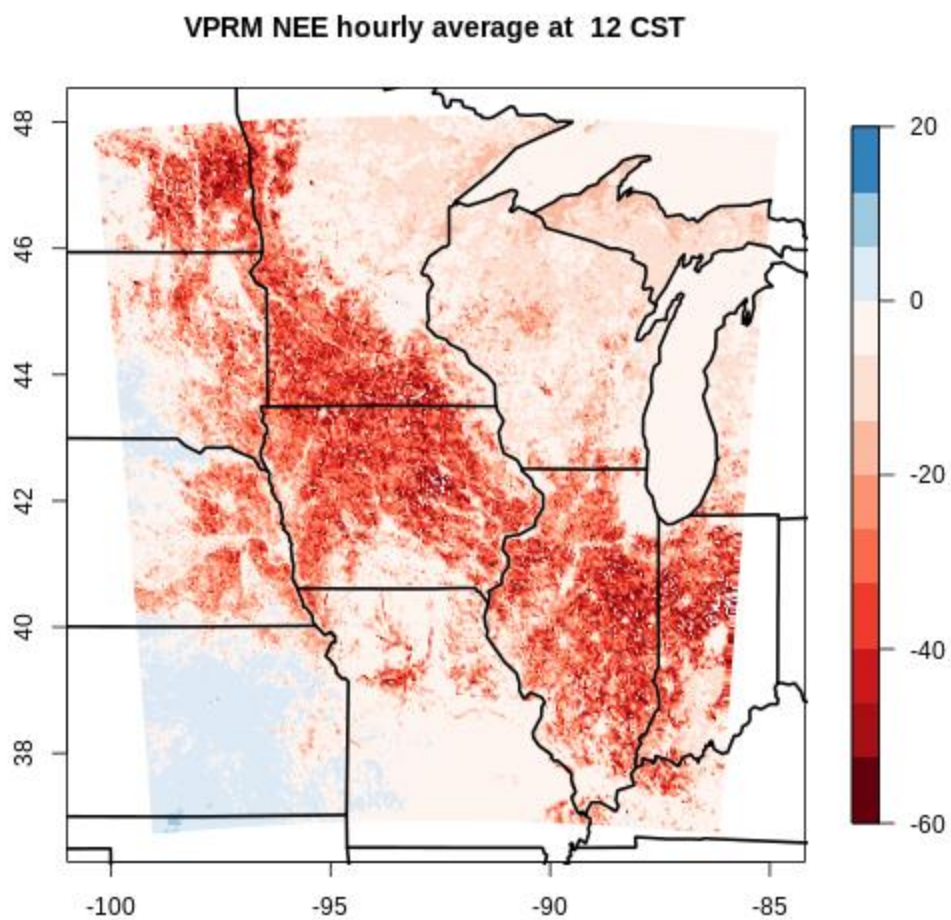
Figure 6.22 NEE flux hourly average (from August 1st, 2012 – August 7th, 2012) at 12 am CST when using invert VPRM parameters and multi-crop.
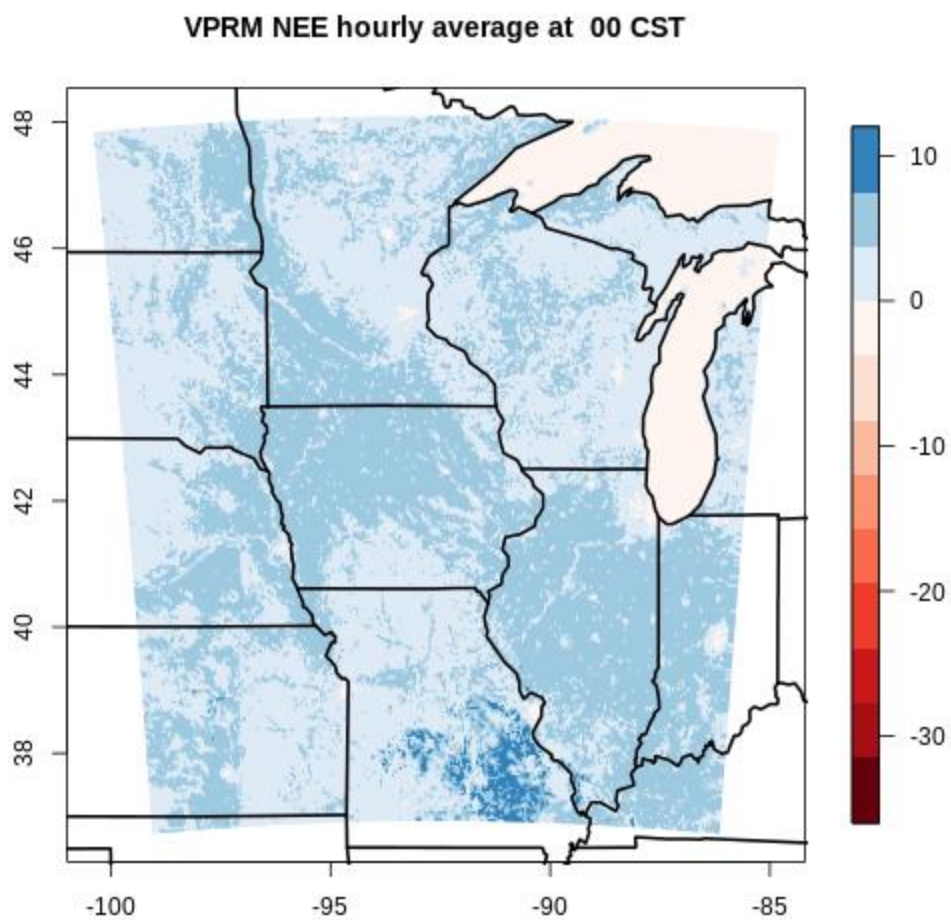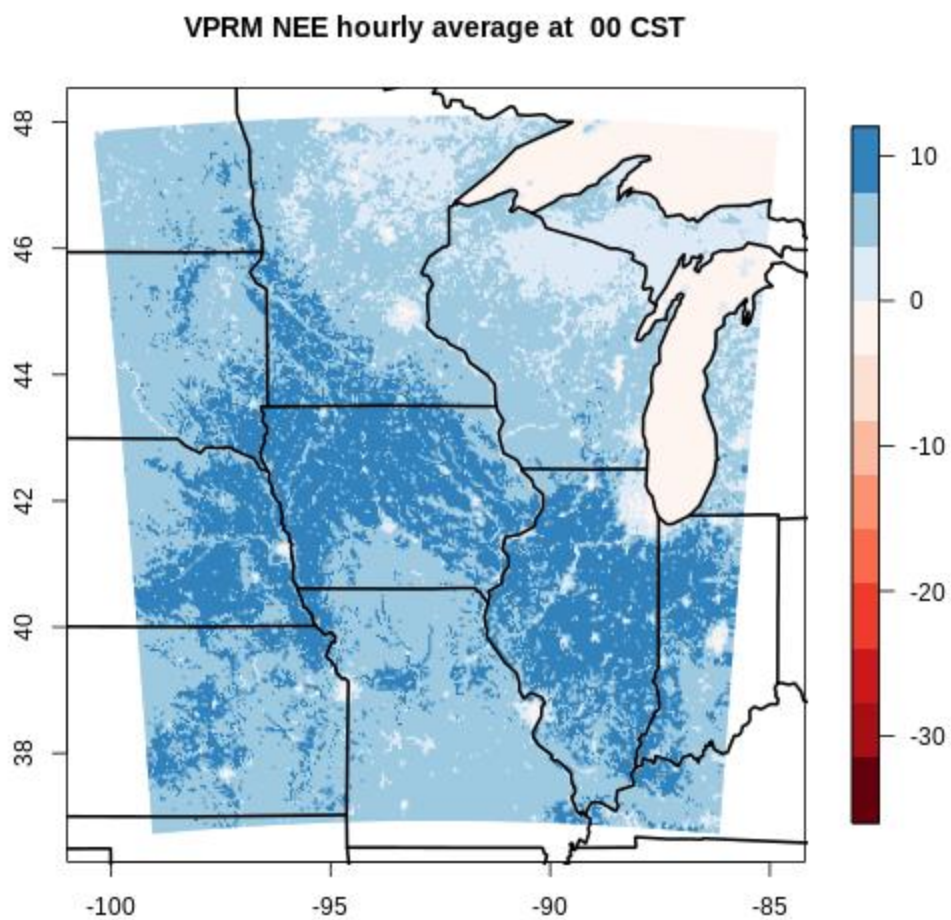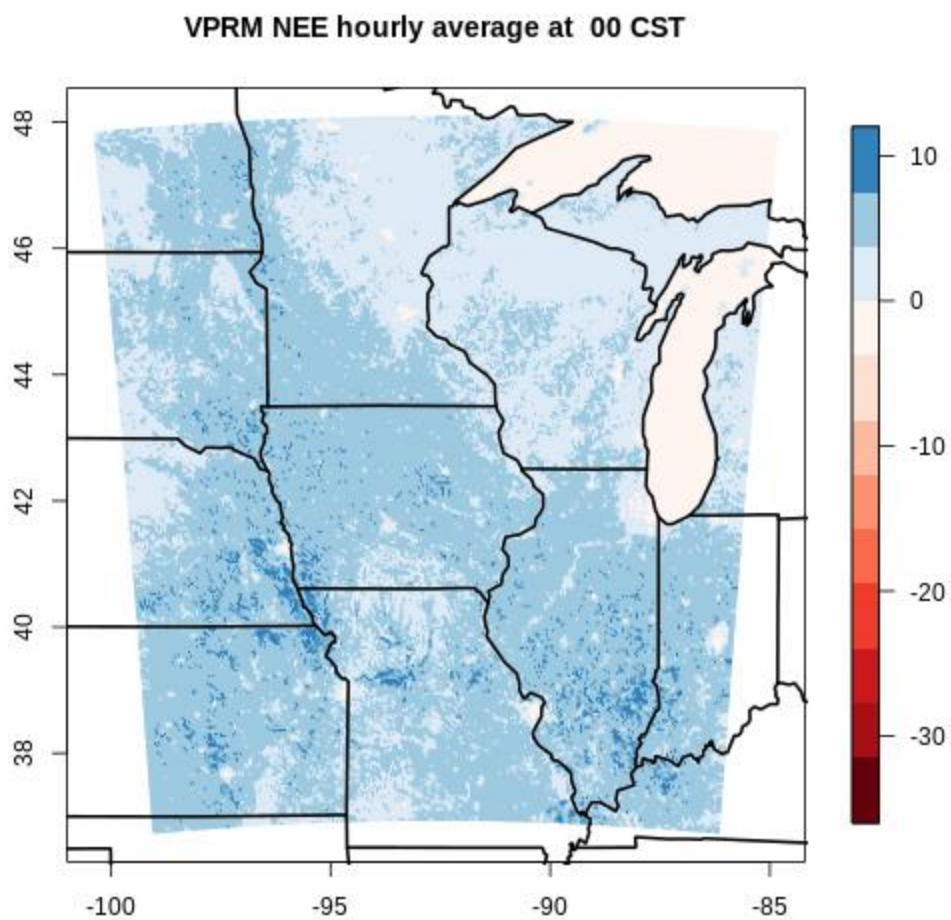
CHAPTER 7 SUMMARY AND RECOMMENDATIONS

7.1 Summary

The main objective of this research was to develop a methodology to reduce uncertainty in estimates of CO_2 fluxes and concentrations by improving current bottom up biosphere and transport model performance and utilizing top-down inversion data assimilation methods. The WRF-VPRM biosphere and transport model was the major tool used for reducing the biosphere flux estimate uncertainties. First, we studied the model transport configurations to identify the PBL scheme, the number of vertical layers, and horizontal resolutions which yielded the lowest prediction errors. Then, we reduced the uncertainty in bottom-up biosphere flux estimates by separation of corn from soybean in the land cover inputs and performed the VPRM model parameter optimization against Ameriflux NEE data. Both month by month and growing season optimizations were performed to capture the peak of the growing season. Finally, we utilized a data assimilation technique (top-down approach) to obtain a new set of VPRM parameters using Ameriflux optimized parameters as prior parameters.

The YSU PBL scheme was found to improve the prediction of daytime and nighttime CO_2 concentrations over the MYJ method at all tower levels. The maximum error reduction was 17.1% during nighttime at the WBI tower at the 99 m level. The concentration predictions were found to be sensitive to the vertical resolution, with the largest impacts during nighttime and early morning at the 30 m tower level. The monthly average RMSE when using 41 vertical layers was reduced by 19.5% at 11 pm CST compared to a 31 vertical layer simulation. WRF-VPRM with higher horizontal resolution was shown to capture more details of the biosphere flux estimates. The differences of the monthly average net fluxes between WRF-VPRM and Carbon Tracker were significant, 71%, 18%, and 62% in June, July, and August, respectively.

Using growing season optimized VPRM parameters for corn and soybean, the model usually overestimated NEE at the beginning of the growing season (June) and could not capture the high uptake at the peak time of the plant growth in August. Monthly optimized parameters significantly reduced the RMSE at corn and soybean sites. Although the simulation with the multi-crop parameters yielded higher daytime CO_2 drawdown, the separation of corn and soybean are still critical due to significant differences in the biosphere fluxes and their effects on CO_2 vertical profiles.

A series of sensitivity simulations in which one parameter at a time was perturbed by 20% showed that carbon dioxide concentrations are very sensitive to α and λ, with the maximum changes of CO_2 concentrations of 6.6 (1.7%) and 10.2 (2.2%) ppm at WBI tower, respectively. The results from the inversion study that assimilated CO_2 concentrations from a series of towers in the Midwest yielded significantly higher PAR_0 and λ of soybean, but lower PAR_0, λ, and α of corn compared to the Ameriflux optimized (Prior) parameters. The simulation with these optimized parameters decreased the CO_2 drawdown, which increased the daytime predicted CO_2 concentrations. The RMSE during the daytime was reduced from 11.6 ppm to 7.8 ppm.

The 7 day average fluxes over the Midwest calculated by the three different methods (top-down optimization, with corn and soybean separated, Ameriflux optimized parameters, and original parameters and single crop) were 12.9, 15.1, and 10.8 μmol m^{-2} s^{-1} at 12 pm, and 4.4, 6.1, and 3.4 μmol m^{-2} s^{-1} at 12 am, respectively. The differences between the top-down parameters and the Ameriflux optimized parameters indicate that the use of a top down approach is important since the diversity of the biosphere may not be captured by the Ameriflux towers, which are known to have limited footprint areas.

This research has provided a methodology to reduce the uncertainty in estimates of CO_2 fluxes and concentrations. The high resolution model is important for more accurate biosphere flux estimates. The separation of corn and soybean is critical because of the different photosynthesis rates of the two crops can cause significant differences in

the biosphere fluxes. Since the WRF-VPRM model can be used to estimate CO_2 biosphere fluxes at high resolutions and at any location, it allows States/Cities to obtain accurate biosphere fluxes at a high resolution. The more accurate biosphere flux estimates will ease policy makers in evaluating carbon mitigation policies' benefit, thus encourage more implementation of the sequestration policies.

Possible sources of uncertainties may also come from the accuracy of input data including EVI and LSWI values, Ameriflux NEE data, and radiation. Accuracy of land cover map can also cause errors in the estimates. The SYNMAP and CDL land cover show significant discrepancy in cropland areas (58.1% versus 34.8%). VULCAN anthropogenic emission for the year 2002 was used without extrapolation to 2008. These uncertainties can be reduced by improving quality of the input data.

7.1.1 The major contributions of this research are as follows.

We separated corn and soybean from other crops and optimized the VPRM parameters for those crops against the Ameriflux data both monthly and growing season. The separation of corn and soybean is critical for accurate CO_2 biosphere flux and concentration due to their different photosynthesis and respiration rates.

We performed the data assimilation to obtain VPRM parameter using atmospheric CO_2 concentrations over the Midwest. To our knowledge, a data assimilation method has not been used to retrieve VPRM parameters. The top-down approach is useful for verifying the VPRM parameters obtained from the bottom-up approach. It can be used to improve a bottom model. By optimizing VPRM instead of the biosphere fluxes, the parameters can also be applied to other domain to obtain the fluxes and concentrations.

A number of future research activities are anticipated. One is to explore the effect of the time period on the top down inversion. The current results are based on a single 7 day period. Another important issue is to characterize the uncertainties in the system on

additional key inputs including land cover, EVI and LSWI values, radiation. For example, how sensitive are the results at the WBI tower to the surrounding land cover inputs. Also the top down inversion method can be extended to simultaneously assimilate concentration and flux measurements.

7.2 Recommendations

The WRF-VPRM respiration equation, which is a function of temperature and two parameters, may need some modification. This is difficult to capture the plant nighttime respiration fluxes in different seasons and atmospheric conditions. More variables should be added to the model's respiration term especially the EVI (which highly correlate to Leaf Area Index and plants' respiration, http://adsabs.harvard.edu/abs/2006AGUFM.B43A0252S) and atmospheric conditions. Higher respiration fluxes were observed under stable atmospheric conditions (Juszcsak et al., 2012). The model also applies the same VPRM parameter values to calculate nighttime and daytime respiration fluxes.

T_{min}, T_{max} and T_{opt} may play an important role in the biosphere flux estimates. Here, we used T_{max} of 40 ^{o}C. When air temperatures are higher than T_{max}, the model assumes no photosynthesis occurs but we still observed quite strong uptake from photosynthesis from the tall towers.

At the early growing season, the EVI values should be significantly lower than the peak growing season. However, we observed quite high EVI values at some Ameriflux sites at the beginning of the growing season which may cause by atmospheric contaminations. We would also recommend on investigating LSWI and W_{scale} effects on plants photosynthesis.

REFERENCES

Aber, J. D., & Federer, C. A. (1992). A generalized, lumped-parameter model of photosynthesis, evapotranspiration and net primary production in temperate and boreal forest ecosystems. *Oecologia, 92*(4), 463-474.

Ahmadov, R., Gerbig, C., Kretschmer, R., Koerner, S., Neininger, B., Dolman, A. J., et al. (2007). Mesoscale covariance of transport and CO2 fluxes: Evidence from observations and simulations using the WRF-VPRM coupled atmosphere-biosphere model. *Journal of Geophysical Research-Atmospheres, 112*(D22)

Ahmadov, R., Gerbig, C., Kretschmer, R., Korner, S., Rodenbeck, C., Bousquet, P., et al. (2009). Comparing high resolution WRF-VPRM simulations and two global CO2 transport models with coastal tower measurements of CO2. *Biogeosciences, 6*(5), 807-817.

Baker, D. F., Law, R. M., Gurney, K. R., Rayner, P., Peylin, P., Denning, A. S., et al. (2006). TransCom 3 inversion intercomparison: Impact of transport model errors on the interannual variability of regional CO2 fluxes, 1988-2003. *Global Biogeochemical Cycles, 20*(1)

Emery, C. A., E. Tai, & G. Yarwood. (2001). *Enhanced meteorological modeling and performance evaluation for two texas ozone episodes*. Novato, CA: ENVIRON International Corp.

Enting, I. G., & Mansbridge, J. V. (1991). Latitudinal distribution of sources and sinks of Co2 - results of an inversion study. *Tellus Series B-Chemical and Physical Meteorology, 43*(2), 156-170.

Falge, E., Baldocchi, D., Olson, R., Anthoni, P., Aubinet, M., Bernhofer, C., et al. (2001). Gap filling strategies for defensible annual sums of net ecosystem exchange. *Agricultural and Forest Meteorology, 107*(1)

Gerbig, C., Dolman, A. J., & Heimann, M. (2009). On observational and modelling strategies targeted at regional carbon exchange over continents. *Biogeosciences, 6*(10), 1949-1959.

Gerbig, C., Lin, J. C., Wofsy, S. C., Daube, B. C., Andrews, A. E., Stephens, B. B., et al. (2003). Toward constraining regional-scale fluxes of CO2 with atmospheric observations over a continent: 1. observed spatial variability from airborne platforms. *Journal of Geophysical Research-Atmospheres, 108*(D24), 4756.

Grell, G. A., Peckham, S. E., Schmitz, R., McKeen, S. A., Frost, G., Skamarock, W. C., et al. (2005). Fully coupled "online" chemistry within the WRF model. *Atmospheric Environment, 39*(37), 6957-6975.

Gurney, K. R., Law, R. M., Denning, A. S., Rayner, P. J., Baker, D., Bousquet, P., et al. (2002). Towards robust regional estimates of CO2 sources and sinks using atmospheric transport models. *Nature, 415*(6872), 626-630.

Hong, S. (2010). A new stable boundary-layer mixing scheme and its impact on the simulated east asian summer monsoon. *Quarterly Journal of the Royal Meteorological Society, 136*(651), 1481-1496.

Hu, X., Nielsen-Gammon, J. W., & Zhang, F. (2010). Evaluation of three planetary boundary layer schemes in the WRF model. *Journal of Applied Meteorology and Climatology, 49*(9), 1831-1844.

Huete, A. R., Liu, H. Q., Batchily, K., & vanLeeuwen, W. (1997). A comparison of vegetation indices global set of TM images for EOS-MODIS. *Remote Sensing of Environment, 59*(3), 440-451.

Intergovernmental Panel on Climate Change (IPCC) Report (2007).

Janssens, I. A., Freibauer, A., Ciais, P., Smith, P., Nabuurs, G. J., Folberth, G., et al. (2003). Europe's terrestrial biosphere absorbs 7 to 12% of european anthropogenic CO2 emissions. *Science, 300*(5625), 1538-1542.

Jung, M., Henkel, K., Herold, M., & Churkina, G. (2006). Exploiting synergies of global land cover products for carbon cycle modeling. *Remote Sensing of Environment, 101*(4), 534-553.

Juszczak, R., Acosta, M., & Olejnik, J. (2012). Comparison of daytime and nighttime ecosystem respiration measured by the closed chamber technique on a temperate mire in poland. *Polish Journal of Environmental Studies, 21*(3)

Keeling, C. D., Whorf, T. P., Wahlen, M., & Vanderplicht, J. (1995). Interannual extremes in the rate of rise of atmospheric carbon-dioxide since 1980. *Nature, 375*(6533), 666-670.

Kumar, S. (2007). Fourth assessment report of the intergovernmental panel on climate change: Important observations and conclusions. *Current Science, 92*(8), 1034-1034.

Lauvaux, T., Gioli, B., Sarrat, C., Rayner, P. J., Ciais, P., Chevallier, F., et al. (2009). Bridging the gap between atmospheric concentrations and local ecosystem measurements. *Geophysical Research Letters, 36*

Law, B. E., Falge, E., Gu, L., Baldocchi, D. D., Bakwin, P., Berbigier, P., et al. (2002). Environmental controls over carbon dioxide and water vapor exchange of terrestrial vegetation. *Agricultural and Forest Meteorology, 113*(1-4), 97-120.

Lin, J. C., & Gerbig, C. (2005). Accounting for the effect of transport errors on tracer inversions. *Geophysical Research Letters, 32*(1), L01802.

Liu, D. C., & Nocedal, J. (1989). On the limited memory bfgs method for large-scale optimization. *Mathematical Programming, 45*(3)

Loveland, T. R., Reed, B. C., Brown, J. F., Ohlen, D. O., Zhu, Z., Yang, L., et al. (2000). Development of a global land cover characteristics database and IGBP DISCover from 1 km AVHRR data. *International Journal of Remote Sensing, 21*(6-7), 1303-1330.

Mahadevan, P., Wofsy, S. C., Matross, D. M., Xiao, X. M., Dunn, A. L., Lin, J. C., et al. (2008). A satellite-based biosphere parameterization for net ecosystem CO2 exchange: Vegetation photosynthesis and respiration model (VPRM). *Global Biogeochemical Cycles, 22*(2)

Peters, W., Jacobson, A. R., Sweeney, C., Andrews, A. E., Conway, T. J., Masarie, K., et al. (2007). An atmospheric perspective on north american carbon dioxide exchange: CarbonTracker. *Proceedings of the National Academy of Sciences of the United States of America, 104*(48), 18925-18930.

Rodenbeck, C., Houweling, S., Gloor, M., & Heimann, M. (2003). CO2 flux history 1982-2001 inferred from atmospheric data using a global inversion of atmospheric transport. *Atmospheric Chemistry and Physics, 3*, 1919-1964.

Xiao, X. M., Hollinger, D., Aber, J., Goltz, M., Davidson, E. A., Zhang, Q. Y., et al. (2004). Satellite-based modeling of gross primary production in an evergreen needleleaf forest. *Remote Sensing of Environment, 89*(4), 519-534.

APPENDIX A VPRM OPTIMIZED PARAMETERS FOR GRASSLAND

AND DECIDUOUS FOREST

Table A.1 VPRM optimized parameters for grassland at Fermi Prairie (USIB2)

Approaches	Period	λ (μmol CO_2/ μmol PPFD)	PAR_0 (μmol PPFD m^{-2} s^{-1})	α (μmol CO_2 m^{-2} s^{-1} /$^{\circ}$C)	β (μmol CO_2 m^{-2} s^{-1})
Prior	-	0.0667	314	0.0269	0
Mahadevan et al., 2008	2001-2003	0.213	542	0.028	0.72
Approach 1	Growing season	0.0609	1913	0.1715	0.5146
Approach 2	Growing season	0.0745	1422	0.2523	0
Monthly optimization	April	0.2111	216	0.1711	0
	May	0.1459	614	0.2826	0
	June	0.121	763	0.2922	0
	July	0.0906	1084	0.2645	0
	August	-	-	-	-
	September	0.0742	452	0.2288	0
	October	0.0517	389	0.1588	0

Table A.2 VPRM optimized parameters for deciduous forest

Approaches	Sites	Period	λ (μmol CO_2/ μmol PPFD)	PAR_0 (μmol PPFD m^{-2} s^{-1})	α (μmol CO_2 m^{-2} s^{-1}/$^{\circ}$C)	β (μmol CO_2 m^{-2} s^{-1})
Prior	-	-	0.08645	648	0.3258	0
Mahadevan et al., 2008	-	2000-2003	0.127	570	0.271	0.25
Approach 1	USMOz	Growing season	0.0656	981	0.0881	1.042
	USMMS	Growing season	0.0556	1233	0.0647	2.21
		Average	*0.0606*	*1107*	*0.0764*	*1.626*
Approach 2	USMOz	Growing season	0.1023	664	0.2756	0
	USMMS	Growing season	0.0624	1115	0.2121	0
		Average	*0.0824*	*890*	*0.2439*	*0*
Monthly optimization	USMOz	April	0.2434	222	0.1741	0
	USMMS	April	0.0873	267	0.1753	0
		Average	*0.1654*	*245*	*0.1747*	*0*
	USMOz	May	0.1054	504	0.269	0
	USMMS	May	0.0731	546	0.2416	0
		Average	*0.0893*	*525*	*0.2553*	*0*
	USMOz	June	0.1168	560	0.3265	0
	USMMS	June	0.0625	1226	0.2162	0
		Average	*0.0897*	*893*	*0.2714*	*0*
	USMOz	July	0.0882	955	0.2819	0
	USMMS	July	0.057	1571	0.2207	0
		Average	*0.0726*	*1263*	*0.2513*	*0*

Table A.2 continued

Approaches	Sites	Period	λ (μmol CO_2/ μmol PPFD)	PAR_0 (μmol PPFD m^{-2} s^{-1})	α (μmol CO_2 m^{-2} s^{-1}/^oC)	β (μmol CO_2 m^{-2} s^{-1})
	USMOz	August	0.0776	1031	0.2922	0
	USMMS	August	0.0632	1304	0.2177	0
		Average	*0.0704*	*1168*	*0.255*	*0*
	USMOz	September	0.1432	593	0.3023	0
	USMMS	September	0.0735	917	0.2055	0
		Average	*0.1084*	*755*	*0.2539*	*0*
	USMOz	October	0.2646	405	0.2069	0
	USMMS	October	0.0747	677	0.2027	0
		Average	*0.1697*	*541*	*0.2048*	*0*

Note: growing season optimization used data from April 1st to Oct 31st 2008

APPENDIX B CO_2 FLUXES AND CONCENTRATIONS PLOTS OF

SINGLE AND MULTI-CROP SIMULATIONS
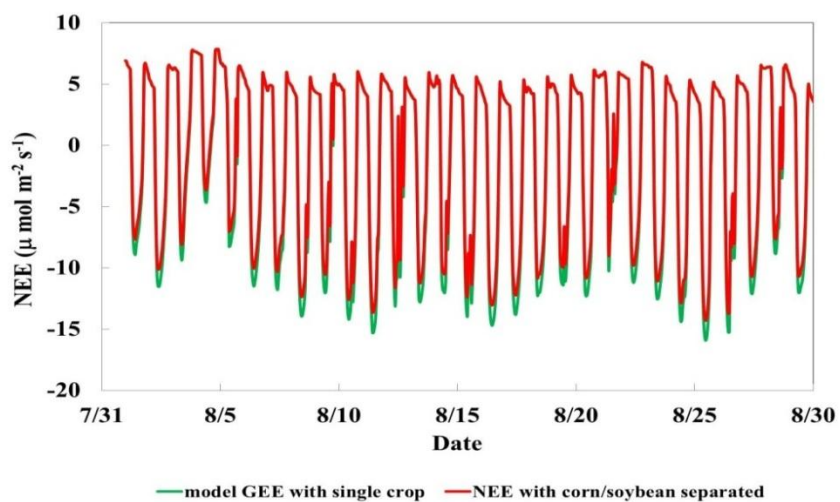
Figure B.1 Biosphere fluxes from single and multi-crops simulation at Centerville tower
in August 2008.
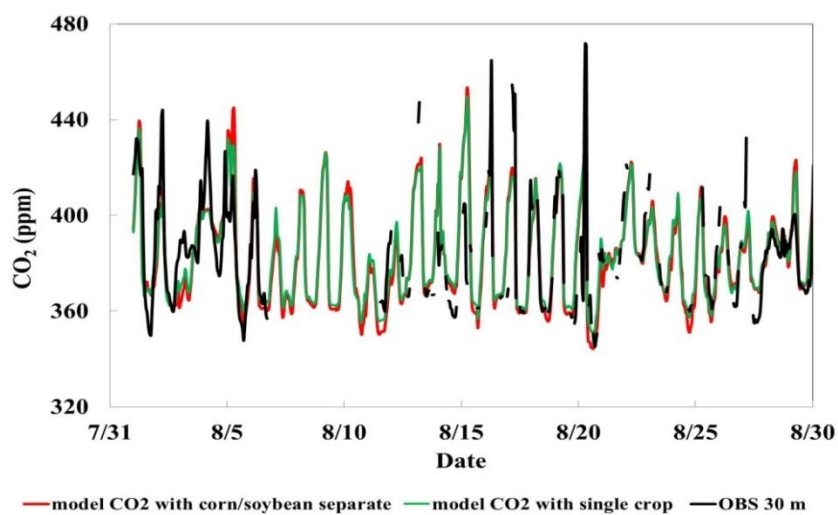
Figure B.2 CO_2 concentrations from single and multi-crops simulation at Centerville
tower at 30 m in August 2008.
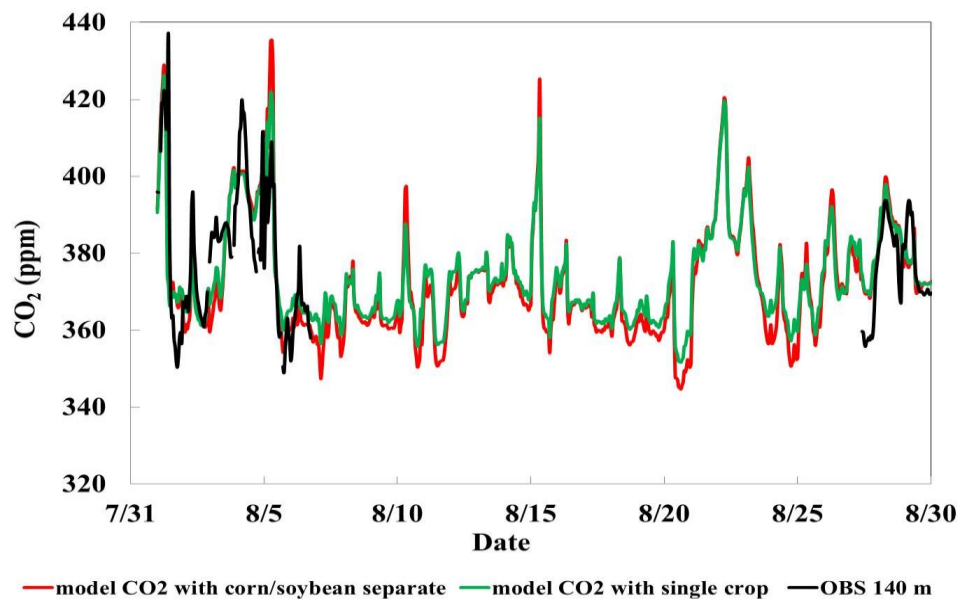
Figure B.3 CO$_2$ concentrations from single and multi-crops simulation at Centerville tower at 140 m in August 2008.
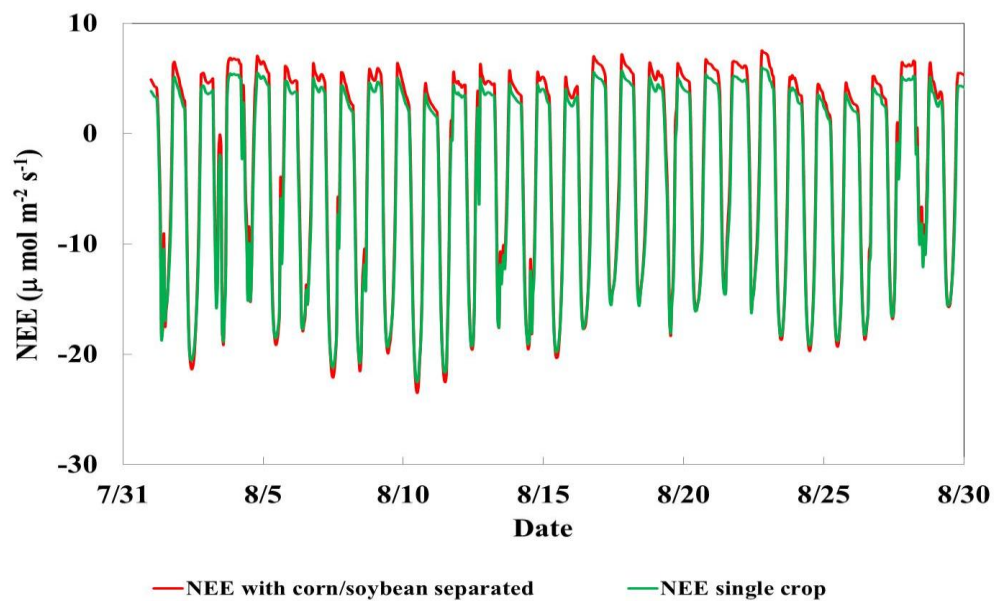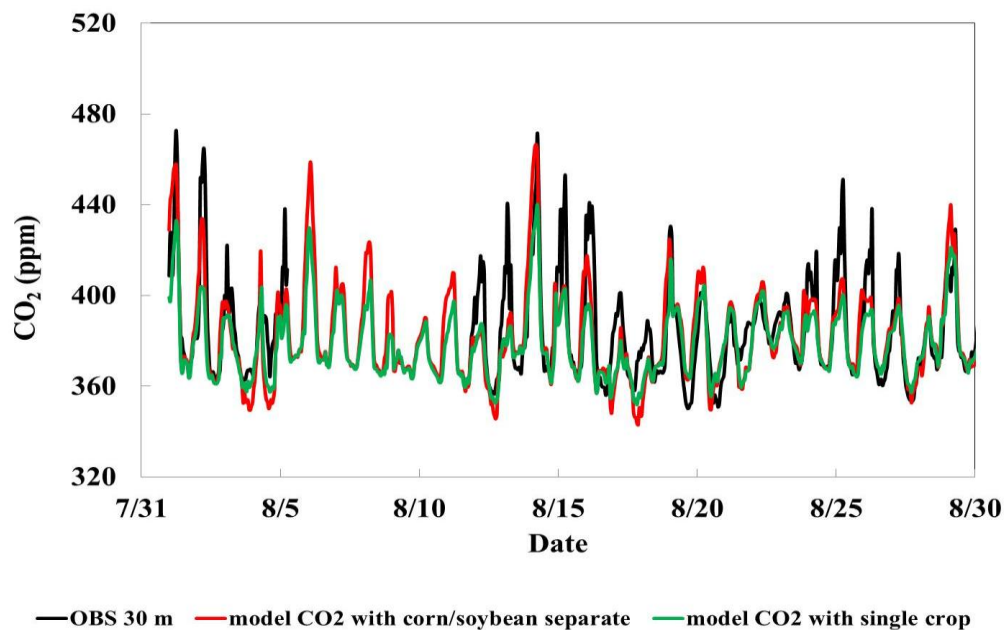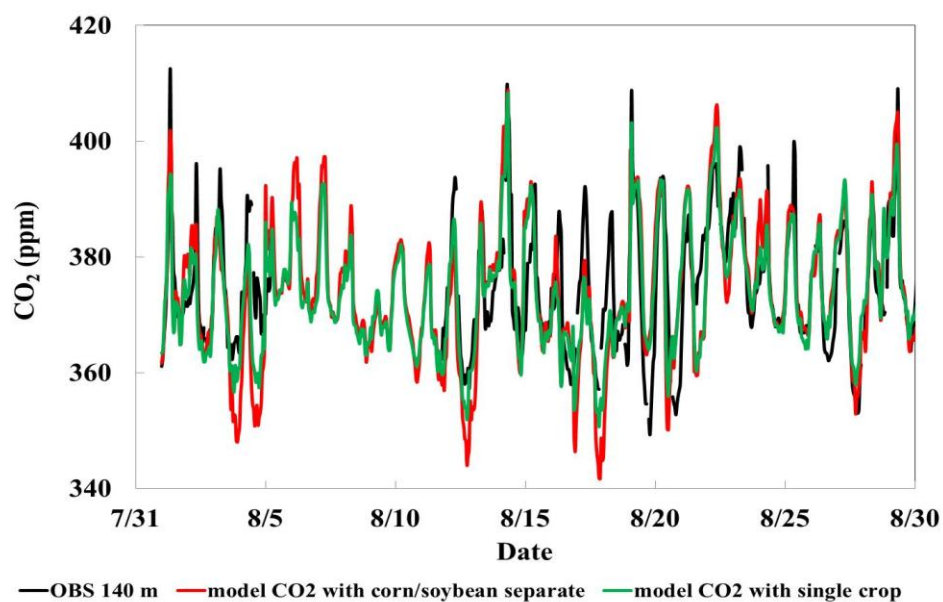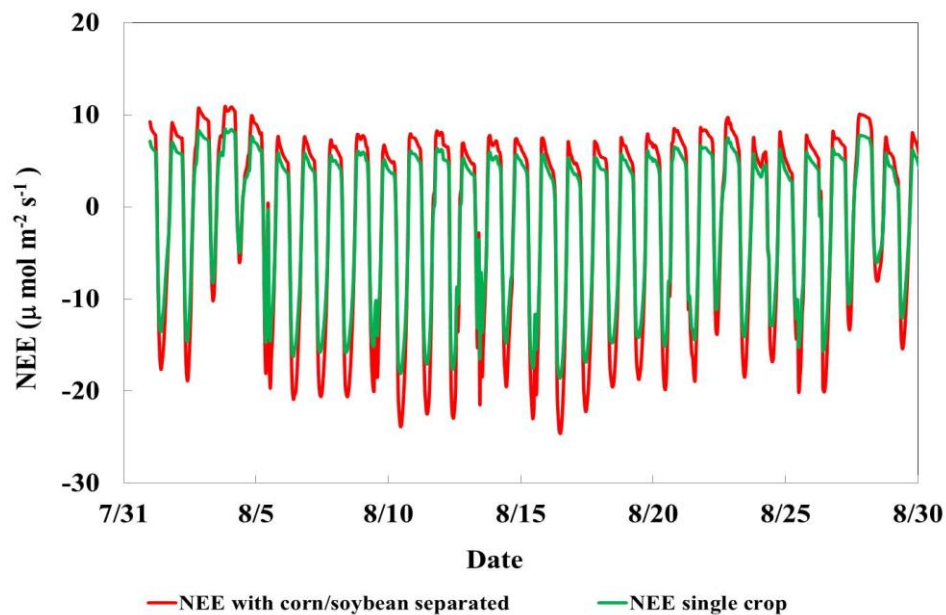

Figure B.4 Biosphere fluxes from single and multi-crops simulation at Galesville tower in August 2008.

Figure B.5 CO_2 concentrations from single and multi-crops simulation at Galesville tower at 30 m in August 2008.

Figure B.6 CO_2 concentrations from single and multi-crops simulation at Galesville tower at 140 m in August 2008.

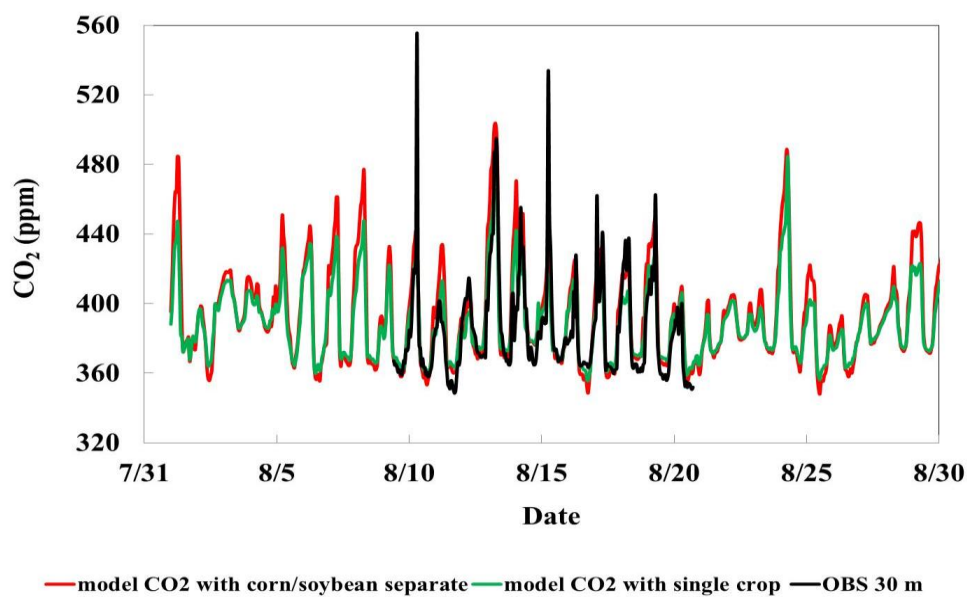Figure B.7 Biosphere fluxes from single and multi-crops simulation at Mead tower in August 2008.

Figure B.8 CO_2 concentrations from single and multi-crops simulation at Mead tower at 30 m in August 2008.
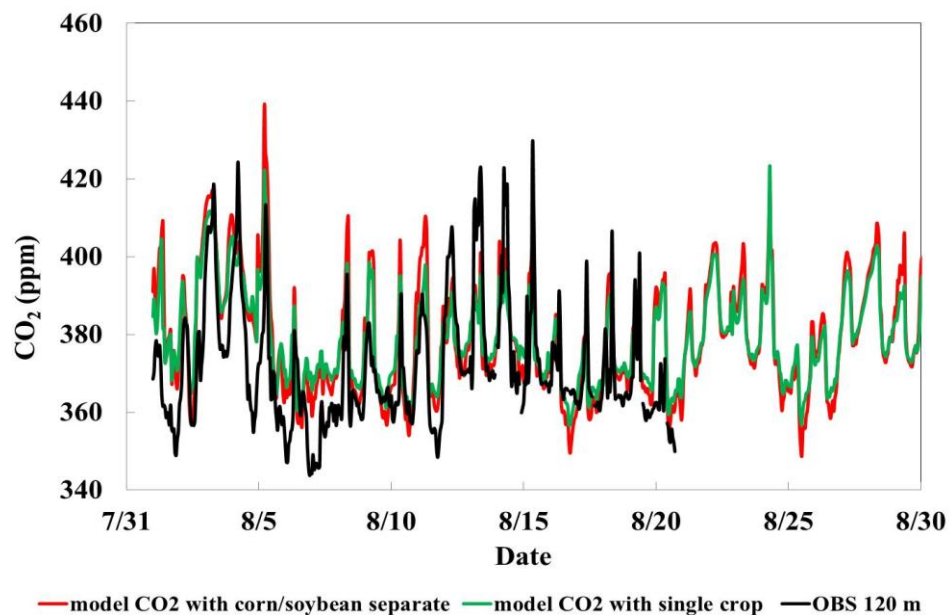
Figure B.9 CO_2 concentrations from single and multi-crops simulation at Mead tower at 120 m in August 2008.
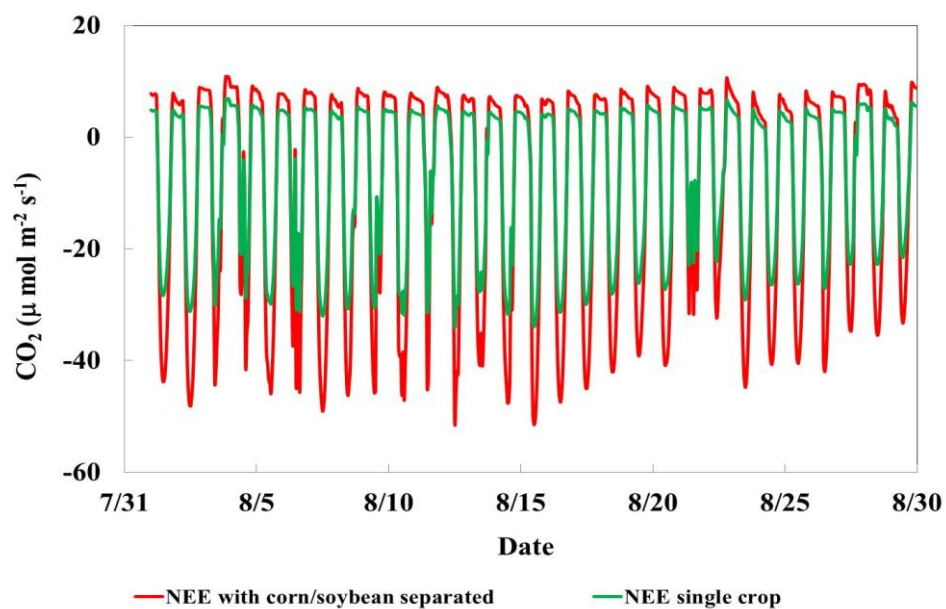

Figure B.10 Biosphere fluxes from single and multi-crops simulation at Round Lake tower in August 2008.
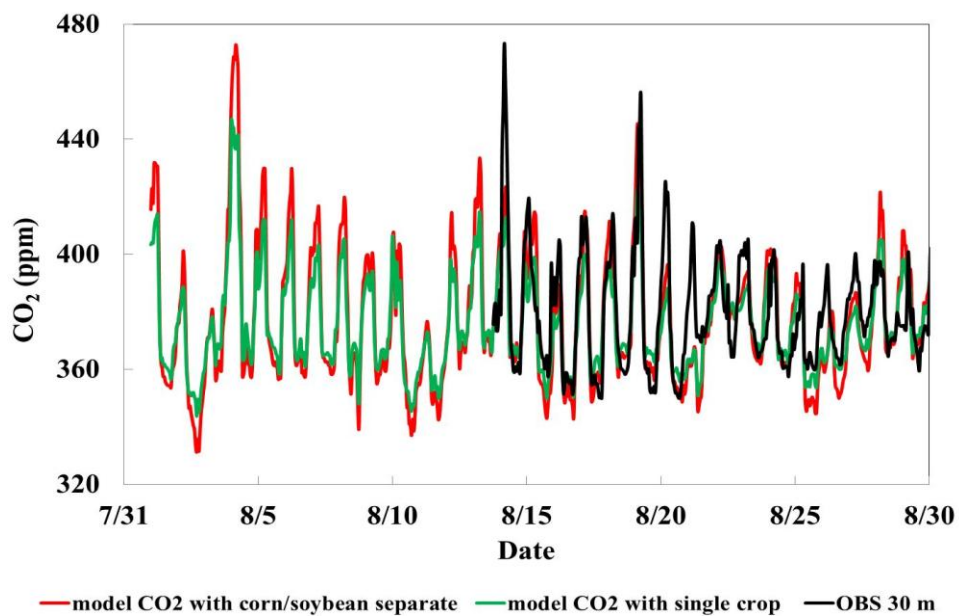
Figure B.11 CO_2 concentrations from single and multi-crops simulation at Round Lake tower at 30 m in August 2008.
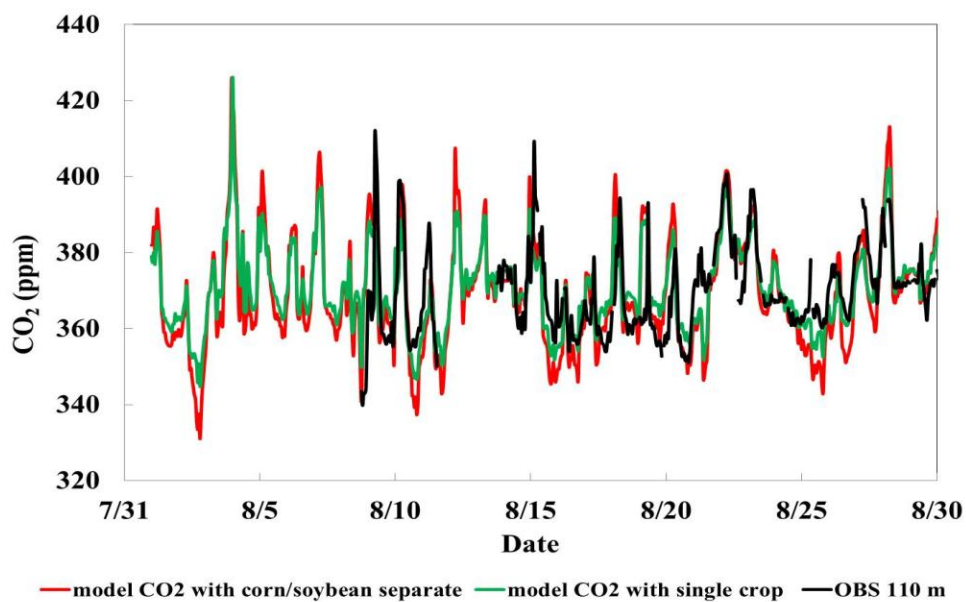

Figure B.12 CO_2 concentrations from single and multi-crops simulation at Round Lake tower at 110 m in August 2008.

Table B.1 Land cover at the tower location (4x4 km pixel).

Sites/ Vegetation Classes	Deciduous (%)	Soybean (%)	Corn (%)	Grassland (%)	Others (%)
Ameriflux towers					
- USNe1, NE	-	5.7	22.1	72.1	-
- USNe2, NE	-	5.7	22.1	72.1	-
- USNe3, NE	-	23.4	25.8	42.1	C3 crops (8.6)
- USIB1, IL	1.6	2.7	7	4.5	Urban/built-up/water (84.4)
- USIB2, IL	4.5	7.9	13.5	28.9	Urban/built-up/water (45.1)
- USMOz, MO	84.1	-	-	15.9	-
- USMMS, MN	100	-	-	-	-
- USBkg, SD	-	22	16.1	59.2	C3 crop (2.7)